

## Review

## Overview of Wells-Dawson Polyoxometalates: from structure and functionalization to application

Daria Nowicka<sup>a</sup>, Nahir Vadra<sup>a,b</sup>, Ewelina Wieczorek-Szweda<sup>a</sup>, Violetta Patroniak<sup>a</sup>, Adam Gorczyński<sup>a,\*</sup><sup>a</sup> Adam Mickiewicz University in Poznań, Faculty of Chemistry, Uniwersytetu Poznańskiego 8, 61-614 Poznań, Poland<sup>b</sup> Universidad de Buenos Aires, Facultad de Ciencias Exactas y Naturales, Departamento de Química Inorgánica, Analítica y Química Física and CONICET-Universidad de Buenos Aires, Instituto de Química Física de los Materiales, Medio Ambiente y Energía (INQUIMAE), Buenos Aires C1428EGA, Argentina

## ARTICLE INFO

Dedicated to Professor Jean-Marie Lehn on the occasion of his 85th birthday.

## Keywords:

Wells-Dawson POM  
Polyoxometalates  
Hybrid organic-inorganic  
Functional materials  
Post-functionalization approaches

## ABSTRACT

Wells-Dawson polyoxometalates (WD POMs) are an important subgroup within the diverse family of POMs. In the last two decades, there has been remarkable progress in the structure modification and post-functionalization of WD POMs, which has unlocked their enormous potential across various domains, including energy materials, catalysis (photocatalysis, electrocatalysis), functional materials (sensors, optical materials, electrochromic materials, magnetic materials) or biology/medicine (anticancer and antibacterial activities). What makes these systems particularly captivating is their highly adaptable topological structure, combined with the versatile functionalization methods and consequently their precise design and control, which transfers into a wide range of applications. In our comprehensive review, we focus on the exploration of their intricate structural characteristics which play a pivotal role in their functional properties. Moreover, the exciting and promising applications of WD POMs across various areas of science disciplines are highlighted. Our aim is to shed light on the current state of the art, identify emerging trends, and provide insights into the potential future directions of WD POM research, which are still being expanded, especially given the rapid development and continuous progress in the design of novel WD POM subunit functionalities. By doing so, we hope to contribute to a better understanding of these remarkable materials and inspire further innovation in their utilization.

## 1. Introduction

Polyoxometalates (POMs) are a group of metal-oxo nanoclusters in the class of inorganic compounds, represented by the general formula  $[X_nM_mO_o]^{n-}$ , where X = heteroatom, M = early transition metal (TM) ion in the highest oxidation state ( $W^{6+}$ ,  $Mo^{6+}$ ,  $V^{5+}$ ) [1–16]. In general, POMs are formed by the condensation of oxygen atoms and an early TM ion under appropriate conditions (pH, solvent, reducing agents, temperature, rate and sequence of addition, type of heteroatoms, type of cations, etc.) thus forming polyhedra, which are linked to each other via edge and corner sharing [17–22]. Metal-oxo nanoclusters are classified into different types, with the principal ones being Lindqvist  $[M_6O_19]^{n-}$  [23], Keggin  $[XM_{12}O_{40}]^{n-}$  [24], Wells-Dawson  $[XM_{18}O_{62}]^{n-}$  [25], Silverton  $[XM_{12}O_{42}]^{n-}$  [26], Preyssler  $[X^{n+}P_5W_{30}O_{110}]^{(15-n)-}$  [27] and Anderson-Evans  $[XM_6O_{24}]^{n-}$  [28,29] types (Fig. 1). The possibility of self-assembly in various geometric archetypes and sizes contributes to the diverse nature of the compounds and affects their characteristics

such as charge density and redox properties [20,30]. The versatility and variety of POM properties have led to the publication of numerous papers and reviews in the last decades. An important area of research focuses on POM nanoclusters as precursors to forming organo-inorganic hybrid materials [2]. The process of POM functionalization occurs in a covalent and/or ionic manner. The combination of inorganic precursors with organic functionalities via covalent binding is a significant branch of hybrid materials chemistry due to synergistic interactions between organic and inorganic parts [18]. Moreover, published works have explored ways to diversify physicochemical properties for potential applications as well as to understand structure–function relationships in a wide variety of areas such as catalysis [31–43], photocatalysis [44–52], magnetism [53–57], energy [58–70], biology/medicine [71–80], and others [81–87].

However, although comprehensive and recent reviews of several of the archetypical POM systems have been reported [88–97], an in-depth discussion of Wells-Dawson POMs (WD POMs) has been unexpectedly

\* Corresponding author.

E-mail address: [adam.gorczynski@amu.edu.pl](mailto:adam.gorczynski@amu.edu.pl) (A. Gorczyński).<https://doi.org/10.1016/j.ccr.2024.216091>

Received 5 April 2024; Accepted 10 July 2024

Available online 30 July 2024

0010-8545/© 2024 The Authors. Published by Elsevier B.V. This is an open access article under the CC BY license (<http://creativecommons.org/licenses/by/4.0/>).

missing. In fact, the latest published review that focuses on WD nano-clusters dates as far back as 2003 [31] and it summarized related developments in this group for the period 1990–2002. The versatility of WD structures has led in the last decades to exploring ways to diversify their physicochemical properties: for example, modification of the internal counterions or templates (Se, P, S, Te, Sb, Ge), modification of addenda atoms (V, Mo, W) by other coordination metals leading to CAP (trilacunar or monolacunar) or belt modification, and the formation of non-conventional WD POMs such as open or sandwich WD POMs. Furthermore, besides the changes that typically occur in the WD POM structure, the properties are also influenced by post-functionalization processes, such as for example single-, double-linker modularity-generating hybrid materials and others leading to the formation of for example polymeric systems based on WD POMs. Structurally modified and post-functionalized WD POMs show an unparalleled range of properties, from systems capable of mimicking enzymes to materials for supercapacitors or batteries. Despite the numerous limitations associated with speciation in solution at different pH ranges, the modification of POM structures, such as the adjustment of the electronic properties of acidity or polarity and post-functionalization, researchers started to probe into biological properties, such as anticancer and antibacterial activity. Thanks to their valuable redox properties, they find numerous applications in catalysis, be it photocatalysis or electrocatalysis. Modified WD POMs have gained features such as stability in solution and in the solid, have shown potential host roles for magnetic ions, and their structure has become rigid and highly symmetric, all of which has made them encouraging compounds in the design of new molecular magnetic devices. Owing to dynamic developments in the synthesis, characterization and application of new WD POMs since the most recent review, 567 papers have been published on WD POMs, of which 293 have appeared in the last 10 years (Fig. 2).

The purpose of this work is to provide a comprehensive review of developments related to WD POMs centered on the growing interest in this class of compounds. Firstly, structural modifications made in this family of POMs are analyzed in a rational and orderly form, followed by the synthetic strategies used for these modifications. Subsequently, the post-functionalization processes of WD POMs together with the synthetic strategies are thoroughly discussed. Finally, the properties and recent applications in areas such as energy transfer, photo- or electrocatalysis, sensors, magnetism, biology and other functional materials are critically evaluated.

## 2. Structure of WD POMs

WD POMs are one of the more common types of POMs of the general formula  $[X_2M_{18-n}Y_nO_{62}]^{n-}$ , where X = heteroatom/template (P, Si, S, As, etc.), M = early transition metal ion/addenda atom (Mo, W), Y = other metal coordinate (V, Cr, Sn, Co, etc.),  $n = 1, 2$  or  $3$  [98–101] (Fig. 3) and interestingly enough, the first example of a WD POM was developed and published as early as in 1953 [25].

The overall structure can be grouped according to the exterior cap and belt positions, which are mostly oxometallates of molybdenum, tungsten or vanadium at their highest oxidation states, and the internal *p*-block elements which form so-called templating oxoanion heteroatoms. A modification to the original WD POM structure by incorporating another metal ion in the cap position contributes to building variable structures such as dimers or tetramers and facilitates functionalization [101–104]. Nonetheless, belt modification is also important as it leads to the formation of non-classical POMs such as open WD POMs [105–108] (Fig. 4).

### 2.1. Templates/Heteroatoms

WD clusters may differ from each other in their inner heteroatoms which are enclosed in the 3D structure of POMs [98,99,109–112] (Fig. 5). Unlike the classical WD POMs containing two  $[XO_4]^{n-}$  moieties in their structures, e.g.  $[PO_4]^{3-}$  [113–116],  $[AsO_4]^{3-}$  [113,114,117,118],  $[SO_4]^{2-}$  [119–122],  $[ClO_4]^-$  [123], non-classical types are generated by the incorporation of non-tetrahedral moieties, such as pyramidal  $[XO_3]^{n-}$  groups, e.g.  $[SO_3]^{2-}$  [124–127],  $[AsO_3]^{3-}$  [128],  $[SbO_3]^{3-}$  [129,130],  $[BiO_3]^{3-}$  [131],  $[TeO_3]^{2-}$  [132],  $[SeO_3]^{2-}$  [99,127,133,134], ditetrahedral  $[P_2O_7]^{4-}$  [135], trigonal-hexafluorosodate  $[NaF_6]^{5-}$  [136–139], trigonal-prismatic  $[WO_6]^{6-}$  [140–142] or other octahedral  $[XO_6]^{n-}$ , such as  $[TeO_6]^{6-}$  [141,142],  $[IO_6]^{5-}$  [142,143],  $[SbO_6]^{7-}$  [144] (Table 1). It is noted that owing to the introduction of various heteroatoms into the interior of the structure, the physicochemical properties are effectively modulated and fine-tuned [110], e.g. solubility, conductivity, functionalizing flexibility, specific surface area, degradation, and aggregation.

Classical WD POMs are one of the most well-known and researched types of POMs owing to their interesting properties and auspicious utilization [110].  $[PO_4]^{3-}$  [113–115] moieties are most frequently encountered in the literature as the inner counterions in POM structures, considering the basic POM group. The unusual resemblance to the

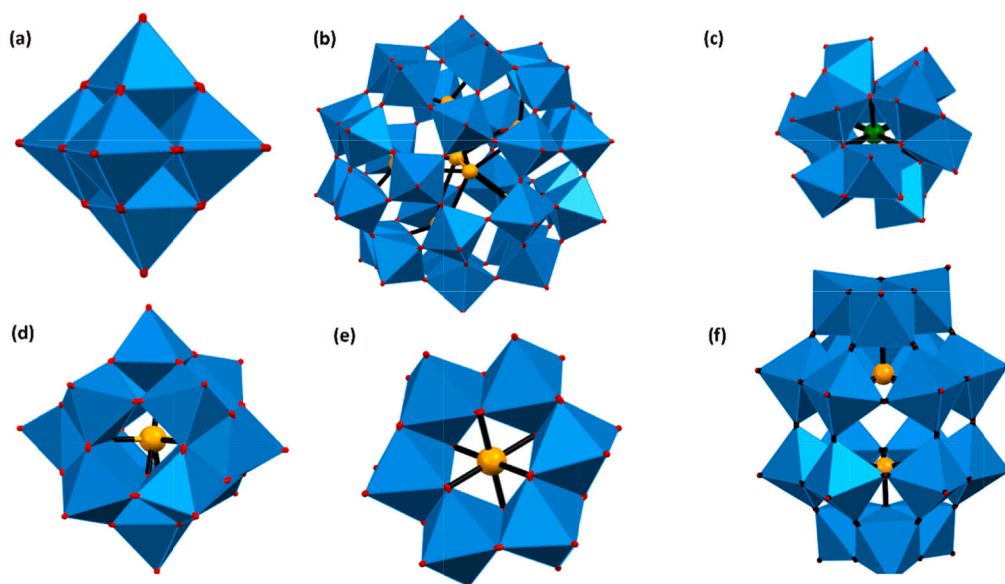


Fig. 1. The most common POM structures: (a) Lindqvist, (b) Preyssler, (c) Silverton, (d) Keggin, (e) Anderson-Evans, and (f) Wells-Dawson.



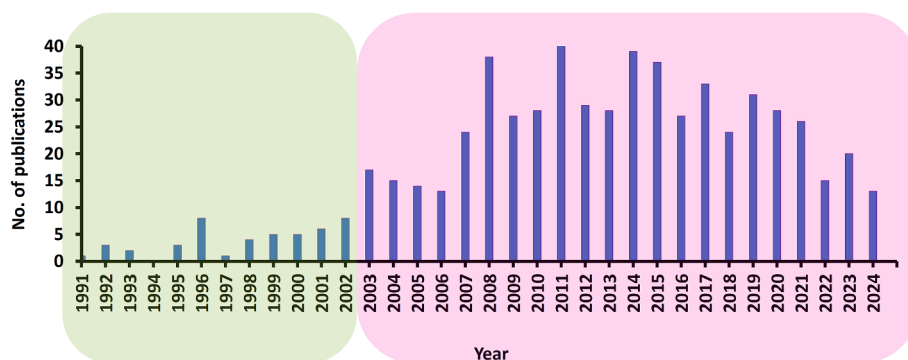


Fig. 2. Number of publications on WD POMs vs. time. Green: Papers summarized in the previous review; pink: papers summarized in this paper.

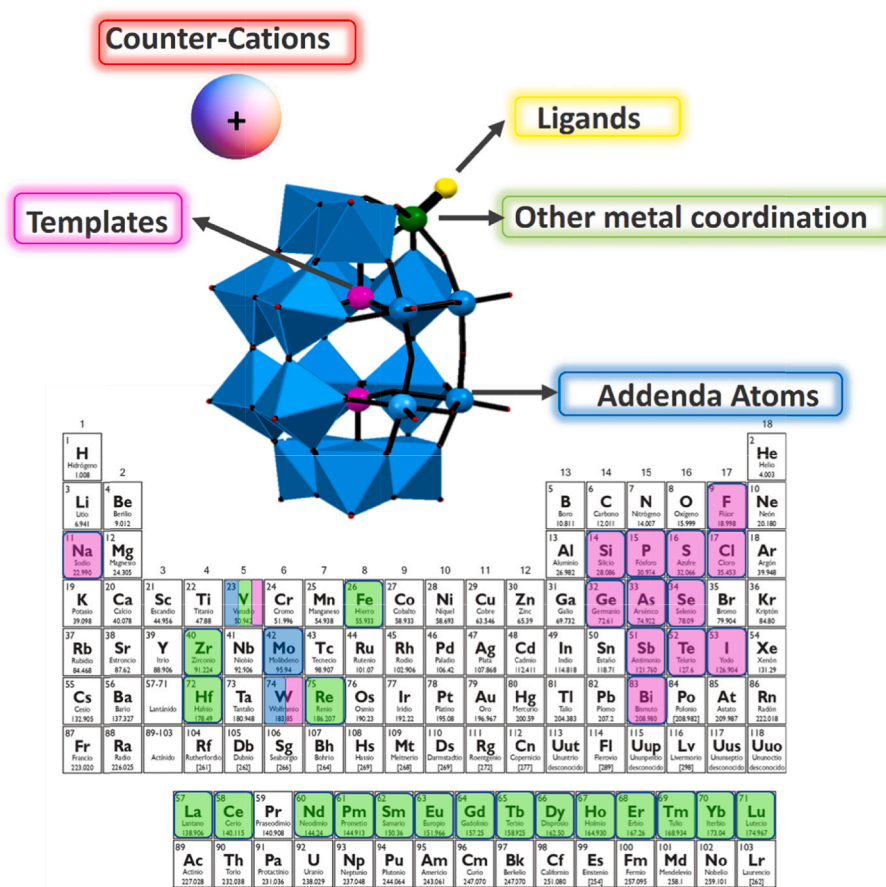


Fig. 3. WD POM structure with modifiable groups highlighted and the periodic table showing elements selected for specific modifications.

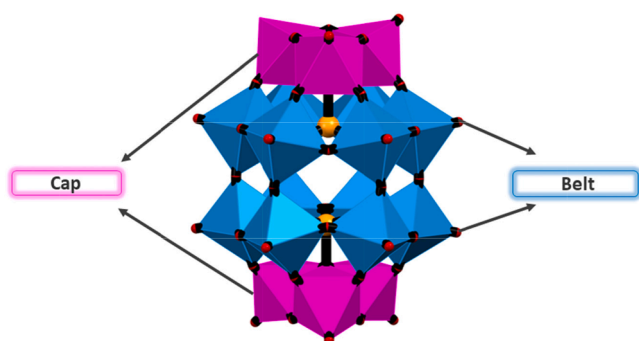


Fig. 4. WD POM structure with cap and belt positions.

phosphorus-centered POM can be seen when arsenic is introduced as the heteroatom. However, the differences between these heteroatoms, such as the larger atomic radius of arsenic and easy oxidation between the  $\text{As}^{\text{III}}/\text{As}^{\text{V}}$  states, modify the electronic properties of the POMs, which can be important for catalysis [113,117]. Remarkably, both arsenic and phosphorus can form a mixed WD POM system, such as arsenate – phosphate – tungstate  $\alpha\text{-[AsPW}_{18}\text{O}_{62}]^{6-}$  as reported by Haouas et al. [147]. Sulfur is the subsequent neighboring element to phosphorus in the periodic table, the introduction of which into the interior of a WD POM structure has a promising effect on its oxidizing properties [121]. Interestingly, WD POM silicotungstates are rarely reported; nonetheless, according to the available literature most of them do not contain any organic compound and no more than five paramagnetic metal atoms can be introduced. This type of POM can be formed by the dimerization of

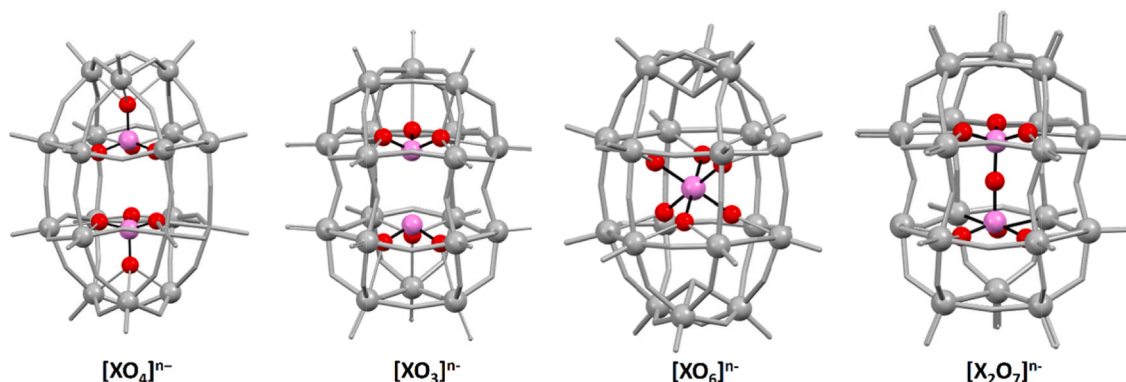


Fig. 5. General structures of classical and non-classical WD POMs with  $[XO_4]^{n-}$ ,  $[XO_3]^{n-}$ ,  $[X_2O_7]^{n-}$  and  $[XO_6]^{n-}$  moieties.

Table 1

Representation of the classical and non-classical WD POM structures containing  $[XO_m]^{n-}$  moieties ( $m = 3, 4$  or  $6$ ) and  $[X_2O_7]^{n-}$ .

General formula of the moiety	Moiety	General formula of the compound	Ref.
$[XO_4]^{n-}$	$[PO_4]^{3-}$	$\alpha\beta\alpha-Na_{16}(Mn^{II}OH_2)_2(Mn^{II})_2(P_2W_{15}O_{56})_2$	[116,115]
	$[AsO_4]^{3-}$	TBA <sub>6</sub> $[\alpha-P_2W_{18}O_{62}] \cdot H_2O$	[113,117,118]
	$[SO_4]^{2-}$	$\alpha\beta\alpha-Na_{16}(Mn^{II}OH_2)_2-Mn^{II}_2(As_2W_{15}O_{56})_2 \cdot 55H_2O$	[119,120,121,122]
		$Na_{16}[Cu_4(H_2O)_2(As_2W_{15}O_{56})_2] \cdot 47H_2O$	
		$K_{14}[As_2W_{19}O_{67}(H_2O)]$	
	$[ClO_4]^-$	$[C_{19}H_{18}N_3]_4[\alpha-S_2Mo_{18}O_{62}]$	[123]
		$(MB)_5[S_2Mo^V Mo^VI_7O_{62}] \cdot CH_3CN$ (MB = $C_{16}H_{18}N_3S$ ) $[Bu_4N]_5[S_2W_{18}O_{62}]$	
	$[SiO_4]^{2-}$	$[Ru^{II}(bpy)_3]_2[\alpha-S_2M_{18}O_{62}]$	[115,105,145]
	$[VO_4]^{2-}$	$[NBu_4]_3[Cl_2W^V W^VI_{17}O_{62}]$	[146]
		TBA <sub>8</sub> $[\alpha-Si_2W_{18}O_{62}] \cdot 3H_2O$	
$[XO_3]^{n-}$	$[VO_4]^{2-}$	$K_7H_2[K(Co(H_2O)_4)_2Co(H_2O)_2(Si_2W_{18}O_{66})] \cdot 22H_2O$	[124,125,126,127]
		$[Dy_2(H_2O)_{6.5}(C_2H_4O_2)_{0.5}Si_2W_{18}O_{66}]^{10-}$	
	$[SO_3]^{2-}$	$[Cu_2(2,2'-bpy)_2(Inic)_2(H_2O)_2][Y(Inic)_2(H_2O)_5]H_3[V_2W_{18}O_{62}] \cdot 5.5H_2O$	[128]
		$(Bu_4N)_4[W_{18}O_{54}(SO_3)_2]$	
	$[AsO_3]^{3-}$	(TEAH) <sub>6</sub> $[H_2W_{18}O_{57}(SO_3)]$	[130,129]
		$(DMAH)_8[W_{18}O_{56}(SO_3)_2(H_2O)_2]$	
	$[SbO_3]^{3-}$	$[W_{18}O_{54}(SO_3)_2]^{4-}$	[131]
		$[W_{18}O_{56}(SO_3)_2(H_2O)_2]^{8-}$	
	$[BiO_3]^{3-}$	$\beta-[W_{18}O_{54}(AsO_3)_2]^{6-}$	[132,132]
		$[SbW_{18}O_{60}]^{9-}$	
$[X_2O_7]^{n-}$ $[XO_6]^{n-}$	$[P_2O_7]^{4-}$	$[Cu(phen)(H_2O)]_2[Cu(phen)(H_2O)_3]_2H[SbW_{18}O_{60}] \cdot 5H_2O$	[135]
		$[H_3BiW_{18}O_{60}]^{6-}$	
	$[NaF_6]^{5-}$	$(C_2H_8N)_{19}Na_{13}[(WO_2)_4(Te_2W_{15}O_{54})_4] \cdot 57H_2O$	[109,136,137,139]
		$(C_2H_8N)_{19}Cs_2Na_{11}[(WO_2)_4(Te_2W_{15}O_{54})_4] \cdot 77H_2O$	
	$[WO_6]^{6-}$	$[H_2Se^{IV}W_{18}O_{60}]^{6-}$	[99,133,134,127]
		$[Se_2W_{18}O_{62}(H_2O)_2]^{8-}$	
	$[TeO_6]^{6-}$	$[W_{18}O_{54}(SeO_3)_2]^{4-}$	[140,142]
		$[W_{18}O_{56}(SeO_3)_2(H_2O)_2]^{8-}$	
	$[TeO_6]^{6-}$	$(N(C_4H_9)_4)_4[(P_2O_7)Mo_{18}O_{54}]$	[135]
		$[(NaF_6)W_{18}O_{54}(OH)_2]^{7-}$	
$[X_2O_7]^{n-}$ $[XO_6]^{n-}$	$[WO_6]^{6-}$	$K_9[NaH_2Zn(H_2O)W_{17}F_6O_{55}]$	[141,141]
		$K_8[NaH_2Mn^{II}(H_2O)W_{17}F_6O_{55}] \cdot 19H_2O$	
	$[TeO_6]^{6-}$	$K_9[NaH_2Ni(H_2O)W_{17}F_6O_{55}] \cdot 15H_2O$	[140,142]
		(TEAH) <sub>6</sub> $[H_4W_{19}O_{62}]$	
	$[TeO_6]^{6-}$	$\alpha-[W_{18}O_{56}(WO_6)]^{10-}$	[141,141]
		Na(DMAH) <sub>6</sub> $[H_3W_{18}O_{56}(Te^{VI}O_6)] \cdot 14H_2O$	
	$[IO_6]^{5-}$	(TBA) <sub>7</sub> $[H_3W_{18}O_{56}(Te^{VI}O_6)] \cdot 4CH_3CN$	[143,143,143]
		$K_6[H_3W_{18}O_{56}(IO_6)] \cdot 9H_2O$	
	$[SbO_6]^{7-}$	(TPA) <sub>6</sub> $[H_3W_{18}O_{56}(IO_6)]$	[109,144]
		(TBA) <sub>6</sub> $[H_3W_{18}O_{56}(IO_6)]$	

TBA: tetrabutylammonium; bpy: 2,2'-bipyridine; TEAH: protonated triethanolamine; DMAH: protonated dimethylammonium; phen: 1,10-phenanthroline; TPA: tetrapropylammonium.

tri-lacunary Keggin-type  $[\alpha-SiW_9O_{34}]^{10-}$  anions [106,115]. There are only a few examples in the literature where other metals, such as selenium or vanadium, were introduced as heteroatoms; however, these metal-oxo nanoclusters are little known and studied [146,148–150]. It is yet noted that despite the fact that they have been little studied, papers are available that discuss their interesting applications. The work of Cronin's group is such an example, in which a core-shell cluster of POM

$[W_{18}O_{54}(SeO_3)_2]^{4-}$  has been shown to act as a potential storage node for metal-oxide-semiconductor (MOS) flash memory [134].

Non-classical WD nanoclusters containing only non-tetrahedral moieties affect the properties and can modulate the physicochemical nature of POMs. Admittedly, almost for all of non-classical WD POMs (except for pyramidal  $[XO_3]^{n-}$  and di-tetrahedral  $[P_2O_7]^{4-}$ ), six Baker-Figgis isomers have been observed ( $\alpha$ ,  $\beta$ ,  $\gamma$ ,  $\alpha^*$ ,  $\beta^*$  and  $\gamma^*$ ) (for

explanation and description, see Sections 2.2.1 and 2.2.2) [109]. The first structure of this group of POMs is  $\alpha$ -[NaF<sub>6</sub>](OH)<sub>2</sub>W<sub>18</sub>O<sub>54</sub>]<sup>7-</sup> containing [NaF<sub>6</sub>]<sup>5-</sup> moieties, reported in 1980 by Chauveau et al. [138] and determined in 1990 by Baker's group [151]. In 1994, Kortz and Pope identified the second WD POM,  $\gamma$ -[(P<sub>2</sub>O<sub>7</sub>)Mo<sub>18</sub>O<sub>54</sub>]<sup>4-</sup>, which embeds di-tetrahedral [P<sub>2</sub>O<sub>7</sub>]<sup>4-</sup> [135]. In the next decade, Cronin and co-workers reported a library of WD POMs with octahedral [XO<sub>6</sub>]<sup>n-</sup> moieties with the general formula [H<sub>m</sub>W<sub>18</sub>O<sub>56</sub>(XO<sub>6</sub>)<sup>n-</sup>, where m = 3 or 4; n = 6 or 7; X = I, W or Te [141–143]. Moreover, the possibility of the occurrence of [WO<sub>6</sub>]<sup>6-</sup> moieties was proved in two forms: octahedral and trigonal-prismatic [109,140,141,143]. Noteworthy, in the archetypes with octahedral geometry, the heteroatoms are located at the center of the cluster, unlike in other archetypes [142]. It is noted that Cronin's group developed a stepwise synthesis method using a robotic workflow for discovering new metal clusters which led for example to the discovery of three new tetrametallic POMs with the formula TBA<sub>5</sub>[(A- $\alpha$ -SiW<sub>9</sub>O<sub>34</sub>)<sub>2</sub>FeMn<sub>4</sub>O<sub>2</sub>(Lu(acac)<sub>2</sub>)<sub>2</sub>A<sub>2</sub>] (A = Ag, Na, K; acac = acetylacetonate) reported in [152].

## 2.2. Addenda atoms

An important aspect of POMs are addenda atoms, i.e. transition metals that are part of POM structures, typically Mo, W, V, Nb, and Ta. The metals are of remarkable importance for reactivity and type of displayed function [98,153]. The first group, polyoxomolybdates (POMos), are characterized by their size and shape, being giant clusters in the shape of spheres, wheels and hedgehogs due to the presence of building blocks composed of [Mo<sub>2</sub>O<sub>4</sub>] and [(Mo)Mo<sub>5</sub>] subunits under reducing conditions [154]. A distinctive feature of the second group, polyoxotungstates (POTs), is their occurrence as lacunar precursors which are stable and act as inorganic multidentate ligands, so that they can coordinate with different active species leading to the formation of abundant POM structures [155]. The third group, polyoxovanadates (POVs), provide rich redox chemistry and organometallic frameworks or cages can be formed owing to their structure. In addition, the oxidation of reduced POVs provides a new pathway for the generation of lacunar POVs, which in turn can act as host molecules [156]. The last two groups

of POMs are polyoxoniobates (PONbs) and polyoxotantalates (POTas); their chemistry is hindered and they are characterized by their neutral redox nature, have high negative charge density, their behavior under aqueous conditions is poorly understood and they are base-dependent [157]. Substitution of various addenda atoms is a useful method to modulate the electronic structure of hybrids. For instance, Amin et al. investigated the effects of molybdenum substitution in a wolframium-based cluster and confirmed the significant effect of this modification on the energies of the frontier orbitals of the hybrid [158].

The original WD POM structure is composed of two [XM<sub>3</sub>] moieties that form the cap (3x[XM<sub>3</sub>] per each cap) and two [XM<sub>6</sub>] moieties that form the belt (6x[XM<sub>6</sub>] per each belt). Both the cap and the belt can be modified and rotated resulting in six theoretical rotational isomers:  $\alpha$ ,  $\beta$ ,  $\gamma$ ,  $\alpha^*$ ,  $\beta^*$ , and  $\gamma^*$ . As shown in the study of Contant and Thouvenot, the most stable form of these isomers is isomer  $\alpha$ , and isomer  $\alpha^*$  is less stable ( $\alpha > \beta > \gamma > \gamma^* > \beta^* > \alpha^*$ ) [159]. The  $\alpha$ -[X<sub>2</sub>M<sub>18</sub>O<sub>62</sub>]<sup>6-</sup> anion is composed of two halves of [XM<sub>9</sub>]; subsequently two isomers are formed:  $\beta$  and  $\gamma$  form at high temperatures; the  $\beta$ -isomer forms through a rotation by 60° around the axis leading through both heteroatoms X and the  $\gamma$ -isomer forms through a second rotation by 60° [100,147,160,161] (Fig. 6).

According to calculations by Zhang et al., among the six isomers  $\alpha$ ,  $\beta$ ,  $\gamma$ ,  $\alpha^*$ ,  $\beta^*$  and  $\gamma^*$ , a form of D<sub>3h</sub>-symmetric M<sub>18</sub>O<sub>54</sub>, where M=W, Mo, V, etc. cages, for  $\alpha$ ,  $\gamma$  and  $\beta^*$  isomers, and a form of D<sub>3d</sub>-symmetric M<sub>18</sub>O<sub>54</sub> for  $\beta$ ,  $\alpha^*$  and  $\gamma^*$  isomers are possible. In addition,  $\alpha$ ,  $\beta$  and  $\gamma$  isomers incorporate two eclipsed D<sub>3h</sub> anions, while  $\alpha^*$ ,  $\beta^*$  and  $\gamma^*$  isomers encapsulate two staggered XO<sub>4</sub><sup>3-</sup> D<sub>3d</sub> anions [162]. In summary, the  $\alpha$  and  $\gamma$  isomers have D<sub>3h</sub> symmetry,  $\alpha^*$  and  $\gamma^*$  have D<sub>3d</sub> symmetry and  $\beta$  and  $\beta^*$  have C<sub>3v</sub> symmetry due to the mismatch of the inner anions and the outer cage, as confirmed in the report from Poblet's group [163].

Of the six isomers predicted by Baker and Figgis in 1970, only four isomers ( $\alpha$ ,  $\beta$ ,  $\gamma$ , and  $\gamma^*$ ) have actually been observed [162,164]. It is noted that the incorporation of non-tetrahedral moieties into a WD structure (see Section 2.1) enhances the complexity of cap-rotational isomerism [162] which was underscored in a paper by Cronin's group with a WD species including trigonal-prismatic WO<sub>6</sub><sup>6-</sup> moieties as heteroatoms, which confirmed the greatest stability for the  $\gamma$  isomer using DFT calculations, different from the stability of isomers in classic WD

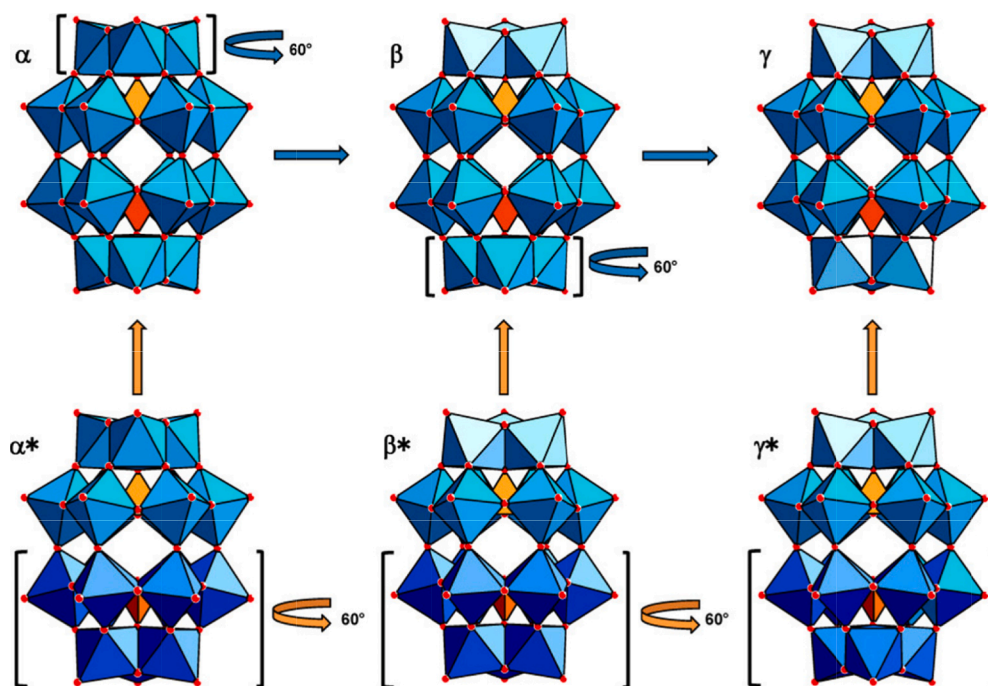


Fig. 6. Theoretical rotational WD POM isomers ( $\alpha$ ,  $\beta$ ,  $\gamma$ ,  $\alpha^*$ ,  $\beta^*$ , and  $\gamma^*$ ) and their structural relationships. Reproduced from [147] with permission of the copyright holders.

POMs [140]. It is difficult to obtain the most stable isomer  $\alpha$  of a classic WD with the general formula  $K_6[\alpha\text{-P}_2\text{W}_{18}\text{O}_{62}]\cdot 14\text{H}_2\text{O}$  with high purity by selective synthesis due to possible intermediate products [165]. In 2004, Nadjo's group reported the most successful synthesis of a highly pure  $\alpha$ -isomer,  $K_6[\alpha\text{-P}_2\text{W}_{18}\text{O}_{62}]\cdot 14\text{H}_2\text{O}$ , and they produced over 200 g with more than 97% (by  $^{31}\text{P}$  NMR) of the pure isomer  $\alpha$  and with no side products other than isomer  $\beta$  [166]. Additionally, Graham and Finke again obtained  $K_6[\alpha\text{-P}_2\text{W}_{18}\text{O}_{62}]\cdot 14\text{H}_2\text{O}$  using the synthesis method described by Nadjo's group and after one recrystallization they obtained a product with purity increased to 99% of isomer  $\alpha$  [165]. Conducted over the years and by many research groups, the investigation into WD isomers confirms the hypothesis of Contant and Thouvenot [159] on the stability of individual isomers of classical WD species, with the following order of stability:  $\alpha > \beta > \gamma > \gamma^* > \beta^* > \alpha^*$ .

Possible structural modifications of classic WD POMs are shown in the scheme below (Fig. 7) and they are discussed in detail in sections that follow about the modification of cap and belt positions.

### 2.2.1. CAP modification: Trilacunar modification

One of the limitations of WD POM synthesis and their further functionalization is the presence of oxo groups on the WD POM surface which can only bind to a limited number of organic groups to form hybrid materials for further post-functionalization. Therefore, modification of the POM structure is extremely important. One of the most common types of WD modifications is the cap modification in which the WD POM structure,  $[\text{M}_3\text{P}_2\text{W}_{15}\text{O}_{62}]^{n-}$ , is composed of a  $[\alpha\text{-P}_2\text{W}_{15}\text{O}_{56}]^{12-}$  precursor and M ( $\text{M} = \text{V}^{\text{V}}, \text{Ta}^{\text{V}}, \text{Nb}^{\text{V}}, \text{etc.}$ ) [102,167–169]. Inarguably, due to the easier synthetic method, the size of the introduced metal ion and charge of the POM, high-valence  $d$ -block metal ions are usually used to modify the structure. Nonetheless, there are known examples of POMs in which low-valence  $d$ -block metal ions have been used to modify the original structure [167,170].

Among the aforementioned structural motifs, the most popular is the WD POM cap modified by vanadium ions,  $\text{V}^{\text{V}}$  (PWV). It is noted that this type of modification has a considerable impact on subsequent functionalization. Moreover, further functionalization is extremely important, given the limitations of the POM subunit itself, in particular poor chemical stability. The importance and usefulness of this type of

modification are evidenced in the large number of publications reporting the synthesis and structure of PWVs [18,98,102,169,171–182]. The incorporation of three vanadium ions in the cap position of POMs adjusts photochemical and electrochemical properties, but most importantly it allows selective modification at the cap position with linkers, for instance using tris-alcohol organic derivatives or other organic groups. Here we report selected examples of vanadium-substituted WD POMs selected based on their potential in further post-synthetic modification. Cronin's group described a benchmark example of the PWV cluster,  $\text{TBA}_5\text{H}_4[\text{P}_2\text{V}_3\text{W}_{15}\text{O}_{62}]$ , which has been often used for subsequent functionalization with other linkers especially in terms of their single modularity, discussed in detail in Section 2.2 [18,171,172].

Furthermore, the presence of the  $\text{V}_3$  cap in the POM structure contributes to sensitivity to external factors, for instance reducing agents, pH, and nucleophiles [102]. Arguably, due to the three capping vanadium atoms in the  $[\text{P}_2\text{V}_3\text{W}_{15}\text{O}_{62}]^{9-}$  cluster PWV becomes an oxidant, and the WD POM cluster acquires catalytic properties [174,183]. Hence, the WD cluster with the vanadate cap is more reactive in comparison to the tungstate cap [173], which allows selective modification toward hybrid materials via post-functionalization, for instance connecting the WD POM with a chosen organic group through the  $\text{M}-\text{O}-\text{C}$  bond [102]. Interestingly, depending on the synthetic method a cluster with a different location of one, two or three  $\text{V}^{\text{V}}$  metal ions of the vanadium polyhedral can be obtained [183,184].

Tantalum is a different example of a high-valence metal ion which can be used for the cap modification of a WD cluster. It turns out that  $\text{Ta}^{\text{V}}$  incorporation in the WD POM cap results in enhanced reactivity due to an increased polyoxoanion charge and basicity of oxygen atoms bound to  $\text{Ta}^{\text{V}}$  [168]. The investigation into the effect of niobium, another metal from the fifth group of the periodic table, has been reported. Research confirms improved catalytic properties of  $\text{P}_2\text{W}_{15}\text{Nb}_3\text{O}_{62}^{9-}$  in comparison to  $\text{P}_2\text{W}_{18}\text{O}_{62}^{6-}$  and a high level of kinetic control obtained [185]. In addition, Xiao et al. reported a cluster consisting of three  $\text{Nb}_3\text{POM}$  units connected by four  $[\text{M}(\text{H}_2\text{O})_x]^{2+}$  groups as an example of a mixed POM with Lewis acid metal centers enhancing catalytic activity [186]. Moreover, apart from catalytic activities, a di- $\text{Nb}^{\text{V}}$  substituted cluster of WD POM can effectively form coiled polymers not previously reported in the literature [187].

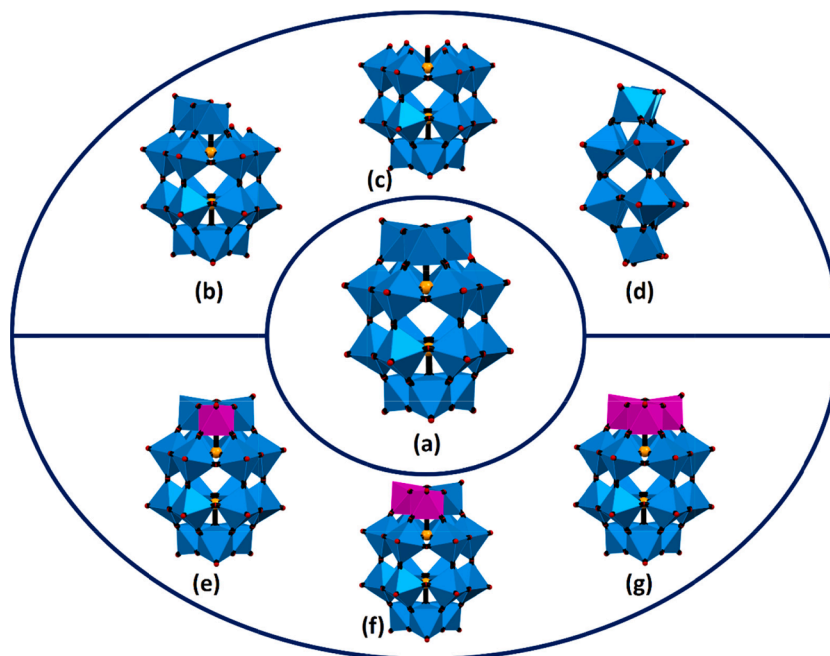


Fig. 7. Modified structures of WD POMs: (a) saturated WD, (b) mono-lacunary WD, (c) tri-lacunary WD, (d) hexa-lacunary WD, (e) mono-substituted WD, (f) bi-substituted WD, (g) tri-substituted WD.



To our knowledge, scientists reported examples of cap modification using a low-valence *d*-block metal ion ( $\text{Co}^{\text{II}}$ ,  $\text{Mn}^{\text{III}}$ ,  $\text{Ni}^{\text{II}}$ ,  $\text{Fe}^{\text{III}}$ ,  $\text{Re}^{\text{IV}}$ ,  $\text{Ti}^{\text{IV}}$ ) [103,167,188–193]. The substitution of the transition metal ion for tungsten increases the negative charge of the polyoxoanion, which results in improved catalytic ability and thermodynamical stabilization of the structure. An example of the  $\text{Mn}_3^{\text{III}}\text{Mn}^{\text{IV}}$  cluster can be mentioned in which a cuban-type system was obtained [188] with single molecule magnet (SMM) magnetic properties (Fig. 8a). Interestingly, it is possible to integrate the cuban type into a WD POM cluster lacunary POM, and while the structural  $\text{Mn}_4$  core geometry is retained, an unexpected change in the sequence of the lowest magnetic levels causes transformation of the  $\text{Mn}_4$  core into a high-spin system without observable slow magnetic relaxation [188].

An interesting example of cap modification was reported by Li et al. who synthesized a series of hexa-Ni-substituted WD POM clusters via a hydrothermal method (Figs. 8b–d). This technique significantly differs from the conventional synthesis technique of WD clusters and results in a shift from a thermodynamic product toward a kinetic one, owing to increased temperature and pressure, which shifts the above chemical equilibrium [190,191]. Three structures of modified WD POMs were determined via single-crystal X-ray and good stability of  $\text{Ni}_6$  clusters was confirmed, in spite of changes in the cap position in the structure. All of those three systems are stabilized via ethylenediamine ligands or their methylated analogs and, noteworthy, the two clusters (the left and middle ones) are isolated compounds but the last one (on the right) is based on  $\text{Ni}_6$ -substituted WD POM segments,  $[\text{Ni}(\text{enMe})_2]^{2+}$  bridges and acetate anions. Interestingly, only for the latter were ferromagnetic magnetic interactions observed, thus confirming how important even subtle structural changes can be [190].

Noteworthy is also the structure of a transition metal-substituted POM  $[\text{M}_3\text{P}_2\text{W}_{15}\text{O}_{62}]^{n-}$  ( $\text{M} = \text{Ti}^{\text{IV}}$ )  $[\alpha\text{-}1,2,3\text{-P}_2\text{W}_{15}(\text{TiO}_2)_3\text{O}_{56}(\text{OH})_3]^{9-}$  due to the generation of multicenter octahedral  $\text{TiO}_6$  active sites which can have semiconductive and photocatalytic properties [192]. Additionally, there is another example of a POM with substitution of  $\text{W}^{\text{VI}}$  atoms in a cluster by  $\text{Ti}^{\text{IV}}$  atoms forming giant “tetrapod”-shaped POMs composed of three main parts: four  $\text{Ti}_3$ -capped WD subunits, four bridging groups of octahedral  $\text{Ti}(\text{H}_2\text{O})_3$  and one encapsulated anion:  $\text{Br}^-$ ,  $\text{I}^-$  or  $\text{NO}_3^-$  [103]. It is noted that similar giant “tetrapod”-shaped polyoxoanions can be obtained using a different transition metal substituent, such as  $\text{Fe}^{\text{III}}$ , with the formula  $[\text{KFe}_{12}(\text{OH})_{18}(\alpha\text{-}1,2,3\text{-P}_2\text{W}_{15}\text{O}_{56})_4]^{29-}$ , published by Cronin’s group [193] (Fig. 8e).

POMs can also be combined into larger superstructures, as shown in a paper by Li et al. [194]. They used a synthetic concept based on

exploiting the chemical nature of the boron atom in boronic acids (electrophilicity and electron deficiency) and features of metal-oxo groups in POMs (nucleophilicity and high electron density) to connect multiple WD POM anions  $[\text{M}_3\text{P}_2\text{W}_{15}\text{O}_{62}]^{9-}$  ( $\text{M} = \text{Ta}^{\text{V}}$  or  $\text{Nb}^{\text{V}}$ ) into POM-based nanostructures using aromatic boronic acid linkages, resulting in giant POM-based nanocapsules with diameters of up to 4 nm, internal cavities and unique high-symmetry architectures [194]. The same research group published other examples of a polymer based on covalently linked POM-organoboronic acid [195,196]. In 2021, they reported for the first time the preparation of polymers with high proton conductivity by the controlled covalent polymerization of  $\text{Nb}_3$ -WD POM and organoboronic acid monomers and the potential for using the resulting polymer as a solid proton conductor [195].

### 2.2.2. CAP modification: monolacunar modification

Apart from the widespread interest in tri-substituted WD POMs resulting from the ability to manipulate the building blocks, control the growth of the structure and modulate the functionalization process [193], there are many literature examples of mono-substituted WD POMs formed by the incorporation of metal ions with high Lewis acid strength, such as  $\text{Mn}^{\text{III}}$ ,  $\text{Ni}^{\text{II}}$ ,  $\text{Co}^{\text{II}}$  etc. [20,101,197], or a high coordination number, such as  $\text{Zr}^{\text{IV}}$ ,  $\text{Sn}^{\text{IV}}$ ,  $\text{Hf}^{\text{IV}}$ ,  $\text{Ln}^{\text{III}}$  etc. [17,20,101,104,198–201], to form mono-lacunary WD POMs.

The first group of the ions (the first row transition metal ions) have a tendency to form monomeric POM structures as exemplified by  $[\text{Co}^{\text{II}}(\alpha\text{-P}_2\text{W}_{17}\text{O}_{61})]^{10-}$ ,  $[\text{Ni}^{\text{II}}(\alpha\text{-P}_2\text{W}_{17}\text{O}_{61})]^{10-}$ ,  $[\text{Cu}^{\text{II}}(\alpha\text{-P}_2\text{W}_{17}\text{O}_{61})]^{10-}$  [20] and  $[\text{Mn}^{\text{III}}(\alpha\text{-P}_2\text{W}_{17}\text{O}_{61})]^{9-}$  [197]. Interestingly, this first group of modifications tend to coordinate with the four terminal oxygen atoms in the lacunar site of the  $\alpha\text{-P}_2\text{W}_{17}\text{O}_{61}^{10-}$  unit in a planar manner due to the typical octahedral coordination expected for the first row transition metals, which may affect the less favorable applications of these systems compared to WD POMs mono-substituted by metal ions with a high coordination number described below [101].

On the other hand, transition metal ions, such as  $\text{Zr}^{\text{IV}}$ ,  $\text{Hf}^{\text{IV}}$ , have enhanced Lewis-acid strength and additionally also have a high coordination number [101]. The incorporation of  $\text{Zr}^{\text{IV}}$ ,  $\text{Hf}^{\text{IV}}$  metal ions into mono-lacunary WD POMs affects the biological properties of modified POMs (see also Section 6.4). Both  $\text{Zr}^{\text{IV}}$ -substituted and  $\text{Hf}^{\text{IV}}$ -substituted WD POMs exist in several forms: 2:2 dimers, 1:1 monomers and 1:2 species, as shown in Fig. 9 [101,198,199,202].

It is noted that the coordination of a lanthanide ion is more likely than that of the first row transition metal ion due to more flexible geometries and a higher coordination number. To the best of our

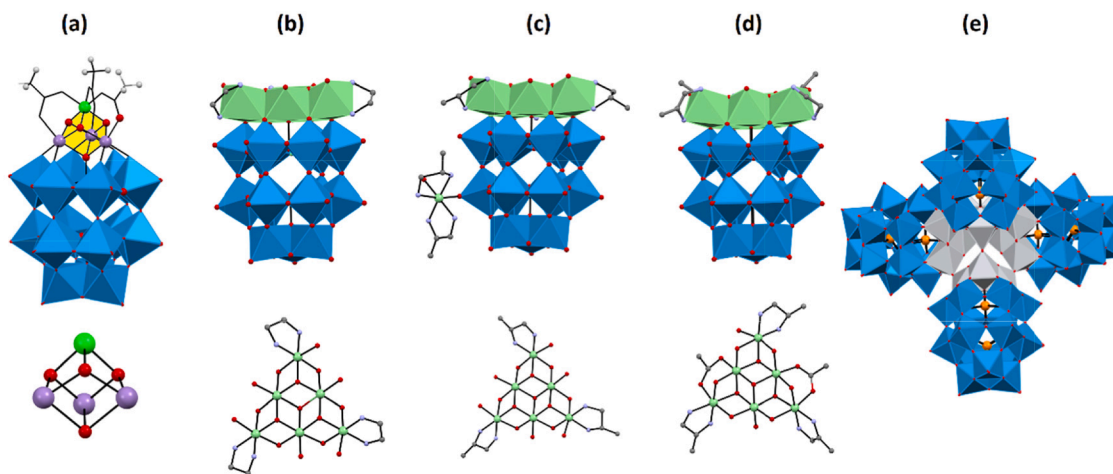


**Fig. 8.** Polyhedral representation and coordination environment of the (a)  $[(\alpha\text{-P}_2\text{W}_{15}\text{O}_{56})\text{Mn}_3^{\text{III}}\text{Mn}^{\text{IV}}\text{O}_3(\text{CH}_3\text{COO})_3]^{8-}$  cluster and (b–d) hexa-Ni cap in three clusters: (b)  $[\text{Ni}_6(\text{en})_3(\text{H}_2\text{O})_6(\mu_3\text{-OH})_3(\text{H}_3\text{P}_2\text{W}_{15}\text{O}_{56})] \cdot 14\text{H}_2\text{O}$ ; (c)  $[\text{Ni}(\text{enMe})_2(\text{H}_2\text{O})][\text{Ni}_6(\text{enMe})_3(\mu_3\text{-OH})_3(\text{H}_2\text{O})_6(\text{HP}_2\text{W}_{15}\text{O}_{56})] \cdot 10\text{H}_2\text{O}$ ; (d)  $[\text{Ni}(\text{enMe})_2]_3[\text{Ni}(\text{enMe})_2(\text{H}_2\text{O})][\text{Ni}(\text{enMe})(\text{H}_2\text{O})_2] \cdot [\text{Ni}_6(\text{enMe})_3(\mu_3\text{-OH})_3(\text{Ac})_2(\text{H}_2\text{O})(\text{P}_2\text{W}_{15}\text{O}_{56})]_2 \cdot 6\text{H}_2\text{O}$ ; (en = ethylenediamine; enMe = 1,2-diaminopropane; Ac =  $\text{CH}_3\text{COO}$ ). (e) Polyhedral representation of giant “tetrapod”-shaped polyoxometalates  $[\text{KFe}_{12}(\text{OH})_{18}(\alpha\text{-}1,2,3\text{-P}_2\text{W}_{15}\text{O}_{56})_4]^{29-}$ .

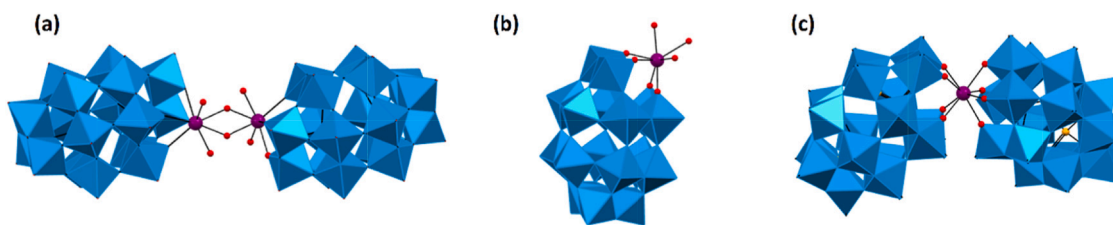


Fig. 9. Representative structures of  $\text{Zr}^{\text{IV}}$ -substituted and  $\text{Hf}^{\text{IV}}$ -substituted WD POMs in various forms: (a) 2:2 dimer; (b) 1:1 monomer and (c) 1:2 species.

knowledge, different monosubstituted  $[\text{Ln}^{\text{III}}(\alpha_2\text{-P}_2\text{W}_{17}\text{O}_{61})_2]^{17-}$  WD POMs ( $\text{Ln} = \text{La}, \text{Sm}, \text{Gd}, \text{Dy}, \text{Nd}, \text{Eu}, \text{Er}, \text{Ho}, \text{Lu}, \text{Ce}, \text{Pr}$ ) [101,104,203–216] have been reported. When comparing different lanthanide ions, slight variation in the distances in the structures of the published compounds between the metal ions and the nearest oxygen atoms is typical of the lanthanide contraction effect [203]. Interestingly, owing to those features, lanthanides are able to coordinate more than one subunit of mono-lacunary WD POMs and generate more complex structures [101,104,213–216]. It is also noted here that two different L and D isomers of the monosubstituted POM subunit can be obtained (Fig. 10a and Fig. 10b). In the dimeric form of POM clusters presented by Wang et al., two lacunary sites existed [200].  $\text{Cs}_{7.5}\text{K}_{0.5}[(\text{H}_2\text{O})_7\text{Dy}^{\text{III}}(\alpha_2, \alpha'_2\text{-P}_2\text{W}_{16}\text{O}_{60})(\text{C}_6\text{H}_5\text{PO})_2)_2] \cdot 42\text{H}_2\text{O}$  and  $\text{Cs}_{7.5}\text{K}_{0.5}[(\text{H}_2\text{O})_7\text{Y}^{\text{III}}(\alpha_2, \alpha'_2\text{-P}_2\text{W}_{16}\text{O}_{60})(\text{C}_6\text{H}_5\text{PO})_2)_2] \cdot 42\text{H}_2\text{O}$  were synthesized in mild conditions to form one lacunar site ( $\alpha_2$ ) in one of the outer caps (Fig. 10c). Metal ion coordination ( $\text{M} = \text{Dy}^{\text{III}}, \text{Y}^{\text{III}}$ ) and the phenylphosphonate induce the opening of the second lacuna ( $\alpha'_2$ ) in the opposite cap. The resulting clusters assemble in a dimeric form connected via  $\text{M}^{\text{III}}$  cap-belt bridges [200] (Fig. 10d).

### 2.2.3. Belt modification

The second significant type of WD modification is related to the belt part, which sparks less interest among scientists than the above-noted cap modification, most plausibly due to more serious problems with the selective etching of XO polyhedra. This alteration involves the

replacement of the WD metal ions ( $\text{Mo}^{\text{VI}}, \text{W}^{\text{VI}}$ ) by surface heterometals such as  $\text{Cu}^{\text{II}}$  [110] (the most common strategy) and rarely by  $\text{Co}^{\text{II}}$  [217],  $\text{Mn}^{\text{III}}$  [218], etc. at the belt position. Xu et al. reported in 2012 a new WD isomer,  $\delta\text{-}[(\text{WO}_5)\text{W}_{17}\text{Cu}(\text{H}_2\text{O})\text{O}_{65}]^-$ , with considerable yields of 55%; they modified the belt site by  $\text{Cu}^{\text{II}}$  incorporation and formation of a  $[\text{WO}_5]$  moiety with a square pyramid shape which causes a  $45^\circ$  rotation of the four-belt square-pyramidal  $[\text{CuO}_5]/[\text{WO}_5]$  (Fig. 11) thus establishing a new type of WD isomerism involving rotation of the belt polyhedra, previously believed to remain unchanged. Jiao, et al. reported the first example of an isomer modified by the  $[(\text{WO}_5)_3\text{W}_{14}\text{Mn}_2\text{O}_{44}\text{Cl}_2]^{12-}$  Jahn-Teller distortion  $\delta$ -WD POM via the incorporation of two  $\text{Mn}^{\text{III}}$  ions which resulted in the formation of a square pyramid in the belt position. The resulting WD POM modified in the belt position using manganese ions, compared to the classical WD POM subunit, showed higher photocatalytic activity toward  $\text{H}_2$  evolution [218].

In the literature, it can be noted that combined cap and belt modifications within the hexa-lacunary  $[\text{H}_2\text{P}_2\text{W}_{12}\text{O}_{48}]^{12-}$  WD is also feasible, and it is characterized by the lack of the six octahedra, more precisely one from each cap position and two from each belt part of the structure [219–225]. Combination of hexa-lacunary WD POMs with transition metal and alkali metal ions usually leads to the formation of a macrocyclic tetramer of  $[\text{P}_8\text{W}_{48}\text{O}_{184}]^{40-}$  [219,220,222,225] but dimers  $[\text{P}_4\text{W}_{24}\text{O}_{94}]^{24-}$  [224], U-shaped trimers  $[(\text{PO}_3\text{OH})_2\text{P}_6\text{W}_{36}\text{O}_{136}]^{46-}$  [226] and cyclic trimers  $[(\text{H}_2\text{O})_3\text{P}_6\text{W}_{39}\text{O}_{147}]^{30-}$  [221,223] have also

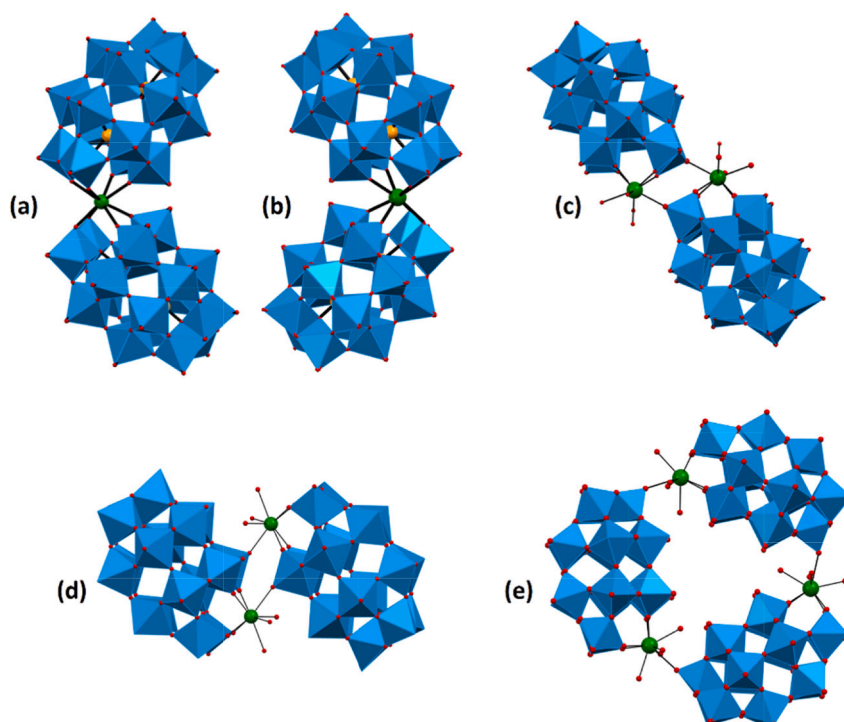
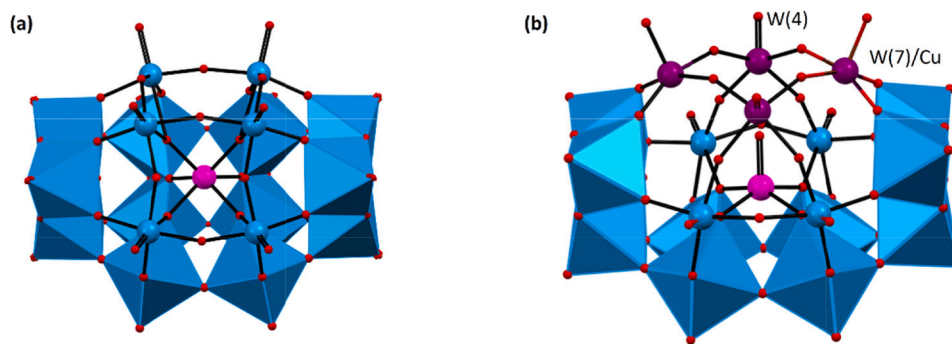


Fig. 10. Representative structures of lanthanide polyanion modifications of (a) L-isomers of  $\text{cis-}[\text{Ln}^{\text{III}}(\alpha_2\text{-P}_2\text{W}_{17}\text{O}_{61})_2]^{17-}$ , (b) D-isomers of  $\text{cis-}[\text{Ln}^{\text{III}}(\alpha_2\text{-P}_2\text{W}_{17}\text{O}_{61})_2]^{17-}$ , (c) “cap to cap”, (d) “cap to belt”, (e) 2:2 type dimeric and trimeric.



**Fig. 11.** Comparison of WD structures between the known isomer, (a)  $\alpha$ - $[(\text{WO}_6)\text{W}_{18}\text{O}_{66}]^{10-}$  (color code: the central  $\text{WO}_6$ : pink; rest  $\text{WO}_6$ : blue octahedra), and the new isomer, (b)  $\delta$ - $[(\text{WO}_5)\text{W}_{17}\text{Cu}(\text{H}_2\text{O})\text{O}_{65}]^-$  (color code: the central  $\text{WO}_5$ : pink; the belt square-pyramidal metal atoms (W(4), W(7)/Cu) and their equivalents: purple; rest  $\text{WO}_6$ : blue octahedra), as an example of belt modification.

been reported (Fig. 12).

To summarize this section, WD POMs can be modified in several ways by removing atoms and forming lacunary WD POMs or substituting original atoms by other elements. Additionally, the reported syntheses allowed a better understanding of the formation mechanism of WD POM polyanions and provided new information on the design of new multifunctional materials that exhibit more effective properties (magnetic properties, photocatalytic activity toward  $\text{H}_2$  evolution, electrocatalytic reduction of  $\text{NO}_x$ ) through modification [100,218,220–223].

### 2.3. Non-conventional WD POM motifs

POM nanoclusters can undergo condensation in a variety of different ways, based on which they are classified into the archetypal POMs, including the classic WD system, as discussed above. Below, we report on the so-called non-conventional or non-typical WD systems which bear certain resemblance to the classical WDs but exhibit enough structural integrity and differences that a separate section is needed.

#### 2.3.1. Open WD POMs

Open WD POMs are an example of the non-conventional modification of POM structures. They are formed by the fusion process of two trivacant Keggin-type  $[\alpha\text{-SiW}_9\text{O}_{34}]^{10-}$  polyoxoanion units combined via W-O-W bonds. The most common in the literature are open WDs containing silicon as the heteroatom, characterized by the ease of capturing transition metal ions in the pocket between the two trivacant Keggin units or as an open container for metals [105]. In these modified compounds five metal atoms are commonly introduced which are paramagnets [106–108,227], such as  $\text{Mn}^{\text{II}}$ ,  $\text{Fe}^{\text{III}}$ ,  $\text{Co}^{\text{II}}$ ,  $\text{Ni}^{\text{II}}$ ,  $\text{Cu}^{\text{II}}$ ,  $\text{Zn}^{\text{II}}$ ,  $\text{Al}^{\text{III}}$ ,  $\text{Ho}^{\text{III}}$ ,  $\text{Gd}^{\text{III}}$ ,  $\text{Ga}^{\text{III}}$ , etc., but modifications are known in which their number is two [228,229], three [105], four [230] or rarely more than five [106] (Fig. 13). The first example of an open WD was reported by Laronze et al. in 2003: the pocket contained potassium and two copper ions [228]. After one year, Kortz's group announced the first example of polyoxotungstate with five  $\text{Cu}^{2+}$  ions incorporated into the pocket between two Keggin units [227]. In the following years, papers began to appear with further novel open WD POMs in which the effect of

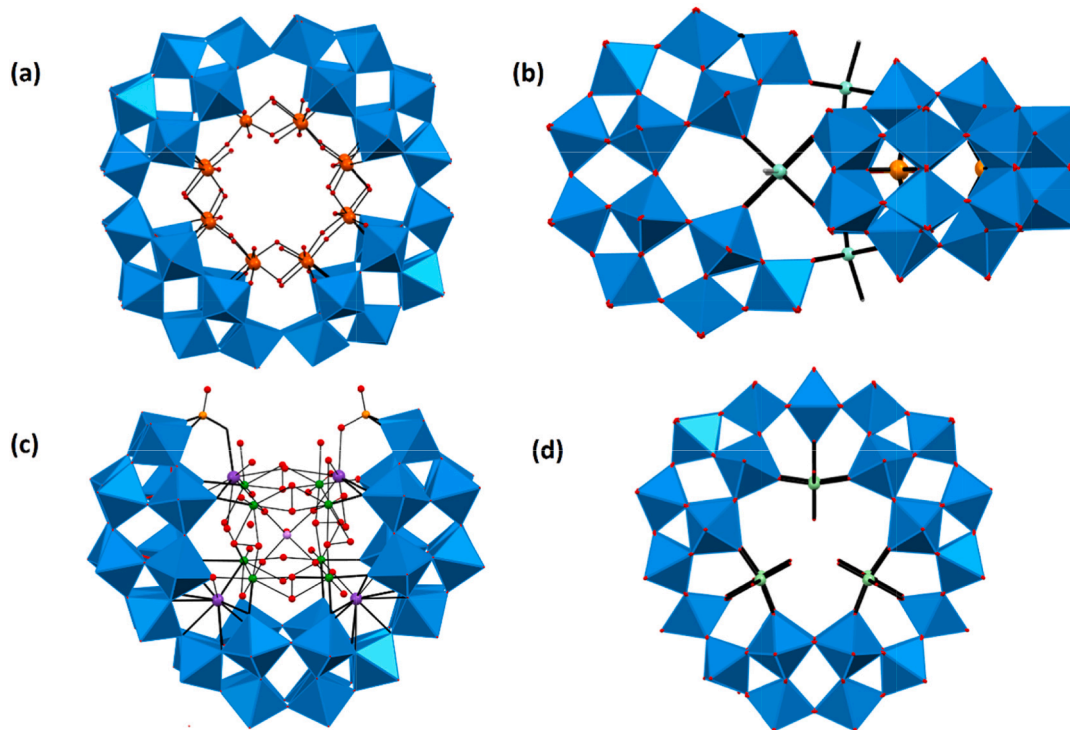


**Fig. 12.** Combined polyhedral/ball-and-stick representation examples of (a) a macrocyclic tetramer of a WD POM  $[\text{P}_8\text{W}_{48}\text{O}_{184}\text{Fe}_{16}(\text{OH})_{28}(\text{H}_2\text{O})_4]^{20-}$ ; (b) dimers  $[\text{P}_4\text{W}_{24}\text{O}_{94}]^{24-}$ ; (c) U-shaped trimers  $[(\text{PO}_3\text{OH})_2\text{P}_6\text{W}_{36}\text{O}_{136}]^{46-}$  and (d) cyclic trimers  $[(\text{H}_2\text{O})_3\text{P}_6\text{W}_{39}\text{O}_{147}]^{30-}$ .



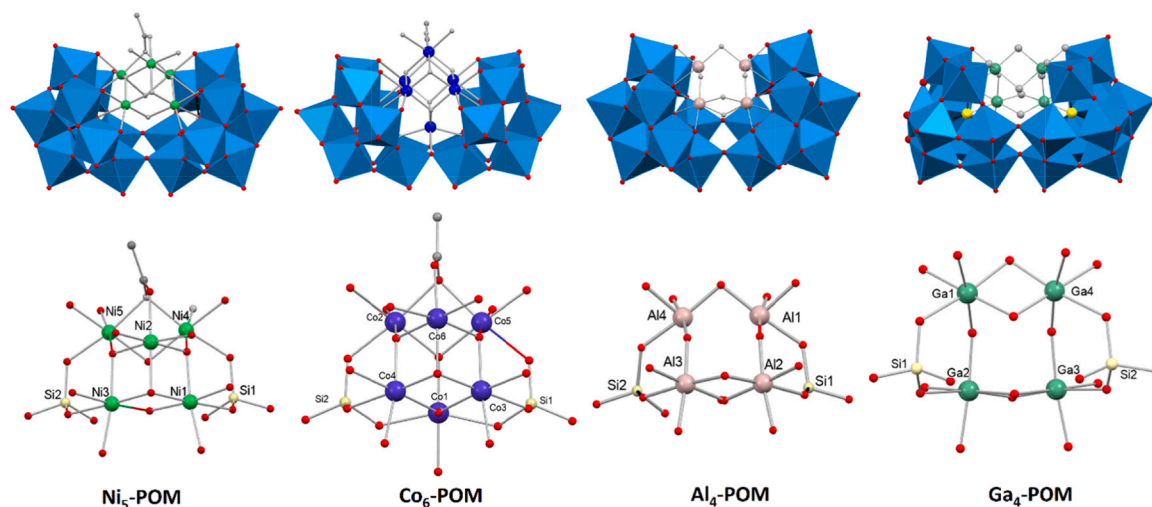


**Fig. 13.** Polyhedral representations and partial structures of the center of metal ions: Ni<sub>5</sub>-POM: Na<sub>2</sub>(C<sub>3</sub>N<sub>2</sub>H<sub>12</sub>)<sub>4</sub>[(Ni<sub>5</sub>(OH)<sub>3</sub>(H<sub>2</sub>O)<sub>4</sub>(CH<sub>3</sub>CO<sub>2</sub>)]-[Si<sub>2</sub>W<sub>18</sub>O<sub>66</sub>]<sup>16-</sup>•12.5H<sub>2</sub>O, Co<sub>6</sub>-POM: (C<sub>3</sub>N<sub>2</sub>H<sub>12</sub>)<sub>3</sub>[(Co<sub>6</sub><sup>III</sup>(OH)<sub>5</sub>(H<sub>2</sub>O)<sub>2</sub>(CH<sub>3</sub>CO<sub>2</sub>)]-[Si<sub>2</sub>W<sub>18</sub>O<sub>66</sub>]<sup>16-</sup>•6H<sub>2</sub>O•(C<sub>3</sub>N<sub>2</sub>H<sub>10</sub>), Al<sub>4</sub>-POM: K<sub>10</sub>[(Al<sub>4</sub>(m-OH)<sub>6</sub>([a,a-Si<sub>2</sub>W<sub>18</sub>O<sub>66</sub>])•28H<sub>2</sub>O and Ga<sub>4</sub>-POM: K<sub>10</sub>[(Ga<sub>4</sub>(OH)<sub>6</sub>([a,a-Si<sub>2</sub>W<sub>18</sub>O<sub>66</sub>])•28H<sub>2</sub>O.

increasing the opening angle of the [Si<sub>2</sub>W<sub>18</sub>O<sub>66</sub>]<sup>16-</sup> open WD skeleton was proved, affecting magnetic properties, and magnetization measurements showed that the multi-metallic core of metal ions in open WD POMs induced strong antiferromagnetic interactions [106,108].

Wang's group reported an interesting example of two open WD POMs: they constructed S-shaped tetrameric germanotungstates with cobalt and nickel in the open pocket in a two-step synthetic procedure shown in Fig. 14. In addition, it is noted that both compounds in the solid state and in aqueous solution had almost identical Raman spectra, confirming the stability of the studied compounds in solution. In addition, the ESI-MS spectra of negative ions and UV spectra showed that both open WD compounds remained stable over a wide range of pH values of 2.7–9.3 and 2.6–9.8, respectively, suggesting their broad applicability [231].

In addition to the incorporation of transition metals into the pocket in the open system of a WD, the introduction of f-block metals has been reported in the literature. In 2011, Patzke's group reported five examples of lanthanoid-containing silicotungstates [Ln<sub>2</sub>(H<sub>2</sub>O)<sub>7</sub>Si<sub>2</sub>W<sub>18</sub>O<sub>66</sub>]<sup>10n-</sup> (Ln = Gd<sup>III</sup>, Tb<sup>III</sup>, Ho<sup>III</sup>) and an example with Dy<sup>III</sup>[Dy<sub>2</sub>(H<sub>2</sub>O)<sub>6.5</sub>(C<sub>2</sub>H<sub>4</sub>O<sub>2</sub>)<sub>0.5</sub>Si<sub>2</sub>W<sub>18</sub>O<sub>66</sub>]<sup>10n-</sup> [145]. The challenge is to obtain open-system WD POMs containing metal ions from the p-block, for instance Al<sup>III</sup> and Ga<sup>III</sup> ions, in their structures, and this was first described in 2016 by Nomiya's group [230]. These are difficult to obtain due to synthetic and structural problems. Arguably, interactions between oxygen atoms in the open WD units and potassium cations in the crystal structures of the Al<sub>4</sub>- and Ga<sub>4</sub>-open structures play a pivotal role in the formation of open WDs with aluminum and gallium ions [230].

### 2.3.2. Sandwich-type WD POMs

Sandwich-type POMs are a large group of transition metal-substituted POMs derivatives (TMSPs) with applications in many areas, e.g. catalysis, biology and materials science [113,167,232–234]. Five principal families of POMs with a sandwich-type arrangement are known, and four of them are derivatives of the trivacant Keggin type polyoxoanion and one is a derivative of the WD structure (Fig. 15). The first group of the four modifications are formed by the combination of two trivacant types: MW<sub>9</sub>O<sub>34</sub><sup>3-</sup> or MW<sub>9</sub>O<sub>33</sub><sup>3-</sup> (M = Fe<sup>III</sup>, Cu<sup>II</sup>, Co<sup>II</sup>, Zn<sup>II</sup>, P<sup>V</sup>, As<sup>III</sup>, As<sup>V</sup>, Si<sup>IV</sup>, Sb<sup>III</sup>, Bi<sup>III</sup>, Se<sup>IV</sup> or Te<sup>IV</sup>), while the fifth modification consists of two encapsulated units of trivacant α-X<sub>2</sub>W<sub>15</sub>O<sub>56</sub><sup>12-</sup> (X = As<sup>V</sup> or P<sup>V</sup>) with potential incorporation of transition-metal cations between two subunits (M = Mn<sup>II</sup>, Fe<sup>III</sup>, Co<sup>II</sup>, Ni<sup>II</sup>, Cu<sup>II</sup>, Zn<sup>II</sup>, and Cd<sup>II</sup>), forming compounds of the formula [M<sub>4</sub>(H<sub>2</sub>O)<sub>2</sub>(P<sub>2</sub>W<sub>15</sub>O<sub>56</sub>)<sub>2</sub>]<sup>n-</sup>. The latter are among the most thoroughly described systems by virtue of easy <sup>31</sup>P NMR analysis [232,235–238].

In 1983, Finke and Droege reported the first example of a sandwich-type POM with the formula P<sub>4</sub>W<sub>30</sub>M<sub>4</sub>(H<sub>2</sub>O)<sub>2</sub>O<sub>112</sub><sup>16-</sup> (M = Co<sup>II</sup>, Cu<sup>II</sup>, Zn<sup>II</sup>) [239] which resulted in a rapidly developing group of non-conventional POMs owing to their catalytic and physicochemical properties that are attracting increased interest [235]. The presence of subunits in the form of a tetranuclear cluster [M<sub>4</sub>O<sub>14</sub>(OH)<sub>2</sub>] where water molecules are attached to the center of the cluster improves the effectiveness of the compounds in applications in electrochemistry, catalysis and materials science [113,117,236,240]. Ruhlmann et al. reported sandwich-type WD POMs with a tetranuclear cluster with Co<sup>II</sup> forming complex ββ-[Co<sub>4</sub>(H<sub>2</sub>O)<sub>2</sub>(P<sub>2</sub>W<sub>15</sub>O<sub>56</sub>)<sub>2</sub>]<sup>16-</sup> at low pH (pH~3) for which isomers

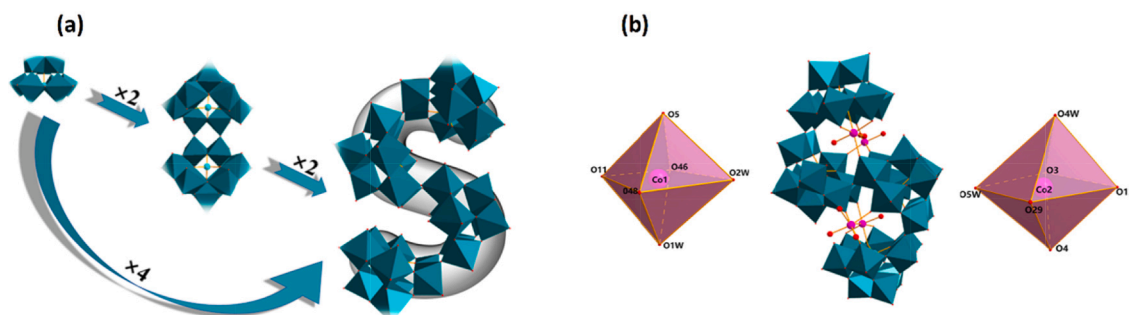


**Fig. 14.** Scheme of S-shaped tetrameric germanotungstates (a) and polyhedral/ball-and-stick scheme of the K<sub>10</sub>H<sub>10</sub>[[Co-(H<sub>2</sub>O)<sub>2</sub>]<sub>2</sub>[Co(H<sub>2</sub>O)<sub>3</sub>]<sub>2</sub>(Ge<sub>4</sub>W<sub>36</sub>O<sub>130</sub>)]•32H<sub>2</sub>O polyanion (b). Reproduced from [231] with permission of the copyright holders.



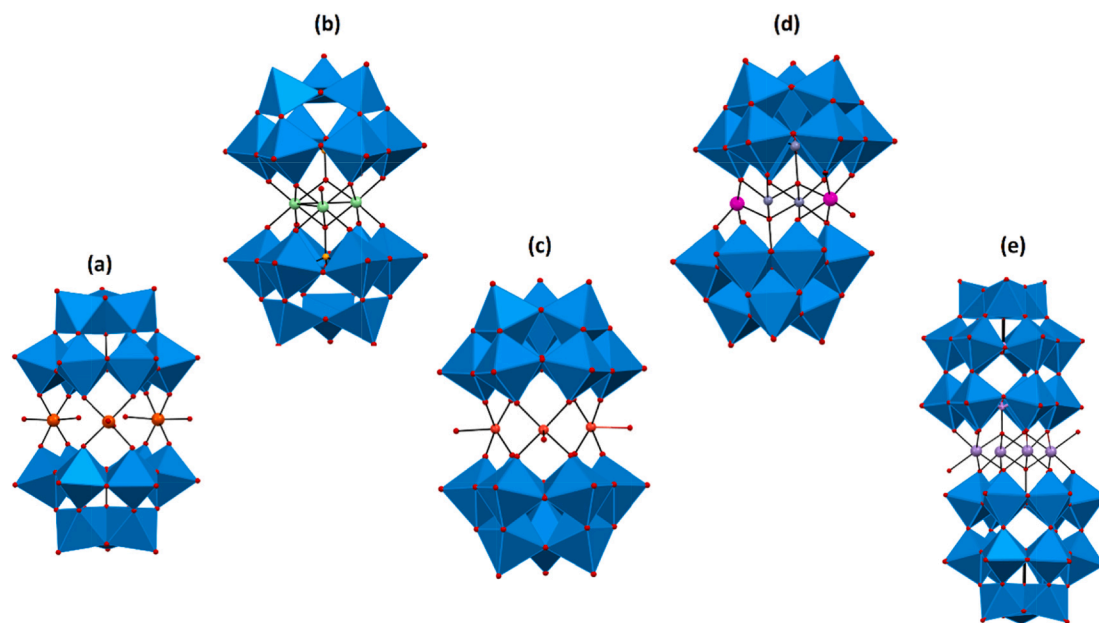


**Fig. 15.** Polyhedral representations of the five principal families of POMs with the sandwich-type arrangement: conventional A-type Keggin sandwich; conventional B-type Keggin sandwich; B-type Keggin sandwich with pyramidal heteroatoms; Tourné B-type Keggin sandwich (transition metal heteroatoms); WD sandwich.

based on  $\alpha$ -[P<sub>2</sub>W<sub>15</sub>O<sub>56</sub>]<sup>12-</sup> units and relationships between them are presented in Fig. 16. The type of connectivity ( $\beta\beta$ ,  $\alpha\beta$  or  $\alpha\alpha$ ) depends on synthesis conditions (pH, concentration, ratio of TM to trivalent moieties), and the number and nature of transition metal ions in the central

sheet. Moreover, in connection with the lability of Na<sup>+</sup> (due to sodium salts in aqueous solution) and their weak binding to the POM unit Co<sub>4</sub>(P<sub>2</sub>W<sub>15</sub>)<sub>2</sub> (blue frame), monovacant NaCo<sub>3</sub>(P<sub>2</sub>W<sub>15</sub>)<sub>2</sub> (violet frame) and divacant Na<sub>2</sub>Co<sub>2</sub>(P<sub>2</sub>W<sub>15</sub>)<sub>2</sub> (yellow frame) lacunary species can be

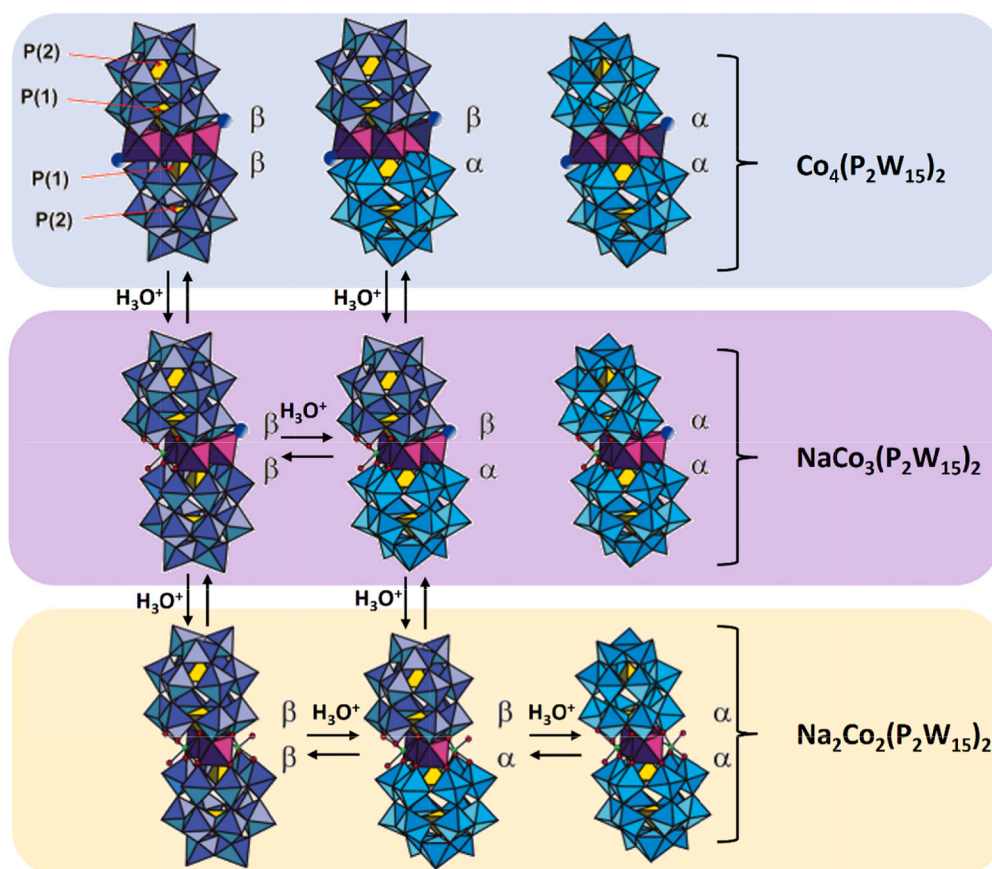


**Fig. 16.** Relationships between isomers of different sandwich-type WD POMs with cobalt-based  $\alpha$ -[P<sub>2</sub>W<sub>15</sub>O<sub>56</sub>]<sup>12-</sup> subunits. Reproduced from [235] with permission of the copyright holders.

distinguished. The interconversion between the isomers is strongly influenced by the pH value, which has been investigated using  $^{31}\text{P}$  NMR, UV–Vis spectroscopy and electrochemistry. In a medium at pH of more than 3.5,  $\alpha\beta\text{-Co}_4(\text{P}_2\text{W}_{15}\text{O}_{56})_2$ ,  $\beta\beta\text{-Co}_4(\text{P}_2\text{W}_{15}\text{O}_{56})_2$  and  $\alpha\beta\text{-NaCo}_3(\text{P}_2\text{W}_{15})_2$  are stable but, interestingly, the  $\text{Na}_2\text{Co}_2(\text{P}_2\text{W}_{15})_2$  they obtained underwent isomerization. On the other hand, isomerization of  $\alpha\beta\text{-Co}_4(\text{P}_2\text{W}_{15}\text{O}_{56})_2$  via  $\alpha\beta\text{-NaCo}_3(\text{P}_2\text{W}_{15})_2$  to  $\beta\beta\text{-Co}_4(\text{P}_2\text{W}_{15}\text{O}_{56})_2$  was observed in lower pH in a range from 2.5 to 3.5.

It is noted that complexes based on electrostatic interactions between zinc tetracationic porphyrin  $[\text{ZnTMePyP}]^{4+}$  and the aforementioned sandwich-type WD  $[\text{M}_4(\text{H}_2\text{O})_2(\text{P}_2\text{W}_{15}\text{O}_{56})_2]^{n-}$  containing four transition metal ions are known [241–243]. Shaming et al. reported films formed via the layer-by-layer method between different porphyrins,  $[\text{ZnTMePyP}]^{4+}$  or  $[\text{ZnOEP}(\text{py})_4]^{4+}$ , and tetracobalt WD sandwich POMs with the formula  $\alpha\beta\beta\alpha\text{-}[\text{Co}_4(\text{H}_2\text{O})_2(\text{P}_2\text{W}_{15}\text{O}_{56})_2]^{16-}$  useful in photocatalysis [242].

### 3. Solution and pH speciation in solution

In aqueous solution, numerous and highly negative-charged species are most frequently formed, hence the determination of dominant POM species is difficult. Therefore, individual speciation profiles need to be investigated in applications in a specific solution [244,245] (Fig. 17).

Stability studies by Contant and Thouvenot show that only the  $\alpha$ -isomer of a WD POM is stable in aqueous solution and all the other isomers undergo transformation to the  $\alpha$ -isomer in the order of  $\gamma \rightarrow \beta \rightarrow \alpha$  [159]. In addition, the rate of WD POM hydrolysis is also dependent on the counterions and follows the trend of  $\text{K}^+ > \text{Na}^+ > \text{Li}^+$  [244].

The common structure of WD POMs with the general formula  $[\text{P}_2\text{W}_{18}\text{O}_{62}]^{6-}$  is stable in acidic media at pH lower than 6 and it degrades at higher pH forming three different species such as mono-lacunary  $[\text{P}_2\text{W}_{17}\text{O}_{61}]^{10-}$ , tri-lacunary  $[\text{P}_2\text{W}_{15}\text{O}_{56}]^{12-}$  and hexa-lacunary  $[\text{H}_2\text{P}_2\text{W}_{12}\text{O}_{48}]^{12-}$  WDs [244,246]. The aforementioned studies from 1985 were also confirmed in the other paper in which Mbomekalle

et al. reported that within the POM of the WD family, compounds with the formula  $[\text{X}_2\text{W}_{18}\text{O}_{62}]^{6-}$  ( $\text{X} = \text{P}^{\text{V}}$  or  $\text{As}^{\text{V}}$ ) in acidic media were stable but monolacunary WD POMs with the formula  $[\text{X}_2\text{MW}_{17}\text{O}_{61}]^{n-}$  ( $\text{X} = \text{P}^{\text{V}}$  or  $\text{As}^{\text{V}}$ ) were more stable in higher pH [232]. Moreover, the pH value also affects the formation of functionalized structures and is associated with partial or complete transformation from trivacant  $\text{P}_2\text{W}_{15}$  with the formula  $\alpha\text{-}[\text{P}_2\text{W}_{15}\text{O}_{56}]^{12-}$  into rarely occurring divacant  $\text{P}_2\text{W}_{16}$  with the formula  $\alpha\text{-}[\text{P}_2\text{W}_{16}\text{O}_{57}]^{8-}$  [247,248] (Fig. 18a). Interestingly, formed by hexa-lacunary species, the macrocyclic tetramer of  $[\text{P}_8\text{W}_{48}\text{O}_{184}]^{40-}$  is stable at lower pH at a range from 1 to 8 [244,246]. The mutual transformations of the different forms of WDs depending on the environment are shown in Fig. 18b.

Moreover, as can be seen in Fig. 19, WD formation depends on the  $[\text{Mo}]/[\text{P}]$  ratio and slows down as the  $[\text{Mo}]$  to  $[\text{P}]$  ratio increases. In addition, in an acidic environment, comparing solutions immediately after preparation (“fresh”) with solutions after up to one month (“aged”), it can be seen that in “fresh” solutions, only the Keggin POM polyanion with the formula  $[\text{P}^{\text{V}}\text{Mo}_{12}\text{O}_{40}]^{3-}$  is found, and no polyanion of the WD type is observed, but after some time in the “aged” solution, both in the case of the  $[\text{Mo}]/[\text{P}]$  ratio = 9 and  $[\text{Mo}]/[\text{P}] = 12$ , a polyanion of the formula  $[\text{P}_2^{\text{V}}\text{Mo}_{18}\text{O}_{62}]^{6-}$  is formed. In addition, for observable anions formed in a pH range of from 6 to 8, a relationship can be seen, arising from the balance of anions  $[\text{HP}^{\text{V}}\text{O}_4]^{2-}$  and  $[\text{P}^{\text{V}}\text{O}_4]^{3-}$  whose occurrence is independent of the  $[\text{Mo}]/[\text{P}]$  ratio and of whether the solution is “fresh” or “aged” [249,250].

### 4. Ionic interactions with counter-cations

Crucial for the self-assembly, solubility, stabilization and function of POMs are the mutual interactions between anionic POMs and organic or inorganic cations [8,251]. Therefore, papers have been published that show the effect of the type of cation and solvent on self-assembly and, consequently, on applications. Given the effect of cations and solvent on the structure in Anderson-Evans POMs [252], it is expected that it is

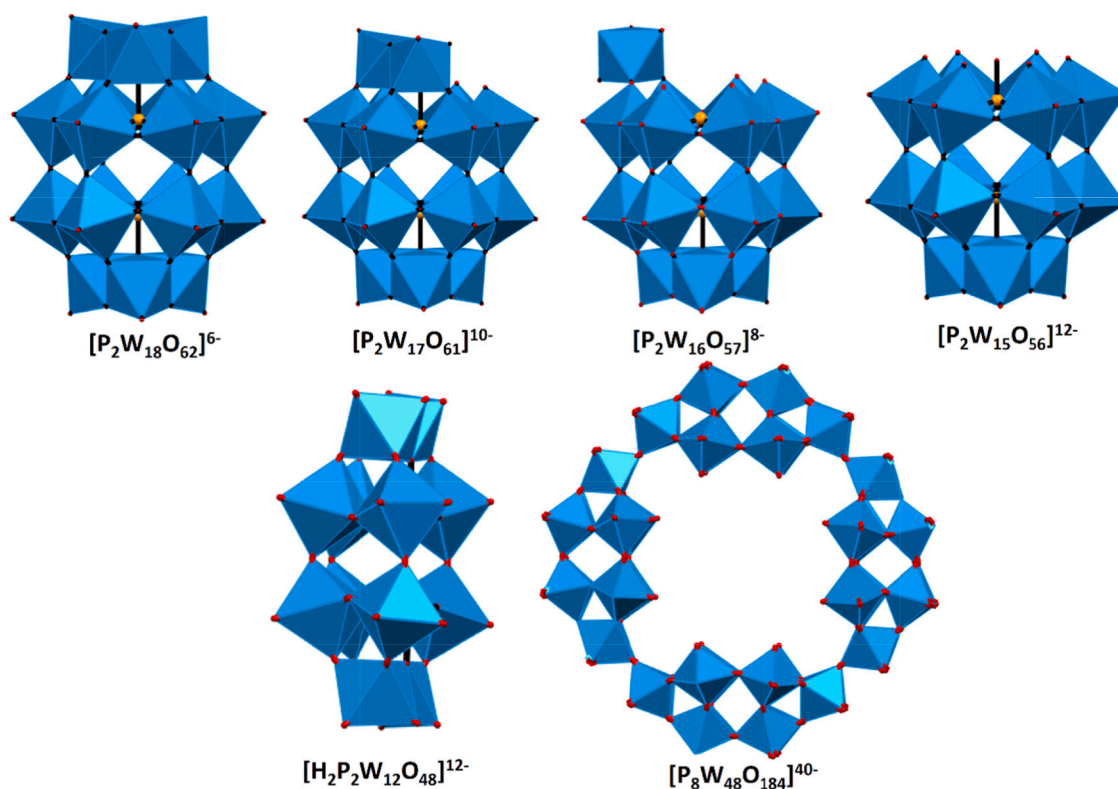


**Fig. 17.** Polyhedral representation of the classical structure of the  $[\text{P}_2\text{W}_{18}\text{O}_{62}]^{6-}$  WD POM and its species such as mono-lacunary  $[\text{P}_2\text{W}_{17}\text{O}_{61}]^{10-}$ , di-lacunary  $[\text{P}_2\text{W}_{16}\text{O}_{57}]^{8-}$ , tri-lacunary  $[\text{P}_2\text{W}_{15}\text{O}_{56}]^{12-}$ , hexa-lacunary  $[\text{H}_2\text{P}_2\text{W}_{12}\text{O}_{48}]^{12-}$  and the macrocyclic tetramer of  $[\text{P}_8\text{W}_{48}\text{O}_{184}]^{40-}$ .

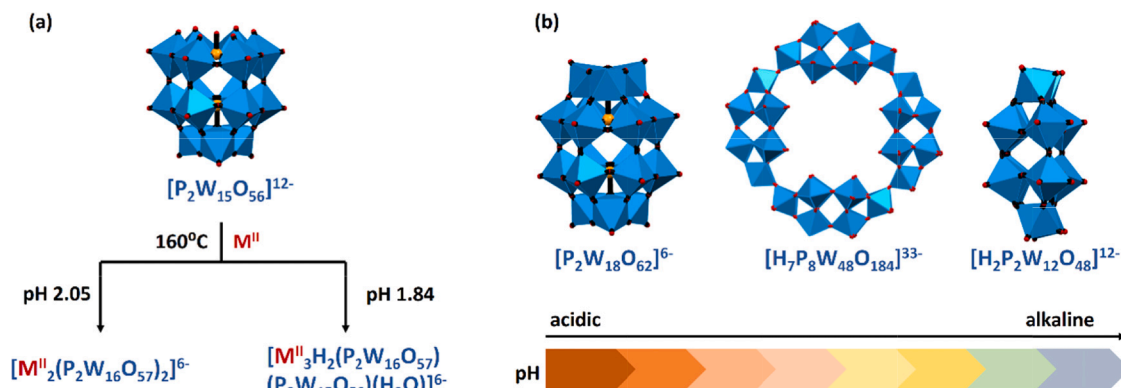


Fig. 18. Scheme of (a) in situ transformation of the trivacant to the divacant form of WD POMs ( $M^{II}$  – transition metal ion); (b) hydrolytic transformation of  $[P_2W_{18}O_{62}]^{6-}$  with an increasing pH value.

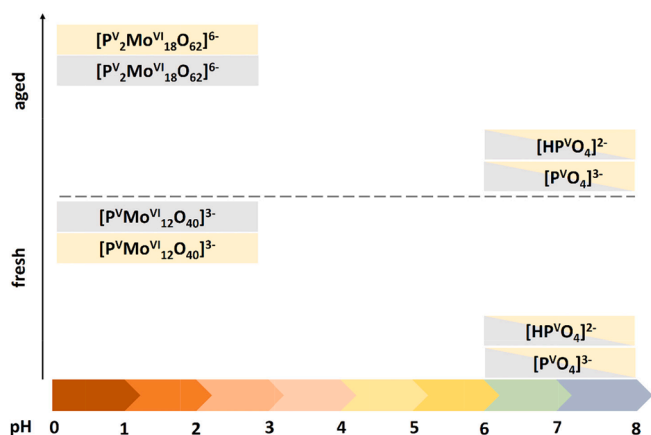


Fig. 19. Scheme of the speciation of selected phosphomolybdates ( $[P^V_2Mo^{VI}_{18}O_{62}]^{6-}$ ,  $[P^V_2Mo^{VI}_{12}O_{40}]^{3-}$ ,  $[HP^VO_4]^{2-}$  and  $[P^VO_4]^{3-}$ ) in fresh prepared and aged (up to 1 month) aqueous solution with a ratio of  $[Mo]/[P] = 9$  (gray filling) and  $[Mo]/[P] = 12$  (yellow filling) in specific pH ranges corresponding to the width of the filling.

similar for WD POMs, but to the best of our knowledge, this requires further research to be confirmed. The self-assembly process of poly-anionic POMs can result from their association with the long chains of alkyl-constituting hydrophobic tails. In the literature the amphiphilic feature of POM hybrids is discussed, which may affect the formation of

surfactant-encapsulated POMs (SEPs) [9,21]. To the best of our knowledge, WD POMs can form only one type of the molecular structure of amphiphilic POMs, such as classical 'head-tail'-type surfactants (Fig. 20a). Various amphiphilic structures of hybrid-POMs can be distinguished depending on the shape and packing parameter of the surfactant, such as micelles, vesicles and bilayers which can be observed using microscopy analyses, for instance STM, TEM, etc. (Fig. 20b) [9].

## 5. Post-functionalization approaches as a means to forming hybrid WD POM assemblies

Hybrid POM platforms, also known as hybrid POM scaffolds, are compounds that consist of reactive organic groups or sites of ligand-like species combined with POMs via covalent, ionic, hydrogen and coordination bonds, etc. [2,3,94,253–256]. In addition, these systems can be used as building blocks in further functionalization aimed to obtain discrete or network materials. The possibility of forming such modified compounds prompted a lot of research groups to develop hybrid POM materials using subsequent organic groups, such as amide, sulfonamide, ester, and thioester groups, and based on organic reactions (Huisgen, Sonogashira, Suzuki coupling, polymerization, metal coordination, etc.) [2] (Fig. 21, Table 2). In essence, two main groups of WD POM functionalization can be distinguished: the first group based on single-linker modularity and the other one based on double-linker modularity, each of which divided into several subgroups.

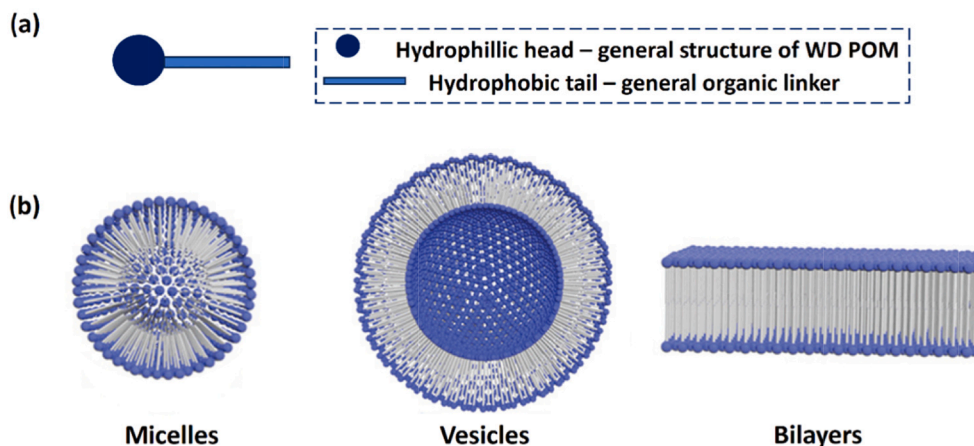
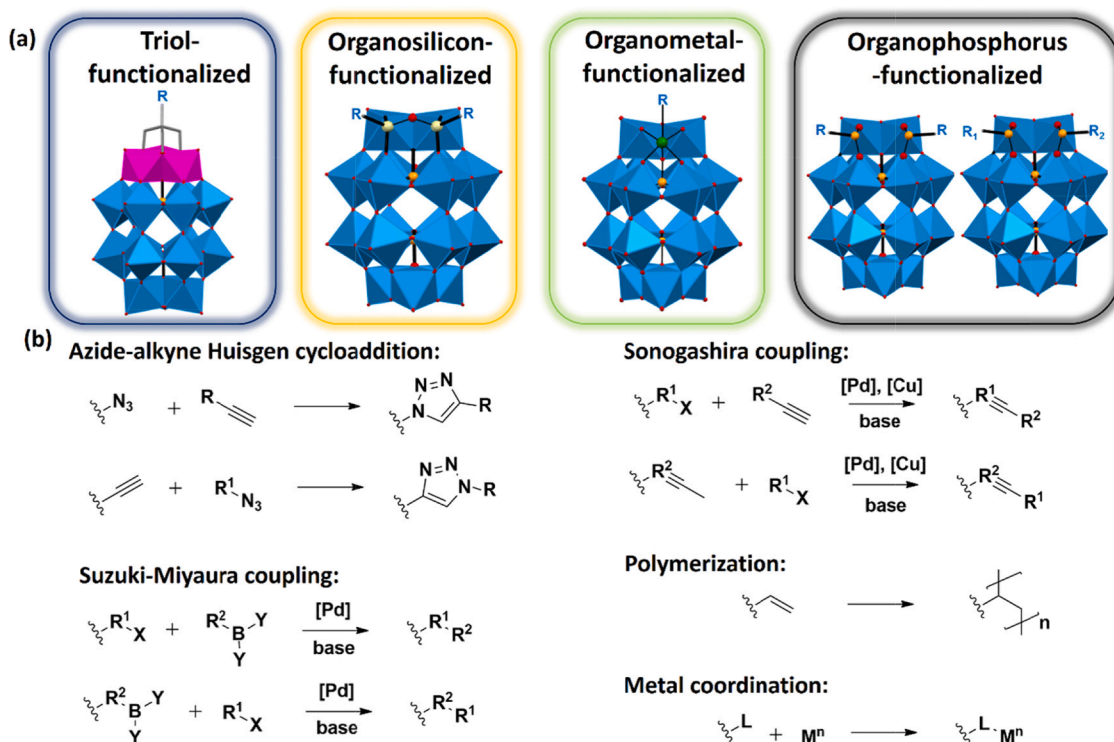


Fig. 20. (a) Scheme of a representative example of the classical 'head-tails' type of WD surfactant. (b) Representative examples of various types of the amphiphilic POM structure: micelles, vesicles and bilayers. Partially reproduced from [9] with permission of the copyright holders.





**Fig. 21.** (a) Selected most commonly studied hybrid WD platforms and functionalization strategies. (b) Typical post-functionalization reactions based on WD POM subunits, where R, R<sup>1</sup>, R<sup>2</sup> = organic moieties; X = halogen; BY<sub>2</sub> = organoborane; L = ligand; M<sup>n</sup> = metal ion.

### 5.1. Single-linker modularity

The first main group of WD POM functionalization (single modification) constitutes a vast group leading to diverse structural hybrid materials with interesting applications. The incorporation of organic moieties into POM backbones ensures facile structural modifications aimed at obtaining anticipated compounds with specific properties [17,174,254–256,258] (Fig. 22).

#### 5.1.1. Trilacunary WD POMs

POMs with organic groups introduced into the cap site are more frequently reported, especially WD tri-vanadium substituted POMs (V<sub>3</sub>POM) due to the easy modulation of structure, stable WD POM scaffolds for the incorporation of redox-active vanadium centers and expanded properties [174,275]. It is noted that the presence of the V<sub>3</sub> substituent improves oxidative properties, thus providing more opportunities in biological [254] and catalytic applications [174]. The major way to this functionalization is the generation of a M–O–C bond connecting the WD POM and an organic group from the second substrate [102]. In 1993 Hill and Hou reported the first alkoxy-POMs obtained through functionalized POMs via the tris(hydroxymethyl) group [276]. Owing to the functionalization of the cap site via tris-alcohol organic derivatives these compounds can be used as building blocks leading to the formation of hybrids via covalent functionalization [173,177,181,254,255,258]. Since the pioneering publication, many papers have been published on using this modification method, and after 16 years, a paper reporting on the modification of the previously developed method appeared in 2009. The new procedure made it possible to insert an organic compound with two hydroxyl groups and an amide group. This work paved the way for new modifications by substituting the POM with carbonyl oxygen from the amide group, making it possible to communicate electron effects between the organic group and the inorganic unit (POM) [175] (Fig. 23). Since 2009, a large number of approaches that use this functionalization to obtain particular hybrids can be found in published works. Dridi et al. reported a series of

novel POMs modified with spironaphthoxazine and spiropyran derivatives [176]. Riffade et al. showed an example of a tri-substituted WD POM modified with picolinamide-diols and formation of a pincer complex using palladium as the catalyst for Mizoroki-Heck coupling [178]. It is noted that not only the amide group is inserted to the POM structure but also different organic groups with carbonyl moieties are used, such as carbamates, thiocarbamates, ureas etc. [174]. Vilona et al. reported several functionalized WD POMs with inserted urea groups and they proved that carbonyl incorporation to WD building blocks caused activation of the urea toward H-bond catalysis [277]. It is noted that Santoni et al. used WD species substituted by the dipyrindyl group for complexation with Re<sup>I</sup> that resulted in the formation of a covalently bond hybrid material [180].

Grafting linear ligands, such as bis(TRIS), tris(TRIS) etc., onto V<sub>3</sub>-capped WD POM leads to the formation of a separate class of hybrids. These materials consist of two or more [P<sub>2</sub>V<sub>3</sub>W<sub>15</sub>O<sub>62</sub>]<sup>9-</sup> units and depending on the amount of subunits known as dumb-bells (two units), triangular (three units) (Fig. 24) and higher species can be obtained which are the most frequently reported by Hill, Hasenknopf and Cronin groups and the main reason for the interest in this class of hybrids is their amphiphilic properties [18,171,278].

An example of the dumbbell modification linked by the bipyridine subunit has been reported by Cronin's research group; they reported a bipyridine-based dumbbell WD hybrid coordinating Zn<sup>2+</sup>. Interestingly, they proved formation of a *trans*-dumbbell WD species and transformation to the *cis* form of the hybrid in DMSO solution upon the coordination of Zn<sup>2+</sup> ions, which returned to the original form after adding EDTA which removed Zn<sup>2+</sup> ions. The authors suggested that this transformation could be further used to manipulate its self-assembly behavior, which arguably mimicked the behavior of protein folding and assembly under the guidance of metal ions [279] (Fig. 25).

#### 5.1.2. Monolacunary WD POMs

A single modification of the WD POM structure includes functionalization by organic groups connected not only with the trilacunary but

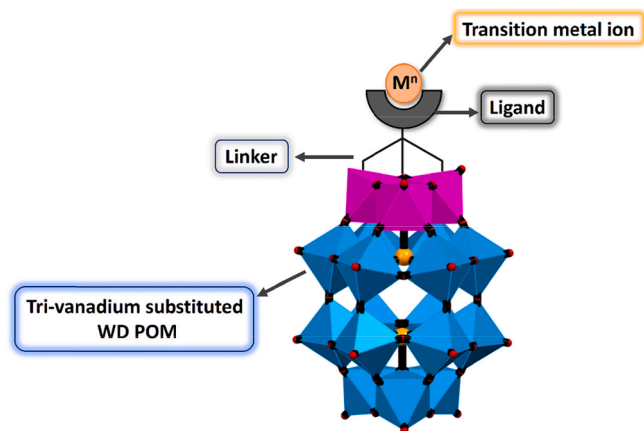


**Table 2**

Representation of functionalized WD hybrids with organic functional groups or metal centers.

General formula of the modularity	General formula of the compound	Ref.
$[P_2W_{15}V_3O_{59}((OCH_2)_3CNH-CO-R)]$	$[P_2W_{15}V_3O_{59}(OCH_2)_3C_{11}H_9N_4O]^{6-}$ $[P_2V_3W_{15}O_{59}(OCH_2)_3CNHCOC_{15}H_{31}]^{6-}$ [COHNC $(CH_2O)_3P_2V_3W_{15}O_{59}(C_4H_9N_4)]^{6-}$ $TBA_{10}H_2[(P_2V_3W_{15}O_{59}(OCH_2)_3CNHCO)_2]$ $TBA_5H[P_2W_{15}V_3O_{62}(C_{20}H_{17}N_4O)]$ $TBA_4H_2[C_{12}H_9O_4NHC(CH_2O)_3P_2W_{15}V_3O_{59}]$ $TBA_5H[C_{16}H_{16}N_3O_6P_2V_3W_{15}]$ $TBA_5H[C_{19}H_{16}N_3BrO_6P_2ReV_3W_{15}]$ $TBA_5H[P_2V_3W_{15}O_{59}((OCH_2)_3CNHCO(CH_3)C=CH_2)]$ $TBA_5H[P_2V_3W_{15}O_{66}C_{19}H_{16}N_3ReBr]$	[102,173,257,171,258,177,180,180,181,259]
$[P_2W_{15}V_3O_{59}((OCH_2)_3C-R)]$	$TBA_{10}H_2[(P_2V_3W_{15}O_{59}(OCH_2)_3CCH_2)_2O]$ $TBA_{10}H_2[C_7H_{14}O_4C(CH_2O)_3P_2V_3W_{15}O_{59}]$ $TBA_5H_2[C_2H_4OC(CH_2O)_3P_2V_3W_{15}O_{59}]$ $TBA_5[HP_2V_3W_{15}O_{59}((OCH_2)_3CCH_2OCH_2C_6H_4)]$	[171,98,98,260]
$[P_2W_{15}V_3-SP]$	$TBA_5[(P_2V_3W_{15}O_{59}(OCH_2)_2C(Et)-NHCO(C_{20}H_{19}N_2O_3))]$	[176]
$[P_2W_{15}V_3O_{59}((OCH_2)_2(R)-CNH-C(=)-R^*)]$	$TBA_{5.95}H_{0.05}[C_{22}H_{21}N_3O_{62}P_2V_3W_{15}]$ $TBA_5[P_2V_3W_{15}O_{59}((OCH_2)_2C(Et)NHC(=O@POM)R)]$	[261,262]
$[P_2W_{17}O_{61}(Sn-R)]$	$[P_2W_{17}O_{61}SnCH_2CH_2C(=O)]^{6-}$ $[P_2W_{17}O_{61}SnCH_2CH_2C(=O)NHCH_2-poly(N,N-diethylacrylamide)]^{7-}$ $TBA_7[P_2W_{17}O_{61}(Sn(CH_2)_2C(O)NH(CH_2)_3(N_3C_2H)CH_2OC(O)C(CH_3)_2SC(S)SC_{12}H_{25})]$ $TBA_7[\alpha_1-P_2W_{17}O_{61}(Sn(CH_2)_2C(O)NH(CH_2)_3N_3)]$ $TBA_7[\alpha_2-P_2W_{17}O_{61}SnCH_2CH_2CON(CH_2)_5]$ $[P_2W_{17}O_{61}(SnCH_2CH_2COOH)]^{7-}$	[17,263,264,264,265,266]
$[P_2W_{16}O_{59}(Zr-R)]$	$Na_{14}[Zr_4(P_2W_{16}O_{59})_2(\mu_3-O)_2(OH)_2(H_2O)_4] \cdot 57H_2O$	[267]
$[P_2W_{17}O_{61}(O(Si-R)_2)]$	$[P_2W_{17}O_{61}(PhSi)_2O]^{6-}$ $[P_2W_{17}O_{61}(O(Si-C_{29}H_{18}N_3)_2)]^{6-}$ $TBA_6[\alpha_2-P_2W_{17}O_{61}(SiC_6H_4CH_2N_3)_2O]$ $TBA_6[P_2W_{17}O_{62}(Si-PhI)_2O]$ $TBA_6[P_2W_{17}O_{61}(Si-Ph-ethynyl-TMS)_2O]$ $TBA_6[P_2W_{17}O_{61}(Si-Ph-ethynylpyrene)_2O]$ $TBA_6[P_2W_{17}O_{61}(Si-Ph-acetylene)_2O]$ $TBA_6[P_2W_{17}O_{61}(SiC_3H_6-I)_2O]$	[268,19,269,270,270,270,270,271]
$[P_2W_{17}O_{61}(P(O)-R)_2]$	$TBA_6[\alpha_2-P_2W_{17}O_{61}(P(O)CH_2CH_2N_3)_2]$ $K_6[P_2W_{17}O_{57}(PO_3H_5C_7)_2] \cdot 6C_4H_9NO$ $K_7(C_2H_8N)_3[Fe(P_2W_{17}O_{57}(PO_3C_{21}H_{14}N_3)(PO_4C_{24}H_{41}))_2]$ $K_4(C_2H_8N)_2[P_2W_{17}O_{61}(P(O)C_{21}H_{14}N_3)(P(O)OC_{24}H_{41})]$ $H_6[P_2W_{17}O_{57}(H_2C_7C_{17}O_4PS)_2] \cdot 3C_4H_9NO$	[269,44,272,273,274]

SP: spiropyran group; TMS: tetramethylsilane.

**Fig. 22.** Scheme of a functionalized tri-vanadium WD POM via an organic ligand capable of coordinating the transition metal ion.

also with the monolacunary site of a WD POM, such as organotin, organosilicon, organophosphorus, etc. functionalization (see Fig. 21a) [9,254,255].

Mayer et al. reported in 2004 the first example of two monolacunary WD POMs with an Si-O-Si anchorage which was confirmed by  $^{29}Si$  NMR studies [268]. Izzet et al. showed the a covalently bond POM-hybrid can consist of two terpyridine subunits connected with  $\alpha_2$ - $[P_2W_{17}O_{61}]^{10-}$  via the Si-O-Si anchorage. This system leads to discrete metallomacrocycles through the self-assembly process with metal ions [19,280]. It is also

noted that an organosilicon WD hybrid covalently bonded with an iridium complex having photophysical properties [281]. In the same paper, Matt et al. reported an example of an organotin hybrid WD species covalently grafted to an iridium(III) complex [281]. Monolacunary tin-substituted WD species form a comprehensive group of functionalized hybrids. The first example of organotin hybrids was reported in 1979 [282] and a number of papers related to this type of functionalization have been published since then [17,263–266]. Boglio et al. reported an example of a tin-substituted WD POM in the cap and belt position that formed two isomers:  $\alpha_2$ - $[P_2W_{17}O_{61}(SnCH_2CH_2COOH)]^{7-}$  (mono-substituted in the cap position) and  $\alpha_1$ - $[P_2W_{17}O_{61}(SnCH_2CH_2COOH)]^{7-}$  mono-substituted in the belt position). The tin-substituted WD hybrids obtained by their research group were subsequently used in a regioselective acylation reaction owing to the nucleophilic character of the W-O-Sn bond and acyl-hybrids were isolated and proved experimentally and computationally [266] (Fig. 26).

Unlike the organotin hybrids, organophosphorus WD hybrids occur very rarely. This type of functionalization is characterized by the presence of two organophosphorus moieties that fill the single vacancy, aligned parallel to the mirror plane, and by the lack of P-O-P anchoring with features that set the organophosphorus hybrids apart from both the organotin and organosilicon species [255]. Even though rare, organophosphorus hybrids are characterized by rich redox chemistry combined with strong electron conjugation between the units and, therefore, they are mainly studied for their electronic properties. In 2008, Boujtita et al. performed the first electrochemical study on a hybrid with a phosphonate moiety with the general formula  $TBA_6[P_2W_{17}O_{61}(POC_6H_5)_2]$ . They proved a reversible redox process involving the organophosphorus hybrid in acetonitrile as solvent [283]. Kastner et al. reported an

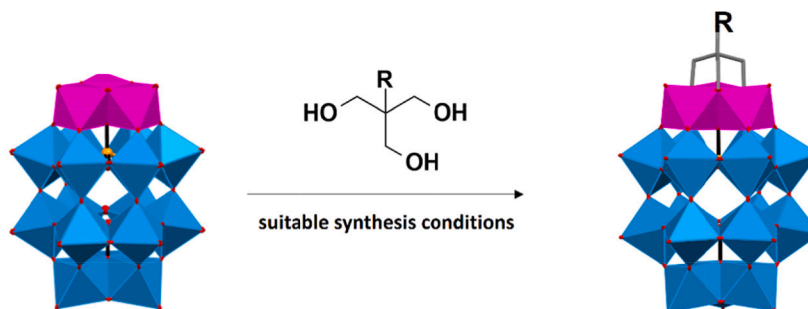
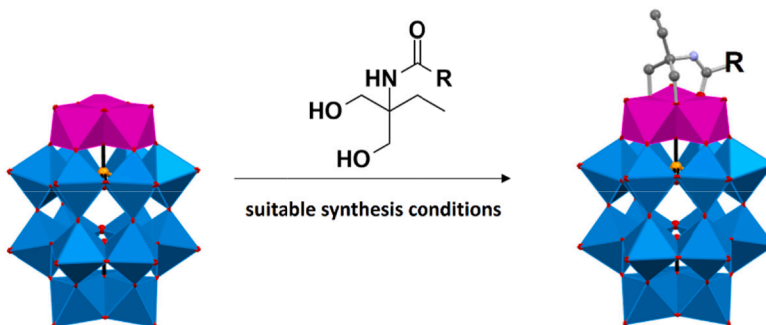
**1993: Functionalization of the cap site *via* tris-alcohol organic derivatives****2009: Functionalization of the cap site *via* with two hydroxyl groups and an amide group**

Fig. 23. Comparison of functionalization methods between the pioneering modification of 1993 and the new modification procedure published in 2009.

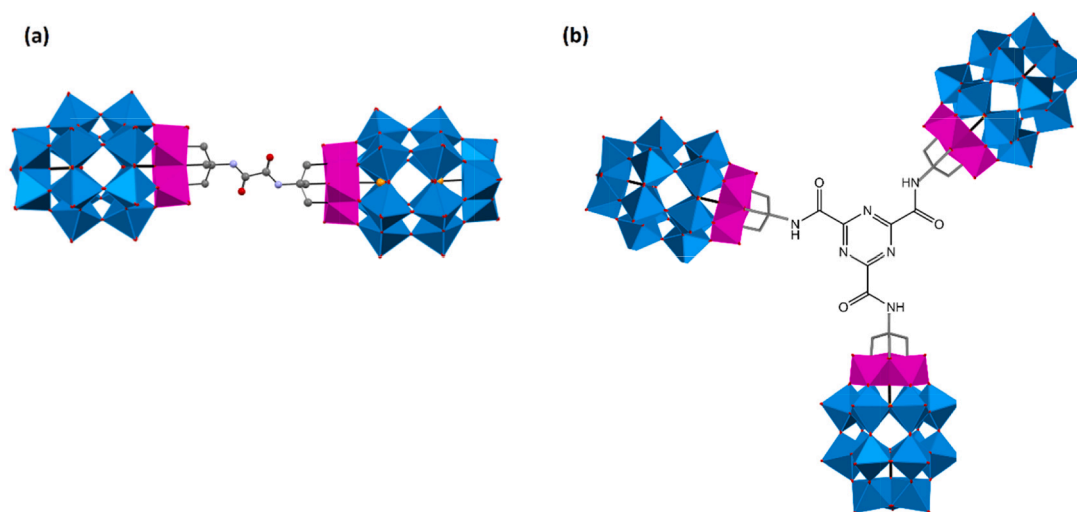


Fig. 24. Scheme of an example of (a) dumbbell (two units) and (b) triangular (three units) species.

example of a redox-active WD POM surfactant consisting of thiol chains which was grafted to a WD structure by phosphonate linkers to form supramolecular aggregates, and this resulted in changes in the redox chemistry of the WD species. In water as solvent, the novel hybrid surfactant formed regular micellar assemblies but the effect of the DMF solvent caused the aggregation to break down to the monomeric form which proved reversible redox chemistry for the aggregates. This transition of the monomeric to the supramolecular form and the accompanying change in physical properties offers opportunities for applications in photocatalysis, catalysis and advanced switchable materials [274].

It is noted that in the case of the formation of hybrid materials by a single linker to the monolacunary site of a POM, there have also been cases of POM-polymer formation as for the modifications discussed above (see Section 5.3 for more information).

### 5.1.3. Various mixed types of POMs

In addition, an interesting example of functionalization reported in 2022 by the group of Tatjana N. Parac-Vogt concerned the combination of subunits of different POM types functionalized with dipentaerythritol ( $R = (OCH_2)_3CCH_2OCH_2C(CH_2OH)_3$ ) and the formation of four heterometallic hybrids of the general formula  $(POM_2-R-POM_1-R-POM_2)$  that combined Lindqvist  $[V_6]$  and Anderson-Evans  $[XMo_6]$  ( $X = Cr, Al$ ) structures and tri-substituted  $[P_2V_3W_{15}]$  WD POM structures [90] (Fig. 27).

### 5.2. Double-linker modularity

The second main group of functionalized WD POMs have double linkers in various sites. Furthermore, three types of this modification are

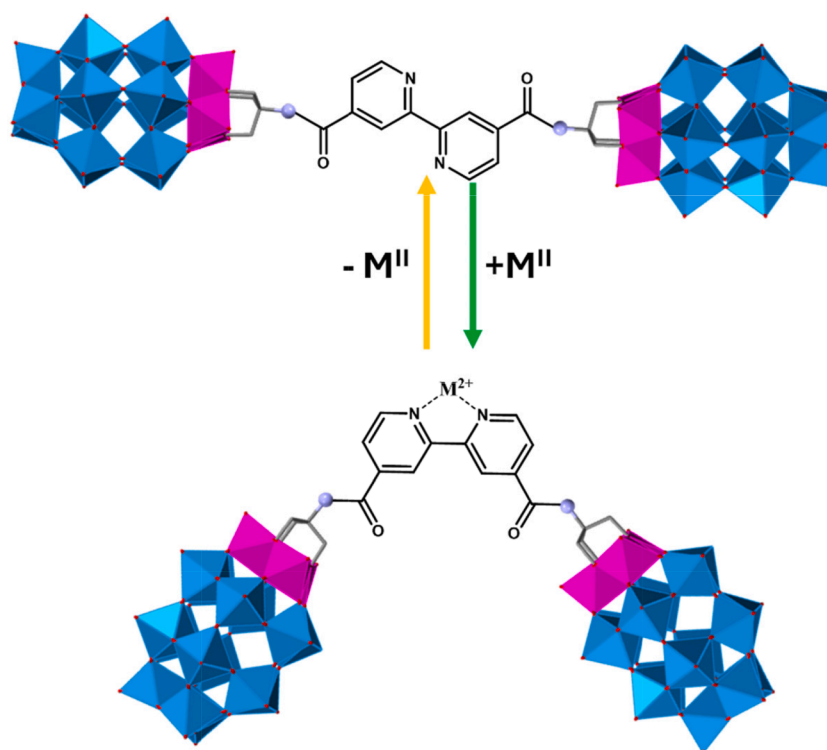


Fig. 25. Scheme of an example of a reversible conformational transformation involving a complexation reaction.

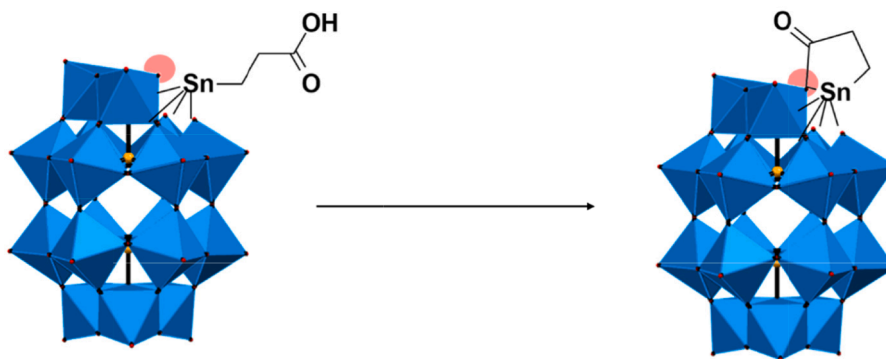


Fig. 26. Demonstration of the use of a tin-substituted WD hybrid for the regioselective acylation of an oxo reaction.

known, such as bent, linear and asymmetrical (Fig. 28). The possibility of functionalization of the primary POM unit gives the opportunity for further post-functionalization, thus improving the activity of compounds in various areas of chemistry.

Pre-functionalized POMs forming hybrids of disilylated WD species are further post-functionalized with additional organic groups to form a bent structure [9,269]. This combination is prepared using effective means, such as Sonagashira coupling reactions most frequently used in the post-functionalization of this type as they provide a rigid connection between the POM and the organic group with photoactive centers [270,284]. Matt et al. reported bent double functionalization in which the POM unit was covalently bond with chromophores to open up a possibility of the potential implementation of this system in photocatalytic devices [270]. Cameron et al. obtained organophosphonate functionalized POMs with photoactive properties. Enhanced photoactivity through the presence of the POM unit was proved in this paper [44].

The second type of WD POM functionalization is the linear modification with double post-functionalization of the POM via a coupling

reaction in suitable reaction conditions. The research group of Tatjana N. Parac-Vogt reported an example of the post-functionalization of a previously prepared iodine-functionalized WD POM with amine substrates in a linear fashion [271]. He et al. showed a copper complex based on POM units formed through the linear functionalization of primary inorganic subunits [131] and another research group, of Han et al., reported linear double post-functionalized WD POMs forming a Cu (II) complex with octahedral and tetragonal pyramidal structure [129].

The last type of double functionalization is asymmetrical POM modification which involves a synthetic challenge and, therefore, the access to such hybrid materials is difficult. In essence, these compounds are desirable as they offer a greater possibility of function and physicochemical activity control of these systems, thus leading to specific and strictly defined applications [272,273]. Hampson et al. reported an example of a cluster consisting of two units with organophosphonate groups with various properties: one of them was terpyridine as a chelating group and the second one was an aliphatic, long-chain subunit [272]. In the following year, Hampson et al. reported an asymmetrical hybrid also based on POM units and two different organic groups: one

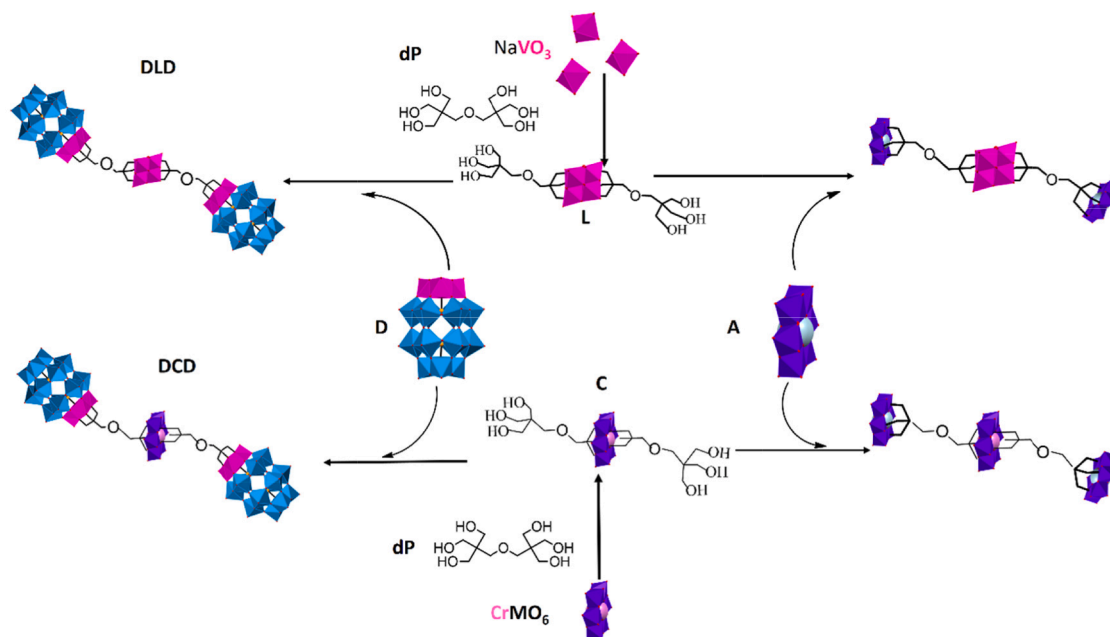


**Fig. 27.** Scheme of heterometallic hybrids with the general formula (POM<sub>2</sub>-R-POM<sub>1</sub>-R-POM<sub>2</sub>) that combine Lindqvist [V<sub>6</sub>], Anderson-Evans [XMo<sub>6</sub>] (X = Cr, Al) and trisubstituted WD POM structures [P<sub>2</sub>V<sub>3</sub>W<sub>15</sub>]. L: [V<sub>6</sub>O<sub>13</sub>((OCH<sub>2</sub>)<sub>3</sub>CCH<sub>2</sub>OCH<sub>2</sub>C(CH<sub>2</sub>OH)<sub>3</sub>)<sub>2</sub>]<sub>2</sub>; A: [Al(OH)<sub>6</sub>Mo<sub>6</sub>O<sub>18</sub>]<sup>3-</sup>; C: [CrMo<sub>6</sub>O<sub>18</sub>((OCH<sub>2</sub>)<sub>3</sub>CCH<sub>2</sub>OCH<sub>2</sub>C(CH<sub>2</sub>OH)<sub>3</sub>)<sub>2</sub>]<sub>3</sub>; D: [P<sub>2</sub>V<sub>3</sub>W<sub>15</sub>O<sub>62</sub>]<sup>9-</sup>; dP: (HOCH<sub>2</sub>)<sub>3</sub>CCH<sub>2</sub>OCH<sub>2</sub>C(CH<sub>2</sub>OH)<sub>3</sub>; ALA: TBA<sub>8</sub>[V<sub>6</sub>O<sub>13</sub>((OCH<sub>2</sub>)<sub>3</sub>CCH<sub>2</sub>OCH<sub>2</sub>C(CH<sub>2</sub>O)<sub>3</sub>(Al(OH)<sub>3</sub>Mo<sub>6</sub>O<sub>18</sub>))<sub>2</sub>]; ACA: TBA<sub>9</sub>[CrMo<sub>6</sub>O<sub>18</sub>((OCH<sub>2</sub>)<sub>3</sub>CCH<sub>2</sub>OCH<sub>2</sub>C(CH<sub>2</sub>O)<sub>3</sub>(Al(OH)<sub>3</sub>Mo<sub>6</sub>O<sub>18</sub>))<sub>2</sub>]; DCD: TBA<sub>12.4</sub>H<sub>2.6</sub>[CrMo<sub>6</sub>O<sub>18</sub>((OCH<sub>2</sub>)<sub>3</sub>CCH<sub>2</sub>OCH<sub>2</sub>C(CH<sub>2</sub>O)<sub>3</sub>(P<sub>2</sub>V<sub>3</sub>W<sub>15</sub>O<sub>59</sub>))<sub>2</sub>]; DLD: TBA<sub>11.4</sub>H<sub>2.6</sub>[V<sub>6</sub>O<sub>13</sub>((OCH<sub>2</sub>)<sub>3</sub>CCH<sub>2</sub>OCH<sub>2</sub>C(CH<sub>2</sub>O)<sub>3</sub>(P<sub>2</sub>V<sub>3</sub>W<sub>15</sub>O<sub>59</sub>))<sub>2</sub>]. Partially modified and reproduced from [90] with permission of the copyright holders.

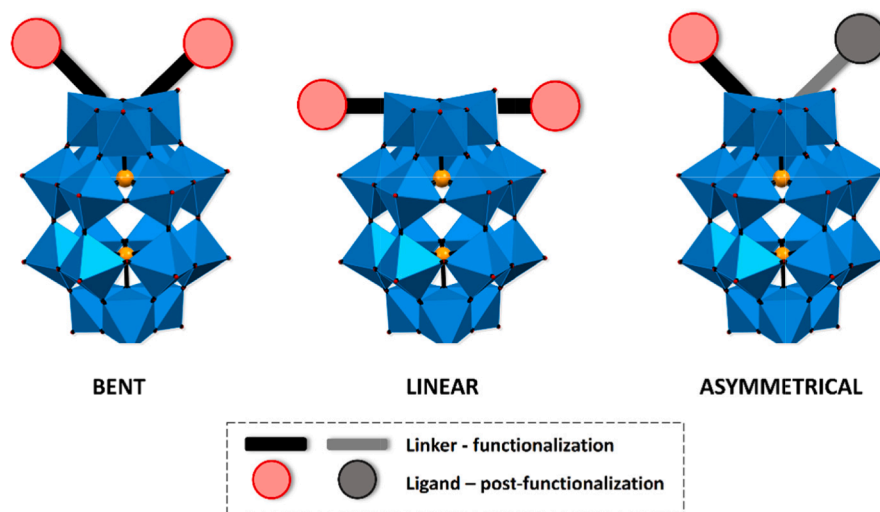


**Fig. 28.** Scheme of the double functionalization of WD POMs involving three types: bent, linear and asymmetrical.

group with terpyridine-coordinating Pt<sup>2+</sup> ions, and the other one without changes, with a long aliphatic chain [273] as in the previously published paper by the same research group [272]. It is noted that it is very difficult to obtain asymmetric functionalized hybrids, and Hampson et al. first obtained a mixture of symmetric and asymmetric products, and then carried out purification to separate the components of the mixture (via addition of a different solvent, centrifugation, and filtration several times) and obtained pure products of hybrid functionalization as confirmed by <sup>31</sup>P NMR analyses (Fig. 29) [272].

### 5.3. Different linker modularity polymers with POMs

#### 5.3.1. Covalent polymeric systems based on POM monomers

Organically functionalized POMs offer the opportunity to

incorporate POMs into polymeric networks. Typically, POM structures are used as components in polymers and self-assembly materials [21]. Miao et al. reported organic polymers with WD POM pendants. The POM was functionalized via a direct M–O–C bond by linking with a norbornene derivative. A study of Ring Opening Metathesis Polymerization (ROMP) revealed that Macromonomers can be polymerized in a controllable manner under mild conditions in the presence of a Grubbs catalyst. The architecture resulting from this process exhibits a well-defined hybrid structure, consisting of an organic backbone and pendant POM groups [285] (Fig. 30). Moreover, a hybrid block copolymer (H-BCP) composed of poly-POM and organic polynorbornene blocks was prepared via living ROMP. The self-assembly properties of H-BCP were investigated, and it was found that in acetonitrile, H-BCP formed micelles with a poly-POM shell and a polynorbornene core,



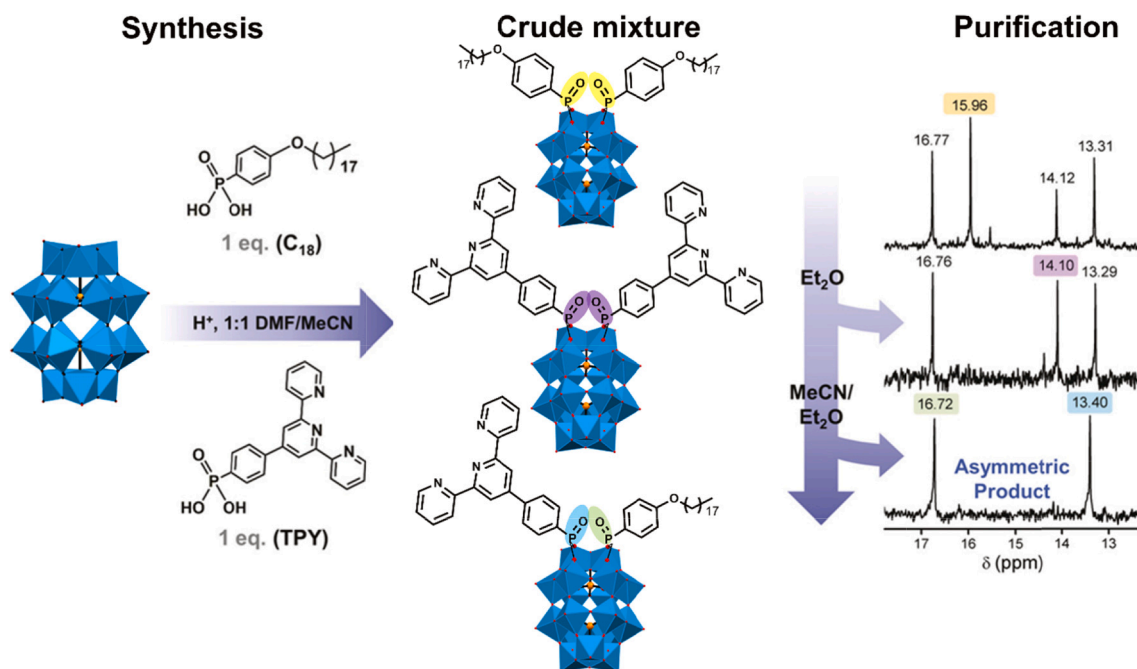


Fig. 29. Scheme of the reaction and purification of the asymmetric functionalized organophosphorus WD hybrid. Partially modified and reproduced from [272] with permission of the copyright holders.

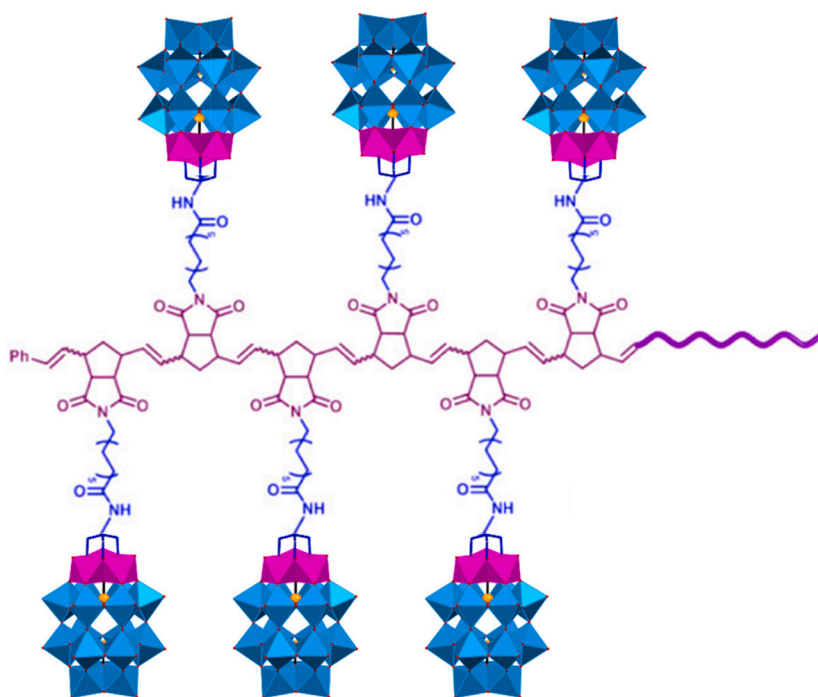


Fig. 30. Scheme of the three-dimensional structure of the hybrid. Partially modified and reproduced from [285] with permission of the copyright holders.

which then formed a hexagonal close-packed pattern [286].

Other interesting materials are copolymer films based on POM-porphyrin hybrids obtained via electrooxidation between porphyrin derivatives and different dipyriddy-substituted WD POMs [179]. Hasenknopf, Lacôte, Ruhlmann et al. published several papers in which they showed a connection between two substituents from the benzene ring with the pyridyl group, and one substituent with POM units [179,261,287].

A POM-based coordination polymer  $(\text{Hbpe})_2[\text{Cu}(\text{pzta})(\text{H}_2\text{O})]$

$[\text{P}_2\text{W}_{18}\text{O}_{62}]$  (pztaH = 5-(2-pyrazinyl) tetrazolate; bpe = bis(4-pyridyl) ethylene) reported by Pang, Ma et al. [288] forms a 3D supramolecular architecture and shows an improved electronic behavior explained in Section 6.1. In this structure each of  $[\text{Cu}(\text{pzta})(\text{H}_2\text{O})]_2^{+}$  complexes connects four neighboring  $\text{P}_2\text{W}_{18}$  anions and forms a straight chain, further interconnected through hydrogen bonds among the terminal oxygen atoms of  $\text{P}_2\text{W}_{18}$  anions to create a polymeric network.

### 5.3.2. WD POM-based polymerization initiators

Because the POM surface can be modified with organic domains, they can be used as inorganic polymerization macroinitiators. There are several examples of research into WD POM-based macroinitiators in Atom Transfer Radical Polymerization (ATRP) and Reversible Addition-Fragmentation chain-Transfer (RAFT).

**5.3.2.1. ATRP macroinitiators.** ATRP, also known as Reverse-Deactivation Radical Polymerization (RDRP) or Controlled Radical Polymerization (CRP), has recently been recognized as one of the ten groundbreaking chemical innovations set to revolutionize our world. This emerging chemical technology holds the potential to contribute significantly to the sustainability of our planet [289]. In 1995, almost simultaneously yet independently, Mitsuo Sawamoto [290] and Krzysztof Matyjaszewski [291] developed one of the earliest and most robust CRP methodologies known as living Atom Transfer Radical Polymerization in the presence of metal complexes. Unlike conventional radical-based polymer manufacturing methods, ATRP stands out by enabling the creation of intricate polymer structures. This is achieved through the use of a special catalyst that incrementally adds one or a few subunits (monomers) at a time to a growing polymer chain. Notably, this living synthetic process can be controlled, allowing the polymerization to be suspended or resumed when needed. Manipulation of the reaction conditions, such as temperature, plays a pivotal role in this capability. ATRP provides an exceptionally resilient means of precisely controlling the chemical composition and architecture of polymers. It ensures the uniform growth of each polymer chain, employing a diverse range of monomers [292]. With over 20,000 citations, ATRP is the most widely used RDRP technique in approximately 40,000 RDRP systems. Its success is attributed to its simplicity and the extensive availability of commercially accessible monomers, initiators, and catalysts.

The first example of well-defined POM-polymer hybrid materials composed of a trivanadium-substituted heteropolytungstate WD POM ( $(\text{Bu}_4\text{N})_5[\text{H}_4\text{P}_2\text{W}_{15}\text{V}_3\text{O}_{62}]$ ) and a conventional polystyrene chain obtained by in situ by the ATRP method was reported by Han et al. in 2009. The macroinitiator was synthesized via a reaction of 2-hydroxyethyl 2-bromoisobutyrate with tris(hydroxymethyl)aminomethane (Tris) in DMF at 70°C. Tris can be covalently linked to a POM cluster, while the 2-methylpropionyl group can initiate the ATRP of styrene (Fig. 31) via the normal (high copper) ATRP methodology. The resulting linear POM-polymer assembled in solution to give hybrid vesicles [293].

Further studies on the POM-polymer hybrid in DMF showed evolution from single macromolecules to vesicles, then to micelles, nanotubes and finally to micelle-stacked domains. The conversion of single macromolecules to vesicles can occur by changing the hydrophobic POM head to a hydrophilic POM head. In contrast, in the further alteration of vesicles into tubular aggregates, an annealing-driven process is necessary [294] (Fig. 32). A recent study demonstrating that the self-assembly of the POM-polystyrene polymer depended on the concentration and differing solubility of the POM and the polymer in DMF [295].

**5.3.2.2. RAFT macroinitiators.** The RAFT method is another form of living radical polymerization providing an excellent platform for the formation of products with high molar mass and controlled properties. In 2013 Lesage de la Haye et al. synthesized for the first time an organo-POM trithiocarbonate RAFT agent in which the macroinitiator was

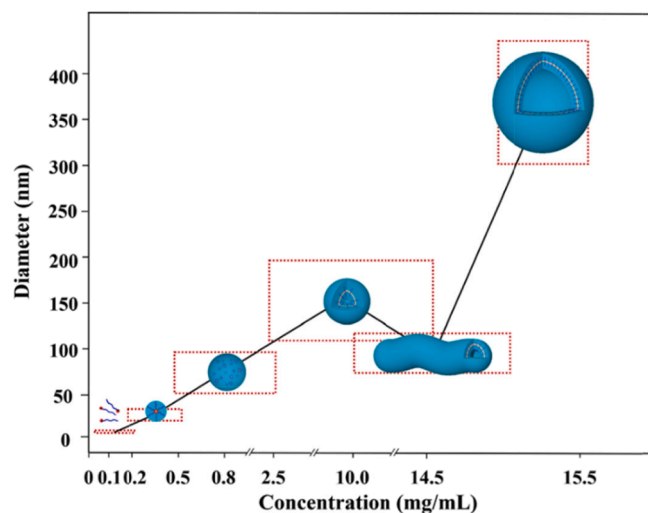


Fig. 32. Morphology of self-assembled aggregates of  $\text{H}_4$ -POM-polystyrene hybrids, the size of which depends on the concentration. The red dotted rectangles correspond to the concentration range of the solutions in which the aggregates formed and the diameter distribution of the aggregates formed, respectively. Reproduced from [294] with permission of the copyright holders.

obtained using trithiocarbonate acid (TTCA) as a classical RAFT agent to enable control of the acrylamide polymerization process. The polymerization reaction was initiated by azobisisobutyronitrile (AIBN) in acetonitrile, with different molar ratios of the monomer while keeping the concentration of the macroinitiator and AIBN constant (Fig. 33a). The polymer hybrid showed photocatalytic activity for the synthesis of silver nanoparticles under UV irradiation [264]. In a further study using the same macroinitiator stable polystyrene-POM composite latex nanoparticles with a size in a range of 50–100 nm were prepared. Core-shell nanoparticles underwent self-assembly during emulsion polymerization. The POM-polymer hybrid latexes were synthesized in the presence of either an amphiphilic organo-POM derivative or a RAFT macroinitiator. 4,4'-Azobis-4-cyanopentanoic acid (ACPA) used as the initiator reacts through the RAFT mechanism with a POM macroinitiator having TTCA in aqueous solution (Fig. 33b). The POM-based RAFT agent stabilized polystyrene nanoparticles. Moreover, the surface of the latexes mediated by POM hybrids retained its photocatalytic activity, as confirmed by using a spatially controlled process involving the germination of silver nanoparticles on the edge of the studied composites, thus confirming the presence of POM moieties at the surface of the nanoparticles in aqueous media [296].

The findings presented above suggest that such WD POM-based polymer hybrids may be used as well-controlled structures in functional materials and lead to the development of the precise control and hierarchical structural construction of the functional aggregates of POM-polymer hybrids.

### 5.3.3. Polymeric POM assemblies

The ability to precisely control the size and topology of hybrid WD POMs as well as their interaction with other components makes them excellent building blocks for the large-scale assembly of supramolecular

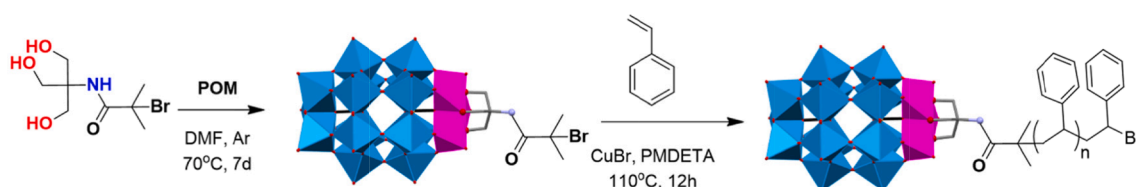
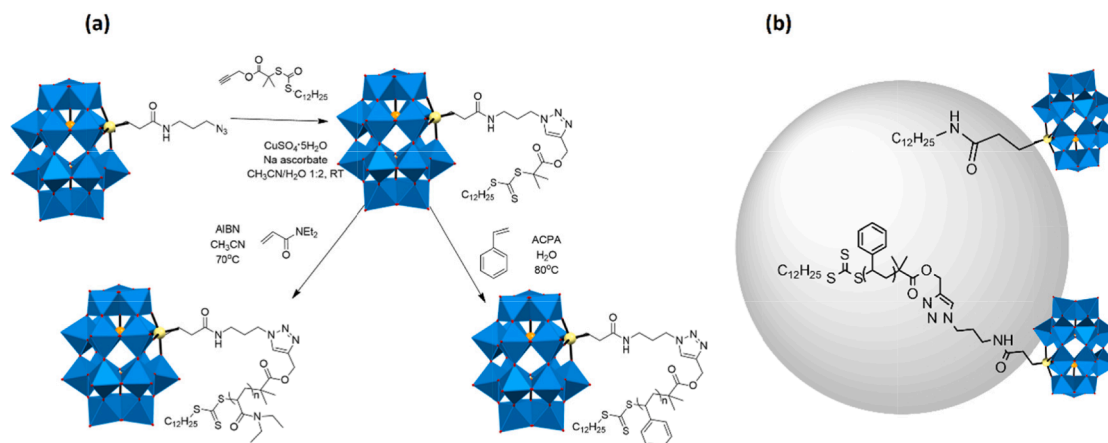


Fig. 31. The first example of POM-polymer hybrid synthesis based on a trivanadium-substituted WD POM.



**Fig. 33.** (a) Example of the synthesis of a WD POM-based polymer using the RAFT method. AIBN: azobisisobutyronitrile; ACPA: 4,4'-azobis-4-cyanopentanoic acid. (b) Examples of polystyrene-POM latexes obtained by the surfactant-free radical emulsion polymerization of styrene in the presence of WD POM derivatives.

hybrid materials.

In 2009, Han et al. presented the first example of a hybrid vesicle assembly composed of a WD POM and polymer chains. The hybrid vehicles were formed by a previously described H<sup>+</sup>-POM polymer obtained via ATRP polymerization, with a hydrophilic inner ring and a hydrophobic shell and core [293]. He and co-workers presented POM-based supramolecular gels through self-assembly formed by nanorolls with lamellar structure. Surfactants such as TBA and triacetate (CTA) encapsulated the K<sub>6</sub>P<sub>2</sub>W<sub>18</sub>O<sub>62</sub> WD structure and assembled into nanorolls in butanone and ethyl acetate and the presence of nanorolls constructed from (CTA)<sub>3</sub>(TBA)<sub>3</sub>P<sub>2</sub>W<sub>18</sub>O<sub>62</sub> and gel formation was confirmed by TEM images [297]. Using a similar approach with a palladium-substituted WD POM, K<sub>15</sub>[Pd<sub>2</sub>(α<sub>2</sub>-P<sub>2</sub>W<sub>17</sub>O<sub>61</sub>)<sub>2</sub>H], promoted the formation of nanorolls constructed from [(CTA)<sub>x</sub>(TBA)<sub>(16-x)</sub>Pd<sub>2</sub>(α<sub>2</sub>-P<sub>2</sub>W<sub>17</sub>O<sub>61</sub>)<sub>2</sub> and hollow spindles, (DTA)<sub>x</sub>(TEA)<sub>(16-x)</sub>Pd<sub>2</sub>(α<sub>2</sub>-P<sub>2</sub>W<sub>17</sub>O<sub>61</sub>)<sub>2</sub> (DTA = decyltrimethylammonium; TEA = tetraethylammonium). The nanorolls and the spindles were formed in chloroform and in aqueous solution, respectively. The authors found an interesting application of such Pd-POM assemblies in Suzuki-Miyaura coupling reactions [298]. A three-component supramolecular hybrid composed of a WD POM, a [Ta<sub>6</sub>Br<sub>12</sub>(H<sub>2</sub>O)<sub>6</sub>]<sup>2+</sup> cluster and γ-cyclodextrin (γ-CD) formed in a specific multi-step recognition was reported by Moussawi et al. Hydrogen bonding and electrostatic interaction enables the formation of a tightly packed cationic cluster between two γ-CDs which bind to the electron-poor POM and form a tubular chain (Fig. 34) [299].

Yin and co-workers reported the formation of monolayer vesicles constructed from a bipyridine-based dumbbell-shaped WD POM [279]. An interesting approach to the formation of novel supramolecular nanostructures self-assembling into a lamellar arrangement was presented by Hu and co-workers. In their work, a WD POM structure was linked via a short organic bond with polyhedral oligomeric silsesquioxane (POSS), resulting in hybrid molecules assembled into layers composed of WD POM and POSS blocks [300]. The combination of WD POM with terpyridine units enables the construction of multiscale nanostructures through metal-driven self-assembly processes. In the

presence of [Co(H<sub>2</sub>O)<sub>6</sub>](NO<sub>3</sub>)<sub>2</sub>, the building block, (TBA)<sub>6</sub>[P<sub>2</sub>W<sub>17</sub>O<sub>61</sub>(O(SiC<sub>29</sub>H<sub>18</sub>N<sub>3</sub>)<sub>2</sub>)], formed nano-organizations, such as a triangle or a square, and assembled into dense nanoparticles with a specific orientation. POM units combined with Co<sup>III</sup> display a different aggregate structure, resulting in worm-like assemblies with enhanced electrostatic interactions (Fig. 35) [301].

In 2019 Lui et al. demonstrated that substitution of a single metal atom in the POM cluster leads to 15 types of clusters, and they used transition metals (Ti, V, Cr, Mn, Co, Ni, Cu, and Zn) and lanthanides (La, Ce, Pr, Nd, Sm, Eu, and Gd). The authors reported a series of single-cluster nanowires, single-cluster nanorings and three-dimensional (3D) superstructure assemblies. Nanostructure formation depends on pH, and pH 4.0 leads to nanoring formation while nanowires form at pH 6.5. The catalytic activity of P<sub>2</sub>W<sub>17</sub>-Mn nanowires toward olefin epoxidation and sensitivity toward H<sub>2</sub>O<sub>2</sub> detection of P<sub>2</sub>W<sub>17</sub>-Eu 3D superstructures presented in this report show different application possibilities of such cluster assemblies [302].

Flexible inorganic polymer chains were also obtained by Zhang et al. in 2020 from K<sup>+</sup> and THA salts of a di-Nb<sup>V</sup>-substituted WD POM through the formation of μ-oxo linkage between Nb<sup>V</sup> = O inorganic blocks. Following the formation of intermolecular Nb-μ-O-Nb linkages, each WD anion repeating unit had a 6- charge [187]. Glöb et al. demonstrated a new surfactant based on a V<sub>3</sub>-capped WD POM structure with a specific linker. In low volumes of water, the POM units were surrounded by nBu<sub>4</sub>N<sup>+</sup> ions to form a micellar structure and were deposited in the liquid phase on a highly oriented pyrolytic graphite, resulting in the formation of two-dimensional molecular layers [260]. Further studies by Glöb et al. on two tris(alkoxo)-ligated polyoxoanions [HP<sub>2</sub>V<sub>3</sub>W<sub>15</sub>O<sub>59</sub>((OCH<sub>2</sub>)<sub>3</sub>C-R)]<sup>5-</sup> (R = CH<sub>2</sub>SMe, NHCOC<sub>6</sub>H<sub>4</sub>SMe) focused on differences in self-assembly on gold depending on ligand functionality. WD POMs with a shorter ligand form a small island on Au(111) and grow vertically, whereas POMs with a longer chain form larger clusters of similar length (Fig. 36) [275].

Zhang and co-workers studied linear poly-POM chains formed with tris(hydroxymethyl)aminomethane cations as substituents on the WD

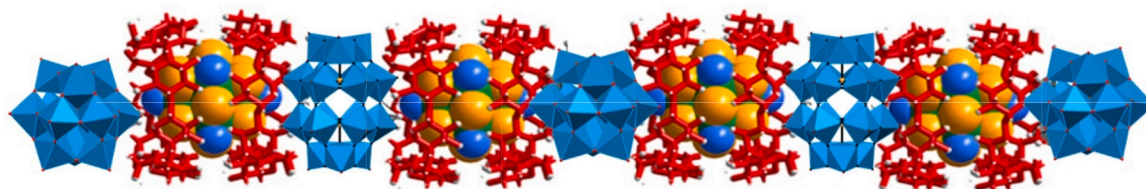


**Fig. 34.** Structural representation based on the X-ray diffraction analysis of a single crystal of the tubular chain showing periodic alternation of a ditopic cation (Ta<sub>6</sub>@2CD)<sup>2+</sup> and [P<sub>2</sub>W<sub>18</sub>O<sub>62</sub>]<sup>6-</sup>. Partially modified and reproduced from [299] with permission of the copyright holders.



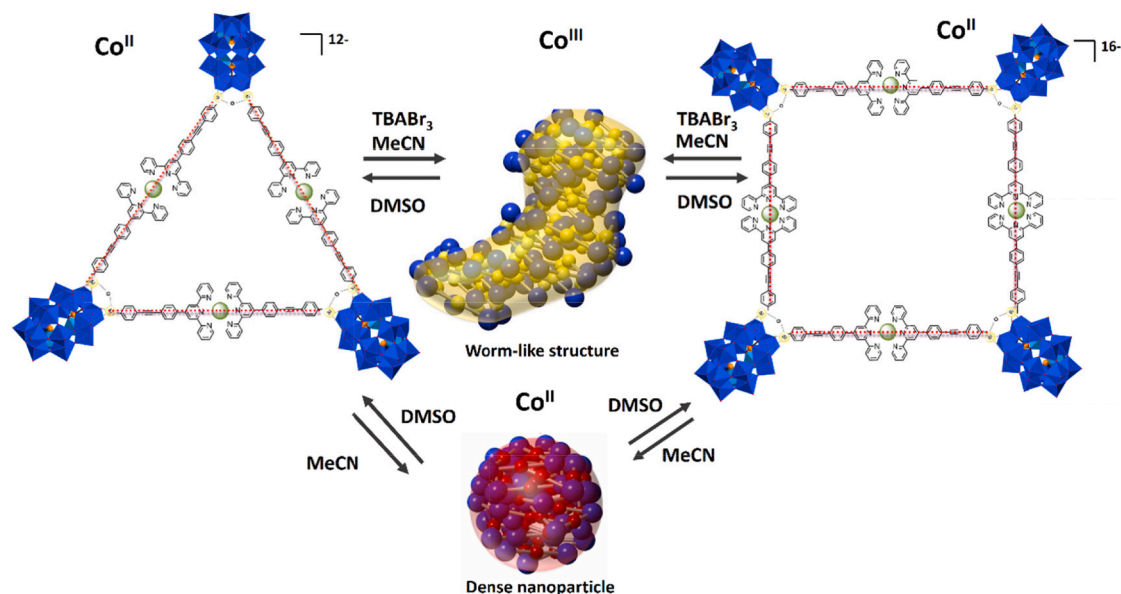


**Fig. 35.** Metal ( $\text{Co}^{\text{II}}$ )-driven formation of a molecular triangle and a square in DMSO ( $\text{Co}^{\text{II}}$ ) and the formation of nanosized aggregates through hierarchical metal-driven self-assembly depending on solvent composition (DMSO/ $\text{CD}_3\text{CN}$  mixtures) and the metal linker charge. For clarity, the supramolecular structures contain only triangles.

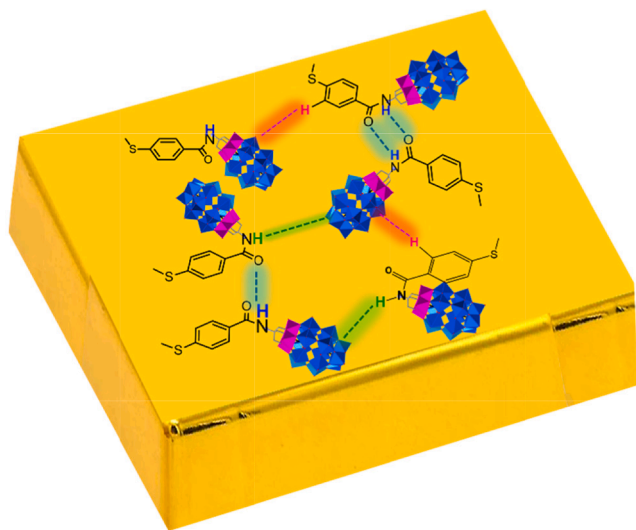


**Fig. 36.** Scheme of the self-assembly of a post-functionalized WD POM on Au(111).

POM anionic core. The authors observed multi-shaped aggregates of single chains of poly-POM units. The shapes of the chains depended on intramolecular interactions. Short-range interactions mimicked straight chains, while long-range interactions mimicked curved and disc-shaped chains [303].

## 6. Different uses of WD POMs

WD POMs are used in many scientific fields: energy-related applications, catalysis, functional materials and biology/medicine (Fig. 37).

### 6.1. POMs as candidates for energy-related applications

Recently, research into new materials for green and sustainable energy sources has increased significantly due to the demand for renewable alternatives and new storage technologies. POMs have gained

prominence and have been the subject of several articles and reviews on energy-related applications due to their unique capabilities (e.g., a high number of metallic centers, high oxidation states, reversible redox processes, multiple electron transfer reactions without altering their structures, etc.) [58,304–307]. However, WD POMs have not been as extensively explored/investigated in this area compared to other types of POMs.

This motivation has led to developments in energy storage technology, such as the use of WD POMs in supercapacitors, which can lead to remarkable results in terms of improved energy storage and delivery capabilities. Using an adsorption method, Madhusree et al. integrated a WD POM with an activated carbon surface. The hybrid electrode showed a capacitance of  $289 \text{ F g}^{-1}$  and achieved cycle stability of 89% over 4000 cycles [308]. An interesting example of the use of WD POMs as redox materials was shown by Mughal et al. Carbon black (Vulcan XC-72R) used as a stabilizing anchor for  $\text{K}_6[\text{P}_2\text{W}_{18}\text{O}_{62}]$  enhanced charge and discharge stability during electrochemical cycling. In voltammetric analysis, the redox activity of a POM and oxidized Vulcan carbon was retained after 500 cycles, while non-oxidized POM-Vulcan lost its redox activity at 250 cycles [309].

An example of hybrid POM nanostructures assembled on a carbon surface was presented by Amin et al. A POM organofunctionalized by (4-(icosyloxy)phenyl)phosphonic acid forms a polar POM head group and non-polar long-chain alkane tails which spontaneously create monodisperse micelles in aqueous media. The deposition of micelles occurs on three different carbon surfaces: (i) glassy carbon (GC), (ii) graphene oxide (GO), where the micelles form a monolayer, and (iii) highly ordered pyrolytic graphite (HOPG) to form a multilayer lamellar structure. Electrochemical analysis showed that GC with multi-redox properties coated with a POM micelle layer is stable and active for up to 100 measurements [310] (Fig. 38).

Deposition of a pseudo-WD-type POM cluster  $[\text{Mo}_{18}\text{O}_{54}(\text{SO}_3)_2]$  on a nanogold surface activates thermally controlled redox behavior, activated by a local electric field, and it accelerates reversible intramolecular redox reactions within the cluster shell. POM nanoclusters containing redox agents are able to eject electrons from the sulfite anion and delocalize them over the POM cage, leading to a reduced state. This process shows potential for applications in molecular electronic devices [311].



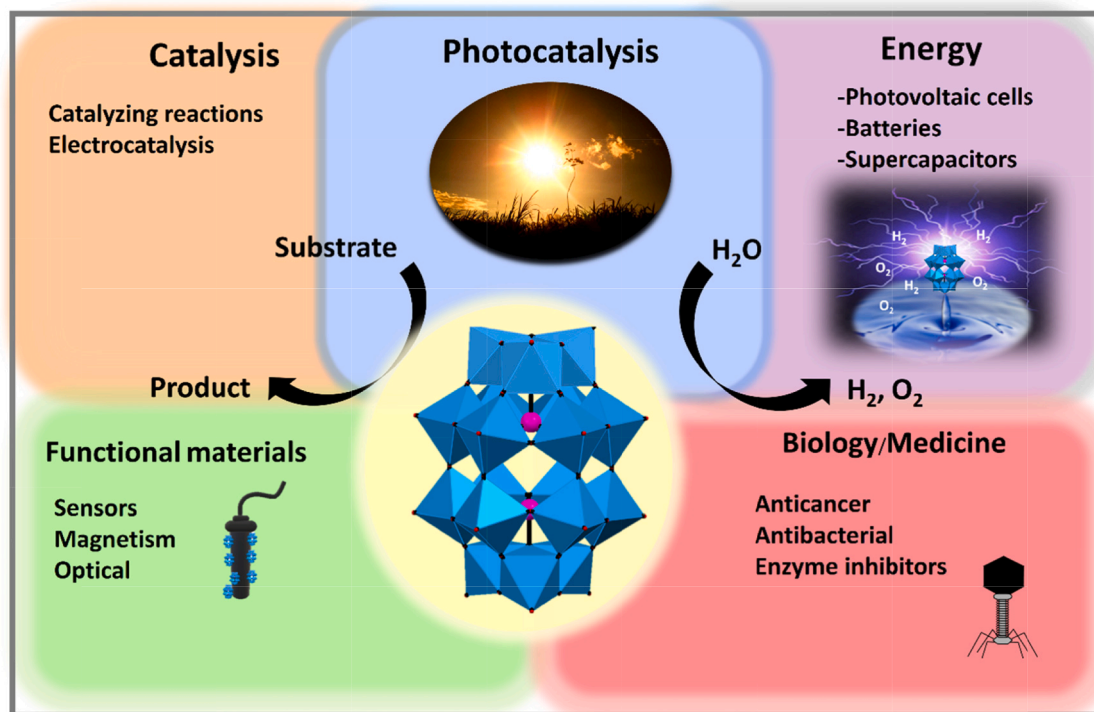


Fig. 37. Scheme of the various applications of WD POMs.

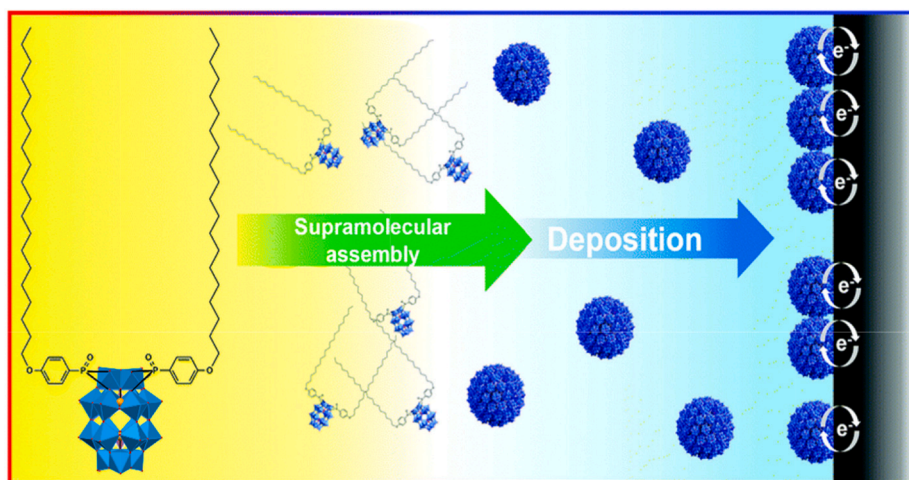


Fig. 38. The model of self-assembly and deposition of a WD POM nanostructure on the carbon surface. Reproduced from [310] with permission of the copy-right holders.

A study of the interaction of WD POM films with an aluminum electrode as a POM/Al cathode showed that six electrons were transferred from the electrode to the  $(\text{NH}_4)_6[\text{P}_2\text{W}_{18}\text{O}_{62}]$  and  $(\text{NH}_4)_6[\text{P}_2\text{Mo}_{18}\text{O}_{62}]$  WD POM cluster after reduction. The device presented in this article has demonstrated applicability in optoelectronics as a cathode interlayer material with improved electron injection/extraction efficiency and reduced recombination losses [312]. The multi-electron reduction of films based on both POM ammonium salts on the aluminum and semiconductor surface was studied several years later by the same research group. They found that the presence of ammonium counterions, POM's LUMO position and Fermi substrate levels affected multi-electron reduction and enabled spontaneous electron transfer [313]. An interesting approach was presented by Bushe et al. in their paper, in which they considered the potential application of POM

molecules as flash memory devices. The core-shell WD POM cluster  $[\text{W}_{18}\text{O}_{54}(\text{SeO}_3)_2]^{4-}$  can be repeatedly reduced, and the selenium moieties can be oxidized. Such a metal-oxide semiconductor can serve as a floating gate and inhibit flash memory charge trapping after the initial excitation step [134]. The role of POMs as an active material in the engineering of resistive random-access memory (RRAM) has been explored by Sterin et al. They demonstrated resistive switching behavior in redox-active POM clusters  $[\text{V}_{10}\text{O}_{28}]^{6-}$  deposited on the top of a glass/ITO layer and coated with Cr/Au contact pads. The new RRAM appliance was capable of storing as well as releasing a large number of electrons and exhibited high endurance, retention, and resistance ratio. Stability of the device was confirmed after as long as 12 months [314].

WD POMs are well-known photosensitive materials with the potential to facilitate multiple electron transfer reactions using light

[218,315]. Unfortunately, most of the excited states of WD POMs can only be generated under UV irradiation (typically at wavelengths of 200–400 nm). Therefore, only a small fraction of sunlight can be converted into electrical energy. Indeed, this has limited applications in the field of photoelectric energy. However, new approaches involving photosensitization of visible light by chromophores have improved photocurrent generation. Among the photosensitization strategies investigated for WD POMs, the most relevant include: (i) electrostatic interactions between anionic POMs and cationic sensitizers [316–318] and (ii) covalent or coordination chromophores coupled to POMs [269,284,319,320].

A significant part of the field has focused on porphyrin [317,319,321–323] which is known to have high absorbance in the visible and near-infrared range. However, most of these photophysical studies have focused on exploring the first light-induced electron transfer and not on the transfer of a second electron, a crucial aspect for solar energy transformation into storable energy such as  $H_2$  or  $O_2$ . In this sense, it is extremely important to carry out a rational design to adapt the hybrid systems to achieve more effective charge transfer properties. Harriman, Odobel et al. [322] described a multi-porphyrin complex consisting of two components, one being ZnTPP-based donors and the other a free porphyrin intermediate compound. Their study was instrumental in promoting directional charge transfer and simultaneously preventing too rapid recombination of the charge between the molecules: WD POM and ZnTPP donors. This enabled POM to store multiple electrons in a single group, an essential requirement for its energetic application. Subsequently, Izzet, Artero, and Proust [324]

showed efficient photoreduction of a WD POM hybrid with an iridium complex:  $[(P_2W_{17}O_{61}-(O(SiC_3H_7)_2N_3O_2Ir)_2)]^{6-}$  in the presence of a sacrificial electron donor. Sequential formation of one-electron and two-electron reduced species was observed with a significantly higher reaction rate for the first reduced species. This hybrid also generated hydrogen under visible light without significant yield loss for more than one week of continuous photolysis.

Hydrogen generation in non-covalently sensitized systems has also been reported. Douvas, Argitis, and Coutsolelos studied the sensitization of W and Mo WD POMs with *meso*-tetrakis(N-methyl-pyridinium-4-yl) porphyrin ( $ZnTMPyP_4^+$ ) [325]. Both sensitized WD POMs showed higher hydrogen generation efficiency compared to those obtained by direct photoreduction. Moreover, the  $[P_2Mo_{18}O_{62}]^{6-}$  (Fig. 39a (left)) catalyst (after sensitization with  $ZnTMPyP_4^+$ ) showed higher efficiency for  $H_2$  evolution than  $[P_2W_{18}O_{62}]^{6-}$  (Fig. 39a (right)). The authors attributed this fact to the lower LUMO position of the  $[P_2Mo_{18}O_{62}]^{6-}$  anion and its higher degree of reduction.

In addition to porphyrins and iridium complexes, metal organic frameworks (MOFs) and supramolecular MOFs (SMOFs) derived from  $[Ru(bpy)_3]^{2+}$  were used as photosensitizers (e.g. UiO MOF [326], MIL-101 [327] or SMOF-cucurbit[8]uril [328]) which showed improved hydrogen evolution. This effect can be attributed to increased three-dimensional organization and enhanced association between the cationic photosensitizer and the anionic catalyst in these systems. However, a disadvantage of these strategies consists in the use of precious metals such as ruthenium. Recently, Lv and co-workers reported noble metal-free POM@MOF systems with efficient hydrogen

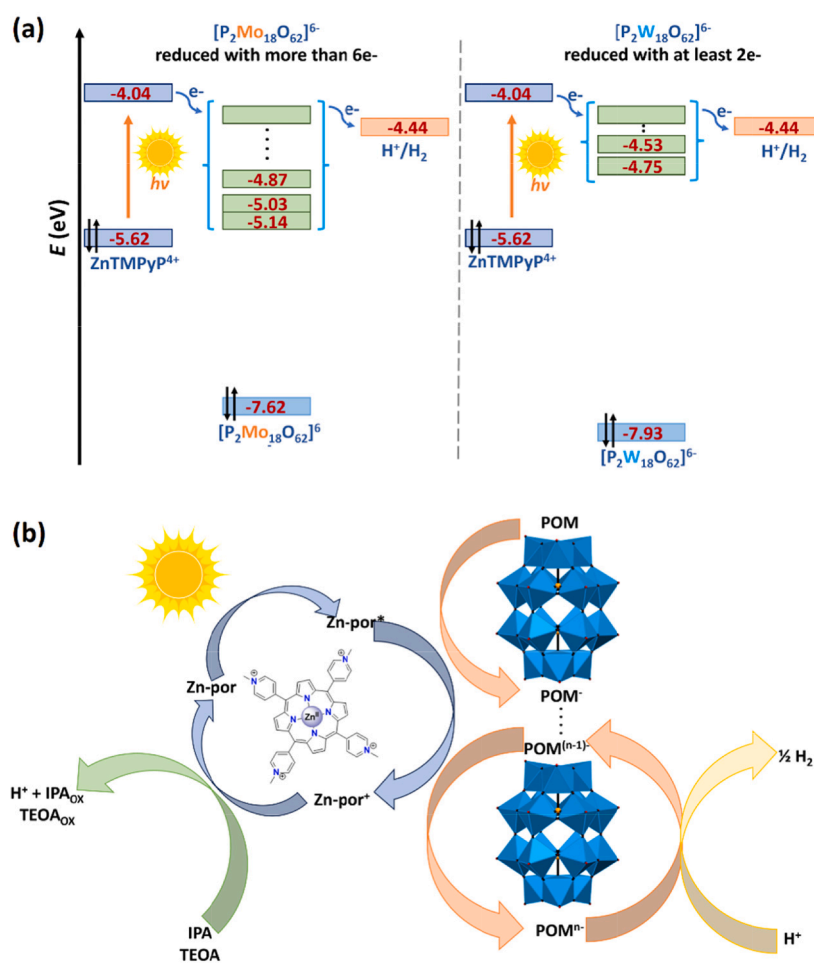


**Fig. 39.** (a) Scheme of a simplified molecular orbitals diagram presenting the  $ZnTMPyP_4^+$ -sensitized multi-electron reduction of two WD-type POM catalysts:  $[P_2Mo_{18}O_{62}]^{6-}$  and  $[P_2W_{18}O_{62}]^{6-}$ , for efficient  $H_2$  evolution. (b) Illustration of highly efficient  $H_2$  evolution by the  $ZnTMPyP_4^+$ -sensitized multi-electron reduction of WD POM catalysts using 2-propanol (IPA) or triethanolamine (TEOA) as the sacrificial electron donor in a water-soluble system; based on [325].

generation using visible light [329]. The compounds were prepared by incorporating Ni-containing POMs ( $\text{Ni}_3\text{PW}_{10}$  and  $\text{Ni}_3\text{P}_2\text{W}_{16}$ ) into the Zr-based MOF (NU-1000). Both compounds showed reproducible photocatalytic hydrogen generation, which was higher in the WD POM@MOF system.

Water oxidation catalysts (WOCs) are also a critical topic for solar fuel production. Hill and co-workers synthesized an open complex of  $[\text{Ni}_5(\text{OH})_6(\text{OH})_2(\text{Si}_2\text{W}_{18}\text{O}_{66})]_{12}$  WD POMs containing penta-nickel and silicotungstate, showing an ability to generate oxygen by oxidizing water in the presence and absence of light by forming complexes with  $[\text{Ru}(\text{bpy})_3]^{n+}$  ( $n = 2$  or  $3$ ) [107].

The unique and tunable electronic properties of POMs have led to the construction of photovoltaic cells for solar cell applications using POMs. It has been observed, for example, that the incorporation of  $\text{P}_2\text{W}_{18}$  films on ITO in organic photovoltaic cells has improved power conversion efficiency [330]. On the other hand, mono-substituted POMs with transition metals,  $\text{P}_2\text{W}_{17}\text{-Co}$  and  $\text{P}_2\text{W}_{17}\text{-Mn}$ , have been used to co-sensitize NiO electrodes, showing higher overall power conversion efficiency compared to other inorganic photosensitizers [331].

Lithium batteries (LiBs) are also in the spotlight in the energy research field because they offer an alternative source of new energy due to their high specific energy density and long lifetime. Energy storage in rechargeable batteries results from reversible redox reactions in active electrode materials. Due to their multi-electron reversible transfer, POMs have received a lot of interest as electrode materials in LiBs [304]. POM can be activated by the coordination of conductive materials and can significantly modify the electronic structure of the clusters. The formation of WD helical hybrids has been shown to improve performance when used as electrodes in LiB [332]. Thus, by having a high number of oxygen atoms and with a lower spatial symmetry, WD POMs are attractive building blocks for different structures and functionalities. For example, Sha and Wang [333] reported complex multi-fold Mesohelices in the structure of a WD POM-based hybrid. The resulting hybrids,  $[\text{Ag}_{26}(\text{Trz})_{16}(\text{OH})_4][\text{P}_2\text{W}_{18}\text{O}_{62}]$  and  $\text{Na}[\text{Ag}_{16}(\text{Trz})_9(\text{H}_2\text{O})_4][\text{P}_2\text{W}_{18}\text{O}_{62}]$  ( $\text{Trz} = 1,2,3$  triazole), were used as anode materials for LiBs, showing higher discharge capacities than those obtained for unfunctionalized  $(\text{NBu}_4)[\text{P}_2\text{W}_{18}\text{O}_{62}]$  or commercial graphite commonly used as reference anodes. Both POM hybrids show excellent performance after 100 cycles and the authors conclude that the regular helical conformation of the composites provides stable charge transmission channels during the discharge-charge process. The surface of GO, a commonly used building block for various nanocomposites, was effectively modified by the covalent binding of ionic liquids and loaded with a WD POM. The use of the prepared nanocomposite as a LiB anode material enhances charge transfer and provides high specific capacitance with a long cycle life over 1000 cycles [334]. A new class of hybrid materials has emerged by introducing the WD POM cluster  $[\text{As}_2\text{Mo}_{18}\text{O}_{62}]^{6-}$  into MOF architectures based on  $\text{Cu}(\text{btp})_2$  ( $\text{btp} = 1,3$ -bis(1,2,4-triazol-1-yl)propane) generating a POMOF. Such a 3D network exhibits stability in air and at different pH values in aqueous solutions and organic solvents. Based on the assessment of reversible capacity and cycling stability, it is a promising anode material for LiBs [335].

Recent studies, from 2022, on lithium-sulfur batteries (LiSBs) based on WD POMs present a solution for dendrite formation and polysulfide conversion. A WD POM-modified polypropylene membrane improves the electrochemical performance of LiSBs and shows initial high specific capacity with excellent cycling stability [336]. A surface modification of MIL-88A(Fe) by a WD POM enables the carbonization of the material to produce a capsule coating with a carbon and  $\text{Fe}_3\text{O}_4$  component. The hollow capsule acts as a sulfur host and can significantly improve the efficiency of the sulfur electrode during the charging and discharging process [337].

The use of an addenda WD POM for energy storage may be challenging. A study of Pratt et al. shows that clusters with higher charge density exhibit poor stability. Consequently, charge storage in a laboratory-scale flow cell demonstrated the worst performance of all

tested addenda POMs [338].

Supercapacitors are also energy storage devices that are gaining importance. They have the ability to deliver a large amount of energy in a short time. Energy storage is based on the combination of electrostatic charge separation (double layer capacitance) and electrochemical charge separation (pseudo capacitance). Ammam et al. synthesized WD POM hybrids with Ru and evaluated the performance of the hybrids deposited on electrodes to be used as supercapacitors in physiological electrolytes as potential storage devices for powered implanted biomedical devices [339]. The hybrid synthesis was carried out in the presence and absence of KI, and two different stoichiometries were obtained:  $[\text{Ru}(\text{bpy})_3]_3\text{POMo}_{18}\text{O}_{62} \cdot n\text{H}_2\text{O}$  and  $[\text{Ru}(\text{bpy})_3]_{3.33}\text{POMo}_{18}\text{O}_{62} \cdot m\text{H}_2\text{O}$ , respectively. The authors showed that there was a strong influence of hybrid composition and supercapacitor behavior. It was found that a hybrid with a higher proportion of Ru(bpy) performed better as a supercapacitor in physiological conditions.

Stretchable supercapacitors reported by Mu et al. constructed with 3-(2-naphthyl)-L-alanine, the  $[\text{H}_6\text{P}_2\text{W}_{18}\text{O}_{62}]$  WD POM and silver powder reveal underwater adhesion properties. In addition, this type of flexible material shows advantages such as adhesion to electrolytes, conductivity, reversible redox behavior and fast electron transfer/storage abilities [340]. The  $\text{P}_2\text{W}_{18}$  WD POM integrated with activated carbon (AC) was studied as a nanohybrid electrode for high-performance supercapacitors in a two-electrode system. The results showed excellent specific capacitance ( $289 \text{ F g}^{-1}$ ) with good energy and power density ( $40 \text{ W h kg}^{-1}$ ) and demonstrated a cycling stability of 89% over 4000 cycles [308].

The use of polymer hybrids is a strategy to reduce POM solubility in electrolytes and increase conductivity in supercapacitors, for example by adding nitrogen compounds to the polymer. Pang, Ma et al. reported and investigated a new coordination polymer,  $(\text{Hbpe})_2[\text{Cu}(\text{pzta})(\text{H}_2\text{O})][\text{P}_2\text{W}_{18}\text{O}_{62}]$  ( $\text{bpe} = \text{bis}(4\text{-pyridyl})\text{ethylene}$ ;  $\text{pzta} = 5\text{-(2-pyrazinyl) tetrazolate}$ ) [288]. The authors showed that the formation of a polymeric WD hybrid had better electronic performance than the  $\alpha\text{-K}_6\text{P}_2\text{W}_{18}\text{O}_{62}$  inorganic analog and other electrodes made of POMs (see Section 5.3.1).

Research into energy storage, either in the form of electrical charge or conversion into chemical fuels, has undoubtedly been a major focus in recent years. In this sense, battolysers (integrated battery-electrolyzers) can function as both batteries and fuel generators and could have a transformative effect on how renewable energy is used [341]. Moreover, finding new mediators capable of accepting more electrons per molecule is crucial for practical applications. Cronin et al. recently showed that the  $[\text{P}_2\text{W}_{18}\text{O}_{62}]^{6-}$  polyoxoanion had remarkable proton-coupled electron redox activity [342]. Under those conditions, the molecule could reversibly accept up to 18 protons and electrons in aqueous solution. The authors showed that the highly reduced  $[\text{P}_2\text{W}_{18}\text{O}_{62}]^{6-}$  WD POM can be used in two ways: firstly it can act as high-performance electrolyte of a flow redox battery (practical discharge energy density:  $225 \text{ Wh l}^{-1}$ ; theoretical energy density: more than  $1000 \text{ Wh l}^{-1}$ ) and can be used as a mediator in an electrolytic cell to produce hydrogen on demand.

## 6.2. Catalysis

POMs are widely used as catalysts due to their high efficiency, resistance to oxidation, degradation and hydrolysis, ability to stabilize ions, and environmental compatibility [31]. POMs and heteropolyacids (HPAs) (containing protons as cations) represent one of the most versatile catalysts due to the multiple active sites, including protons, oxygen, and metals [32]. The protons in HPAs can act as Brønsted acids and participate in acid-catalyzed reactions. Some oxygens are sufficiently basic and are capable of reacting or even abstracting protons from organic substrates. Lewis cation incorporation (in a lacunar POM or through a suitable ligand in a hybrid POM) converts them into catalysts as Lewis acids. However, the most active sites in POMs are on the metal atoms, which are involved in many distinct types of reactions (such as oxidations, acid-catalyzed reactions or other reactions). In turn, the Lewis acidity of POMs may be achieved using high-valent metals [32]. A



wide variety of WD POMs have been extensively used as catalysts in organic transformations, such as chemical oxidation [167,174], in many classical reactions: Diels-Alder, Mannich and Mukaiyama-type [343], Suzuki–Miyaura cross-coupling reactions [344], amide formation [345], cyclization of 1,3-diketones with hydrazines/hydrazides or diamines [346], epoxidation [113], allylation of sulfonyl imines and aldehydes [178], hydrolysis of peptides [199], hydrogenolysis reactions [347], Friedel-Crafts acylation [348], and so on. As in all homogeneous reactions, recovery and reuse of the catalyst can be difficult. In this regard, the inclusion of POM anions as inorganic building units to construct WD POM-based MOFs represents a successful strategy to recover the catalyst at the end of the organic transformation [150].

The catalytic ability of POMs is undoubtedly altered and in many cases enhanced by the introduction of transition metal/lanthanide heteroatoms into their structure (see Section 2.2.2). Cronin et al. investigated the phosphoesterase activity of  $\alpha_2$ -[P<sub>2</sub>W<sub>17</sub>O<sub>61</sub>]<sup>10-</sup> type WD POMs, containing various metals such as Mn<sup>III</sup>, Fe<sup>III</sup>, Co<sup>II</sup>, Ni<sup>II</sup>, and Cu<sup>II</sup>, and other ions such as Y<sup>III</sup>, La<sup>III</sup>, Eu<sup>III</sup>, Zr<sup>IV</sup>, and Hf<sup>IV</sup> [101]. Catalytic activity was studied on 4-nitrophenyl (NPP) and bis-4-nitrophenyl phosphate (BNPP), well-studied model substrates that mimic the phosphoester bond in DNA. The incorporation of the first-row transition metals showed no catalytic activity. In contrast, the second and third groups of POMs modified with lanthanides and Zr<sup>IV</sup> and Hf<sup>IV</sup>, respectively, showed catalytic activity. In the former case, the activity was reported only in NPP and those with Zr and Hf also showed catalytic activity on the more resistant BNPP. The authors attributed these differences to the higher coordination numbers and the capacity to form complexes with flexible geometries of the lanthanides, Zr and Hf. Another consequence of the high oxidation number is the ability to form organized dimeric POM structures. On the other hand, the enhanced Lewis-acid strength from Zr<sup>IV</sup> and Hf<sup>IV</sup> compared to Ln<sup>III</sup> ions enabled more efficient NPP hydrolysis and catalytic activity in more resistant BNPP. In the same way, Wynne et al. showed the potential of WD-substituted hetero-metals, [Zr( $\alpha_2$ -P<sub>2</sub>W<sub>17</sub>O<sub>61</sub>)<sub>2</sub>]<sup>16-</sup> and [Ni( $\alpha_2$ -P<sub>2</sub>W<sub>17</sub>O<sub>61</sub>)]<sup>8-</sup>, to be used as catalysts in the rapid oxidation of a persistent organophosphorus chemical warfare agent analog [349]. A novel decontamination method was employed by the direct application of aqueous POM solutions on the CWA analog and 15 wt% hydrogen peroxide. WD incorporation with Ni<sup>II</sup> and Zr<sup>IV</sup> increased the oxidation rate significantly and reduced the reaction half-lives compared to the slower oxidation without a POM. In the first case, the mechanism involved a direct Ni<sup>II</sup> reaction with hydrogen peroxide generating a reactive species that then the substrate was oxidized. In the case of Zr<sup>IV</sup>-POMs, the process was more complex, with additional active species present in the solution that influenced the rate of substrate oxidation.

### 6.2.1. Photocatalysis

The photocatalytic behavior of POM hybrid materials is the result of UV light irradiation which excites electrons from low-energy states to high-energy states, from oxygen-binding 2p orbitals to (HOMO) metal-binding anti-binding d orbitals (LUMO) [350]. The photoexcitation offers several advantages, such as homogeneous photocatalysis or a light-induced active redox reagent in multi-step photoredox-systems.

Photocatalysis focused on POMs is not only interesting for its energy-related applications but also for its use in the degradation of organic and inorganic pollutants. The major advantage of photocatalysis processes is that experiments can be conducted under mild conditions such as atmospheric pressure and room temperature. As previously noted, many efforts have been made to modify the electronic properties of POMs to take advantage of visible light (see Section 6.1). Newton, Oshio et al. showed that WD POM functionalization with an organophosphonate derivative (4-carboxyphenyl phosphonic acid) reduced the energy gap between HOMO and LUMO [44]. It also shifted the LMCT band to the visible region as compared to non-functionalized WD POMs. This hybrid can photocatalyze the indigo dye (a model impurity) using visible light, unlike non-functionalized POMs. Subsequently, the authors

demonstrated that catalytic activity can be modulated by modifying the substituent at the *para* position of the phenyl ring [130]. They found that catalytic activity depended on the inductive properties of the substituent. Mousavi et al. used a sodium polytungstate POM cluster as an efficient agent to remove toxic auramine-O from aqueous media. The results showed that up to 100% of impurities were degraded within 110 min irradiation time of the WD POM cluster [351].

Photocatalytic capacity has also been explored using non-classical WD POMs, or “WD-like” (similar to WD POMs but with a non-tetrahedral group added to each [M<sub>18</sub>] cluster). These include inorganic–organic hybrids containing the SbO<sub>3</sub> pyramidal group in a WD POM based on an organic ligand ((Ni(phen)<sub>3</sub>)[SbW<sub>18</sub>O<sub>60</sub>](H<sub>3</sub>O)<sub>3</sub>·7H<sub>2</sub>O) [130]. This hybrid showed excellent catalytic activity and selectivity in the degradation of RhB at pH 3 using visible light. The authors suggest that this type of structure may have enhanced catalytic activity as it contains a lone pair of electrons in [W<sub>18</sub>].

The high solubility of WD POMs and the growing interest in designing efficient and recyclable heterogeneous catalysts have prompted the exploration of a variety of approaches to this problem. Several selected supports to immobilize POMs have been shown to play a dual role by modifying some of the physicochemical characteristics of the POM and enhancing the adsorption capacity of the substrates to react with the active species [352]. Metal oxides, for example, are a widely studied group with several types of POMs. In this respect, Wu, Guo, and co-workers showed the effect of immobilizing H<sub>6</sub>P<sub>2</sub>W<sub>18</sub>O<sub>62</sub> on TiO<sub>2</sub> [353]. These composites were successful in the photocatalytic degradation process of aqueous parathion-methyl insecticide solution using visible light. This effect was attributed to the synergy effect between the POM and anatase TiO<sub>2</sub>, porous structures, and the narrow bandgap of the composites. The coupling of H<sub>6</sub>[P<sub>2</sub>W<sub>18</sub>O<sub>62</sub>] and TiO<sub>2</sub> produces a decrease in conductivity band levels, resulting in a smaller bandgap than the POM or the support alone. This group later showed a similar effect by coupling H<sub>6</sub>[P<sub>2</sub>W<sub>18</sub>O<sub>62</sub>] to tantalum pentoxide (Ta<sub>2</sub>O<sub>5</sub>) [354]. In addition to metal oxides, the effect on heterogeneous photocatalytic properties was investigated using hybrid organic–inorganic POMs. The reported organic–inorganic hybrids were based on cucurbituril derivatives and WD POMs which showed photocatalytic activity in the degradation of methyl orange and rhodamine-B using visible light [355].

### 6.2.2. Electrocatalysis

POMs are also widely used as electrocatalysts (mediators) in electrochemical reactions, and they catalyze electron transfer between the electrode and electrolyte solution. Undoubtedly, the functional versatility of WD POMs is evidenced by the large number of papers reporting a wide range of modified WD POMs as electrocatalysts [356]. Among the modifications of WD POMs that present interesting electrocatalytic properties, noteworthy is the introduction of vanadium into the structure of a tungstic or molybdo-tungstic POM [356–358]. The electrocatalytic capacity of non-conventional WD POM structures (e.g. WD-sandwiched clusters [247], open WD-tungstosilicates [105] or metal–organic framework based on WD POM [359,360]) has also been studied. Some of the major electrocatalytic processes using WD POMs include the reduction and oxidation of nitrogen oxides [120,357,361–364], reduction processes resulting in molecules of biological interest (e.g. NADP<sup>+</sup>, L-cysteine) [356,357], oxyanions (such as chlorate, bromate, iodate) [120,247,355,363,365] or hydrogen peroxide [105,360,363,365,366]. A recent study on the mechanism responsible for the super-reduction of fully inorganic POM salts by Chen et al. showed that the protonation and agglomeration of WD structures in aqueous solution promoted H<sub>2</sub> production [367].

## 6.3. Functional materials

### 6.3.1. Sensors

The most salient features of a POM sensor include sensitivity,



selectivity, detection limit, stability and linear range. The remarkable electrocatalytic properties of WD POMs and the numerous works reported in this field have made it possible to understand and study many fundamental aspects for using these systems as electrochemical sensors. In addition, other methods such as colorimetric or fluorescence have been investigated [368]. Some examples of WD POMs used for sensing are summarized in Table 3.

### 6.3.2. Optical materials

POMs are potential candidates as novel nonlinear optical (NLO) materials. For example, WD POMs modified with transition metals have been prepared to obtain non-centrosymmetric structures (a requirement for second-order NLO materials). Su, Wang et al. [82] have shown in a theoretical study that trisubstituted  $\alpha$ -[P<sub>2</sub>M<sub>15</sub>M'<sub>3</sub>O<sub>62</sub>]<sup>m-</sup> (M=W<sup>VI</sup>, Mo<sup>VI</sup>, and M' = V<sup>V</sup>, Mo<sup>VI</sup>) display good second-order NLO properties. On the other hand, since porphyrins exhibit significant NLO responses, porphyrin-WD POM hybrid systems have been prepared by covalent interactions [257,379]. These systems show remarkable enhancement of the nonlinearity of the hybrids over their corresponding porphyrin precursors.

Tetrameric WD POMs containing lanthanide ions, shown in Fig. 40 [104], exhibit reversible photochromic behavior. After UV irradiation, they can change from white to blue within 6 min and restore their color in the dark for 30 h. The switchable luminescent behavior of Sm-POMs induced by their photochromism opens up a new perspective for the development of optical materials. A WD POM ([H<sub>2</sub>N(CH<sub>3</sub>)<sub>2</sub>]<sub>10</sub>H<sub>3</sub>[SeO<sub>4</sub>M<sub>5</sub>(H<sub>2</sub>O)<sub>7</sub>(Se<sub>2</sub>W<sub>14</sub>O<sub>52</sub>)<sub>2</sub>].40H<sub>2</sub>O M = Dy, Gd) was encapsulated by CTA and formed a nanoscale material with photoluminescent properties. The authors showed that CTA, a cationic surfactant, can regulate morphology and tune multicolor optical behavior [380].

### 6.3.3. Electrochromic materials

Electrochromic (EC) materials are characterized by color change after electrochemical reduction or oxidation. POMs exhibit this property and can be modulated through molecular design [100]. Organic cations, such as poly(styrenesulfonate) (PSS) and polyallylamine hydrochloride (PAH), have been used to prepare films based on WD POMs with

different modifications to explore their electrochromic properties. For example, a film formed by incorporating Neutral Red (NR) [P<sub>2</sub>W<sub>17</sub>/PAH/P<sub>2</sub>W<sub>17</sub>/NR]<sub>35</sub> [83] showed color changes from deep pink to dark violet-blue depending on the reduction rate of P<sub>2</sub>W<sub>17</sub> in response to different applied potentials. It was also observed that the electrochromic properties were affected by the degree of the lacunar structure (PSS/PAH/(P<sub>2</sub>W<sub>18-x</sub>/PAH) [381]. Another example is the adjustable color of PSS/Cu<sup>II</sup>(phen)<sub>2</sub>/[(P<sub>2</sub>W<sub>17</sub>/Cu<sup>II</sup>(phen)<sub>2</sub>)]<sub>n</sub> and PSS/Fe<sup>II</sup>(phen)<sub>3</sub>/[(P<sub>2</sub>W<sub>17</sub>/Fe<sup>II</sup>(phen)<sub>3</sub>)]<sub>n</sub> through the reduction of both the transition metal and the POM at different potentials [382].

An interesting approach to detecting weak visible light induced by an LED source and converted into an electrical signal was reported by Zhang et al. [383]. The introduction of covalently linked Pb<sup>2+</sup> ions formed a new POM-Pb<sub>3</sub>Mo<sub>18</sub> chain complex. The revealed new mechanism promoting the ligand-to-metal charge-transfer (LCMT) process and enhanced electrical conductivity was related to the stabilization of the hole of oxygen atoms due to O → Mo charge transfer.

Wang, Chen and co-workers formed films through the electrodeposition of P<sub>2</sub>W<sub>18</sub> and P<sub>2</sub>W<sub>17</sub> on TiO<sub>2</sub> to fabricate high-performance smart windows. The authors observed, as in the case of (PSS/PAH/(P<sub>2</sub>W<sub>18-x</sub>/PAH) systems, that the degree of lacunar structure affected the performance of smart windows [83]. Mono-vacant lacunary WD-type P<sub>2</sub>W<sub>17</sub> had high optical contrast and higher coloration efficiency than P<sub>2</sub>W<sub>18</sub> [384] (Fig. 41).

### 6.3.4. Magnetic materials

Features such as stability in solution and in the solid-state, the potential role as a host for magnetic ions, rigid and highly symmetric structure and structural integrity after accepting several electrons, have been encouraging characteristics to explore POMs in the design of new molecular magnetic devices [53]. Although numerous papers reported magnetic properties and potential applications in single-molecule magnetism (SMM) or single-ion magnetism (SIM) using POMs, reports using WD POMs are scarcer than the Keggin, Peacock-Weakley, or Anderson-Evans POMs [53,385]. Table 4 shows some examples of WD POMs and their magnetic properties.

Cubane-type (Mn<sup>III</sup><sub>3</sub>Mn<sup>IV</sup>O<sub>3</sub>X) assemblies constitute a well-known family of SMMs. Fang and co-workers condensed cubane-type

**Table 3**

Sensors constructed from WD POMs. Coordination water was omitted.

Compound	Substrate	Detection method	Detection limit [μM]	Linear range [μM]	Ref.
H <sub>10</sub> [Cu(bix) <sub>2</sub> (P <sub>2</sub> W <sub>18</sub> O <sub>62</sub> ) <sub>2</sub> ](bix) <sub>6</sub>	UA	Electrochemistry	0.497	0.259–679	[81]
[P <sub>2</sub> W <sub>17</sub> O <sub>61</sub> M] <sub>n</sub> ; M=Cu <sup>II</sup> , Fe <sup>III</sup> insertion during the electropolymerization of polypyrrole	Hydrogen peroxide	Electrochemistry	M=Cu <sup>II</sup> : 0.3 M=Fe <sup>III</sup> : 0.6	100–2000	[369]
K <sub>8</sub> P <sub>2</sub> W <sub>16</sub> V <sub>2</sub> O <sub>62</sub> and monodisperse bimetallic nanoparticles (Au–Pd)	DA, AA	Electrochemistry	DA: 0.83 AA: 0.43	DA: 2.1–2060 AA: 1.2–1610	[370]
FAD-GDH(C <sub>4</sub> H <sub>10</sub> N) <sub>6</sub> [P <sub>2</sub> Mo <sub>18</sub> O <sub>62</sub> ]/PMA /MWCNT	Glucose	Electrochemistry	–	1000–20000	[371]
(HDA) <sub>3</sub> (TBA) <sub>3</sub> P <sub>2</sub> W <sub>18</sub> O <sub>62</sub> (on GO)	Hydrogen peroxide	Electrochemistry	12.0	500–20000	[372]
αK <sub>8</sub> [P <sub>2</sub> W <sub>17</sub> O <sub>61</sub> Ni <sup>II</sup> H <sub>2</sub> O]	Protons	Electrochemistry	–	pH: 3–7	[373]
AgNPs@DHPA/GO/PGE	LD	Electrochemistry	0.00076	0.003–10	[374]
(H <sub>2</sub> N(CH <sub>3</sub> ) <sub>2</sub> ) <sub>10</sub> H <sub>3</sub> [SeO <sub>4</sub> Eu <sub>5</sub> (H <sub>2</sub> O) <sub>8</sub> ][Se <sub>2</sub> W <sub>14</sub> O <sub>52</sub> ]	Cu <sup>II</sup> Cys	Fluorescence	Cu <sup>II</sup> : 1.24 Cys: 0.217	Cu <sup>II</sup> : 10–250 Cys: 20–140	[149]
[Cu <sub>9</sub> (FKZ) <sub>12</sub> (H <sub>2</sub> O) <sub>8</sub> ][H <sub>3</sub> P <sub>2</sub> W <sub>18</sub> O <sub>62</sub> ] <sub>2</sub> /PPy	Hydrogen peroxide, AA	Colorimetry	H <sub>2</sub> O <sub>2</sub> : 0.07 AA: 0.627	–	[375]
MIL-101(Fe)@H <sub>6</sub> P <sub>2</sub> W <sub>18</sub> O <sub>62</sub> @SWNT	Hydrogen peroxide	Colorimetry	H <sub>2</sub> O <sub>2</sub> : 0.3 Glc: 0.2	H <sub>2</sub> O <sub>2</sub> : 80 Glc: 150	[376]
K <sub>8</sub> [CoP <sub>2</sub> W <sub>17</sub> O <sub>61</sub> ·H <sub>2</sub> O]·16H <sub>2</sub> O/CNTFs	Glucose, AA	Electrochemistry	Glc: 0.42 AA: 0.1	–	[377]
[(n-C <sub>3</sub> H <sub>7</sub> ) <sub>4</sub> N] <sub>4</sub> S <sub>2</sub> W <sub>18</sub> O <sub>62</sub> doped PEDOT	bromate	Chronoamperometry	–	100–2000	[378]

UA: uric acid; DA: dopamine; AA: ascorbic acid; Glc: glucose; LD: levodopa; bix: 1,4-bis(imidazol-1-ylmethyl)benzene; PEI: poly(ethylenimine); FAD-GDH: FAD-dependent glucose dehydrogenase; MWCNT: multiwalled carbon nanotube; HDA: hexadecyltrimethylammonium; GO: graphene oxide; DHPA: WD heteropolyacid; Cys: cysteine; HFKZ: 1-(2,4-difluorophenyl)-1,1-bis[(1H-1,2,4-triazol-1-yl)methyl] ethanol; ppy: polypyrrole; PGE: pencil graphite electrode; MIL-101(Fe): Tris [μ-[1,4-benzenedicarboxylato(2-)-κO1:κO'1]]chloro-μ3-oxotriiron; SWNT: single-walled carbon nanotube; CNTFs: carbon nanotube (CNTs) fibers; PEDOT: poly(3,4-ethylenedioxythiophene).

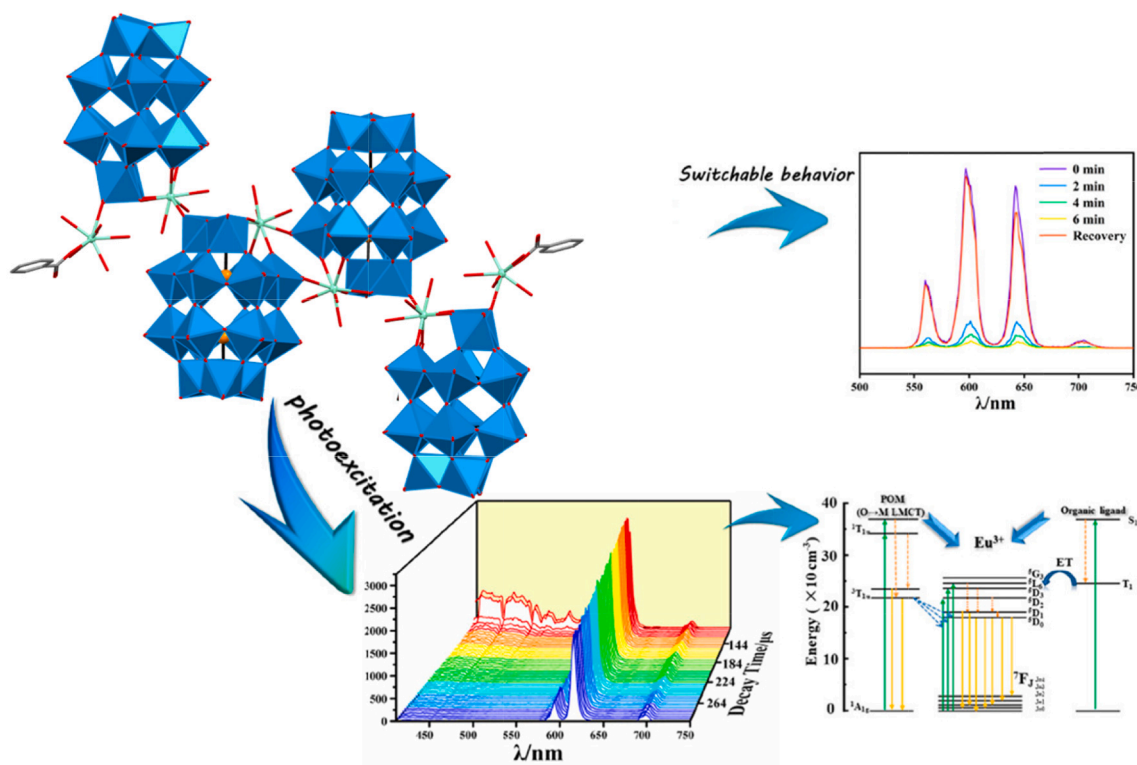


**Fig. 40.** Scheme of photoexcitation and switchable behavior observed for centrosymmetric tetrameric WD POMs containing samarium ions,  $[(P_2W_{17}O_{61})Sm(H_2O)_3Sm(C_6H_5COO)(H_2O)_6]_4[(P_2W_{17}O_{61})Sm(H_2O)_3]$ . Partially modified and reproduced from [104] with permission of the copyright holders.

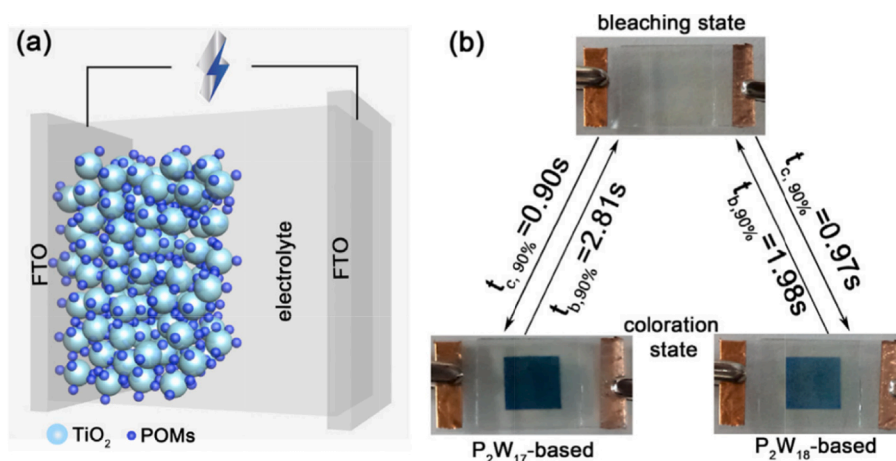


**Fig. 41.** (a) Structure of a POM-based smart window. (b) Images of POM-based smart windows at bleaching and coloration states. Reproduced from [384] with permission of the copyright holders.

$\text{Mn}^{\text{III}}\text{Mn}^{\text{IV}}\text{O}_4$  in the  $[\alpha\text{-P}_2\text{W}_{15}\text{O}_{56}]^{12-}$  lacunar plane to obtain a polyanion,  $[(\alpha\text{-P}_2\text{W}_{15}\text{O}_{56})\text{Mn}^{\text{III}}\text{Mn}^{\text{IV}}\text{O}_3(\text{CH}_3\text{COO})]^{8-}$  (Fig. 42, Compound 1) with a spin  $S = 9/2$  [188]. Surprisingly the polyanion did not exhibit any slowing of magnetization relaxation. The authors attributed the results to the existence of positive axial anisotropy  $D = +0.36 \text{ cm}^{-1}$  that led to the reverse order of the zero-field split substrates, and thus an absence of slow magnetization relaxation. Subsequently, the authors synthesized a sandwich-type polyanion,  $[(\alpha\text{-P}_2\text{W}_{15}\text{O}_{56})_2\text{Mn}^{\text{III}}\text{Mn}^{\text{IV}}\text{O}_6(\text{H}_2\text{O})_6]^{14-}$  [386] (Fig. 42, Compound 2), whose magnetic measurements revealed a system with a spin  $S=21/2$  and  $D = -0.143 \text{ cm}^{-1}$ . The formation of the sandwich-type structure restored the slow magnetization relaxation characteristics typical of  $[\text{Mn}_4\text{O}_4]^-$  based SMMs. The differences observed between these two compounds were attributed to the unexpected sign change in the  $D$  parameter, a consequence of a pronounced

dipole moment of 1 vs. the absence of a dipole moment in 2.

Two types of  $\text{P}_2\text{V}_3\text{W}_{15}$  WD POMs with a metalated ( $\text{M} = \text{Y}^{\text{III}}$ ,  $\text{Yb}^{\text{III}}$ ) phthalocyanine moiety (MPc) connected *via* an exposed organic linker (tris(alkoxo)pyridine) were synthesized by Pitt et al. A SQUID study of the resulting functionalized POMs confirmed intramolecular charge transfer between the MPc and the POM unit and the MPc of one molecule to the POM unit from another molecule [391].

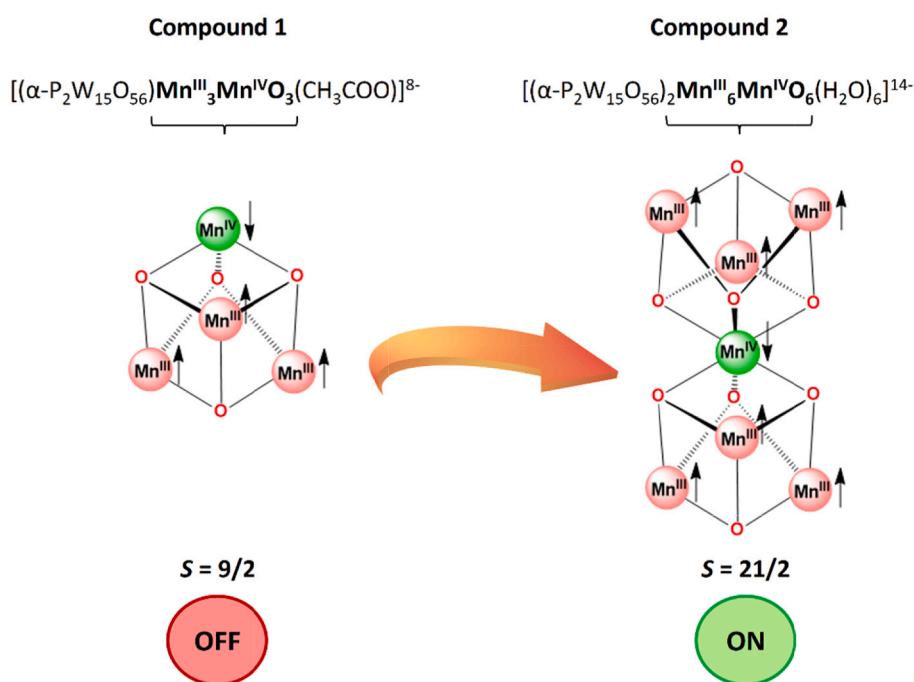
Magnetic properties of  $\text{Cs}_{7.5}\text{K}_{0.5}[(\text{H}_2\text{O})_7\text{Dy}_2^{\text{III}}(\alpha_2, \alpha_2' \cdot \text{P}_2\text{W}_{16}\text{O}_{60}) (\text{C}_6\text{H}_5\text{PO})_2]_{21} \cdot 42\text{H}_2\text{O}$  and  $\text{Cs}_{7.5}\text{K}_{0.5}[(\text{H}_2\text{O})_7\text{Y}^{\text{III}}]_{21}(\alpha_2, \alpha_2' \cdot \text{P}_2\text{W}_{16}\text{O}_{60}) (\text{C}_6\text{H}_5\text{PO})_2]_{21} \cdot 42\text{H}_2\text{O}$  (see [section 2.2.2](#)) were analyzed by Wang et al. and the magnetic susceptibility of the Dy derivative had the characteristics of a single ion magnet [200].

**Table 4**

Compounds based on WD POMs with magnetic properties.

Compound	Magnetic properties	Ref.
$\text{Na}_2(\text{C}_3\text{N}_2\text{H}_{12})_4[(\text{Ni}_5(\text{OH})_3(\text{H}_2\text{O})_4(\text{CH}_3\text{CO}_2))][\text{Si}_2\text{W}_{18}\text{O}_{66}]$	Antiferromagnetic interaction	[106]
$(\text{H}_2\text{bpz})_6[\text{Co}_2(\text{P}_2\text{W}_{16}\text{O}_{57})_2]^\text{a}$	Weak ferromagnetic exchange interaction between Co	[247]
$(\text{H}_2\text{bpz})_6[\text{Co}_3\text{H}_2(\text{P}_2\text{W}_{16}\text{O}_{57})(\text{P}_2\text{W}_{15}\text{O}_{56})$		
$(\text{C}_{16}\text{H}_{18}\text{N}_3\text{S})_5[\text{S}_2\text{Mo}_1^\text{V}\text{Mo}_7^\text{VI}\text{O}_{62}]\text{CH}_3\text{CN}$ .	Weak inter-cluster antiferromagnetic interaction	[120]
$\text{H}_4\text{Li}_6[\beta\text{-P}_2\text{CoW}_{17}\text{O}_{62}]$	Antiferromagnetic Co–Co coupling	[217]
$\text{Na}_{14}[(\alpha\text{-P}_2\text{W}_{15}\text{O}_{56})_2\text{Mn}_6^\text{III}\text{Mn}_6^\text{IV}\text{O}_6]$	Ferromagnetic	[386]
	$\text{Mn}^\text{III}$ – $\text{Mn}^\text{III}$ interaction and antiferromagnetic $\text{Mn}^\text{III}$ and $\text{Mn}^\text{IV}$ , SMM	
$\text{Na}_{32.5}\text{Rb}_{1.5}[\text{Ni}_{14}(\text{OH})_6(\text{H}_2\text{O})_{10}(\text{HPO}_4)_4(\text{P}_2\text{W}_{15}\text{O}_{56})_4]$	Coexistence of both ferro and antiferromagnetic coupling	[387]
$\text{Na}_{12}[\text{Mn}_4^\text{III}(\text{H}_2\text{O})_2(\text{P}_2\text{W}_{15}\text{O}_{56})_2]$	Antiferromagnetic interaction between the four $\text{Mn}^\text{III}$	[388]
$(\text{NH}_2\text{Me}_2)_{13}\text{Na}_3[(\text{Er}(\text{H}_2\text{O})(\text{CH}_3\text{COO})(\alpha\text{-P}_2\text{W}_{17}\text{O}_{61}))_2]$	Antiferromagnetic intramolecular dipolar interaction between the $\text{Er}^\text{III}$ ions	[389]
$\text{Na}(\text{NH}_4)_5[\text{P}_2\text{W}_{15}\text{O}_{56}\text{Ni}_3(\text{H}_2\text{O})_3(\mu\text{-OH})_3(\text{Re}(\text{CO})_3)_3]$	Ferromagnetic coupling	[390]
	interaction between adjacent $\text{Ni}^\text{II}$	
$(\text{nBu}_4\text{N})_4[\text{HP}_2\text{V}_3\text{W}_{15}\text{O}_{59}(\text{OCH}_2)_3\text{C}(\text{C}_5\text{H}_4\text{N})(\text{YC}_{32}\text{H}_{16}\text{N}_8)]$	Non-photoinduced charge transfer between electron donor and acceptor centers	[391]
$(\text{nBu}_4\text{N})_4[\text{HP}_2\text{V}_3\text{W}_{15}\text{O}_{59}(\text{OCH}_2)_3\text{C}(\text{C}_5\text{H}_4\text{N})(\text{YbC}_5\text{H}_4\text{N}_8)]$		
$\text{Cs}_{7.5}\text{K}_{0.5}[(\text{H}_2\text{O})_7\text{Dy}^\text{III}_2(\alpha_2, \alpha'_2\text{-P}_2\text{W}_{16}\text{O}_{60})(\text{C}_6\text{H}_5\text{PO})_2] \cdot 42\text{H}_2\text{O}$	Two predominant slow relaxation process ranges at separate temperature intervals	[200]

Bpz: 3,3',5,5'-tetramethyl-4,4'-bipyrazole.

**Fig. 42.** Scheme of the proposed spin arrangement in the ground state for Compound 1 and 2.

#### 6.4. Biology/Medicine

Tunable POM-macromolecular interaction results from the modification of the POM structure, such as adjustment of electronic properties of acidity or polarity, POM encapsulation, post-functionalization with organic molecules or with metals and other species, and it has inspired several studies on the use of these compounds as therapeutic agents such as for Alzheimer's disease, antibacterial, anticancer, and the like (Table 5).

##### 6.4.1. Anticancer activity

Numerous studies have been reported using POMs as potential anticancer drugs [71]. Antitumor activity against various tumor cell types has been found using inorganic WD POMs [392,393], WD organometallic hybrids [394,395] or WD POMs encapsulated in covalent [396] and supramolecular [397,398] polymeric networks. The proposed mechanisms of POM antitumor activity are diverse and are still under discussion/being investigated [71]. However, WD POMs inhibit processes that play pivotal roles in the proliferation of several types of

cancer, for example in angiogenesis (in particular through binding the fibroblast growth factor [399], CK2 inhibitors [400], inhibition of the DNA-binding activity of AP-2gamma [393] and Sox2 [401], or aquaporin-3 (AQP3) activity [402]. These studies have shown that the size and type of POMs affect inhibitory activity, and the WD type was one of the most efficient inhibitors compared to other POM types.

Additionally, a gadolinium-containing WD POM ( $\text{Gd}_2\text{P}_2\text{W}_{18}\text{O}_{62}$ ) was evaluated *in vitro* and *in vivo* as a magnetic resonance imaging (MRI) contrast agent [229]. Recent studies on WD POMs in combined photothermal and immune anticancer therapy (PTT) show promising results. The authors presented *in vivo* and *in vitro* studies on  $\text{P}_2\text{Mo}_{18}\text{O}_{62}$  in the free form and in a gellan gum hydrogel formulation. Moreover, POM hydrogel incorporation into resiquimod (R848) showed a synergy effect against the 4 T1 cell line. Photothermal agent R848/POM@GG is stable in water, degrades to a nontoxic form in the physiological environment and minimizes POM toxicity against normal tissues [403].

##### 6.4.2. Antibacterial activity

Similarly, it has also been observed that POMs have interesting

**Table 5**Activity of selected WD POMs in the *in vitro* and *in vivo* experiments.

POM	Cell line	Activity	Ref.
Na <sub>6</sub> [P <sub>2</sub> Mo <sub>18</sub> O <sub>62</sub> ]	KB	IC <sub>50</sub> = 34.5 μg/mL	[392]
Na <sub>6</sub> [As <sub>2</sub> Mo <sub>18</sub> O <sub>62</sub> ]	KB	IC <sub>50</sub> = 52.3 μg/mL	
Na <sub>12</sub> [P <sub>2</sub> W <sub>15</sub> O <sub>56</sub> ]·24H <sub>2</sub> O	HeLa	cell viability- 85%	[398]
	MCF-7	cell viability- 79%	
	Vero	cell viability- 37%	
PMAA-ChCl-[P <sub>2</sub> W <sub>15</sub> O <sub>56</sub> ]	HeLa	cell viability- 75%	
	MCF-7	cell viability- 77%	
	Vero	cell viability- 15%	
PMAA-CMCh-[P <sub>2</sub> W <sub>15</sub> O <sub>56</sub> ]	HeLa	cell viability- 68%	[397]
	MCF-7	cell viability- 72%	
	Vero	cell viability- 10%	
K <sub>4</sub> H <sub>3</sub> [(CH <sub>3</sub> OOCCH <sub>2</sub> CH <sub>2</sub> Sn)P <sub>2</sub> W <sub>17</sub> O <sub>61</sub> ]· 11H <sub>2</sub> O	HeLa	IC <sub>50</sub> = 90.2 μg/mL	[394]
	SSMC-7721	IC <sub>50</sub> = 86.3 μg/mL	
K <sub>4</sub> H <sub>3</sub> [(CH <sub>3</sub> OOCCH(CH <sub>3</sub> )CH <sub>2</sub> Sn) P <sub>2</sub> W <sub>17</sub> O <sub>61</sub> ]·11H <sub>2</sub> O	HeLa	IC <sub>50</sub> = 86.7 μg/mL	
	SSMC-7721	IC <sub>50</sub> = 79.1 μg/mL	
K <sub>7</sub> H <sub>2</sub> [(CpTi) <sub>3</sub> P <sub>2</sub> W <sub>15</sub> O <sub>59</sub> ]·5H <sub>2</sub> O	HeLa	IC <sub>50</sub> = 47.2 μg/mL	[395]
	SSMC-7721	IC <sub>50</sub> = 20.8 μg/mL	
(Bu <sub>4</sub> N) <sub>9</sub> [(CpZr) <sub>3</sub> P <sub>2</sub> W <sub>15</sub> O <sub>59</sub> ]	HeLa	IC <sub>50</sub> = 63.3 μg/mL	
	SSMC-7721	IC <sub>50</sub> = 40.6 μg/mL	
K <sub>4</sub> H <sub>5</sub> [(CH <sub>3</sub> OOCCH <sub>2</sub> CH <sub>2</sub> Sn) <sub>3</sub> P <sub>2</sub> W <sub>15</sub> O <sub>59</sub> ]· 10H <sub>2</sub> O	HeLa	IC <sub>50</sub> = 50.1 μg/mL	
	SSMC-7721	IC <sub>50</sub> = 30.6 μg/mL	
K <sub>4</sub> H <sub>5</sub> [(CH <sub>3</sub> OOCCH(CH <sub>3</sub> ) CH <sub>2</sub> Sn) <sub>3</sub> P <sub>2</sub> W <sub>15</sub> O <sub>59</sub> ]·10H <sub>2</sub> O	HeLa	IC <sub>50</sub> = 48.3 μg/mL	
	SSMC-7721	IC <sub>50</sub> = 30.1 μg/mL	
α <sub>2</sub> -K <sub>7</sub> [P <sub>2</sub> W <sub>17</sub> (NbO <sub>2</sub> )O <sub>61</sub> ]·13H <sub>2</sub> O	HeLa	cell viability- 10.0%	[413]
TMC-[P <sub>2</sub> W <sub>17</sub> (NbO <sub>2</sub> )O <sub>61</sub> ]	HeLa	cell viability- 5.0%	
[(n-C <sub>4</sub> H <sub>9</sub> ) <sub>4</sub> N] <sub>6</sub> [P <sub>2</sub> W <sub>18</sub> O <sub>62</sub> ]	CT26	cell viability- 80.0%	
	MC38	cell viability- 80.0%	[30]
	CT26 – tumor- bearing mice	TGI 55.5%	
	MC38 – tumor- bearing mice	TGI 64.3%	

**Table 5 (continued)**

POM	Cell line	Activity	Ref.
[P <sub>2</sub> W <sub>18</sub> O <sub>62</sub> ]@Hf <sub>12</sub> -DBB-Ir	CT26	IC <sub>50</sub> = 3.21 μM	
	MC38	IC <sub>50</sub> = 2.51 μM	
	CT26 – tumor- bearing mice	TGI- 99.7%	
	MC38 – tumor- bearing mice	TGI- 99.0%	
(NH <sub>4</sub> ) <sub>6</sub> [P <sub>2</sub> Mo <sub>18</sub> O <sub>62</sub> ]·14H <sub>2</sub> O	4 T1	cell viability- 90.0%	[403]
[P <sub>2</sub> Mo <sub>18</sub> O <sub>62</sub> ]@GG	4 T1 – tumor- bearing mice	inhibition rate- 90.0%	
R848/[P <sub>2</sub> Mo <sub>18</sub> O <sub>62</sub> ]@GG	4 T1 – tumor- bearing mice	inhibition rate- 99.3%	
K <sub>6</sub> [P <sub>2</sub> W <sub>18</sub> O <sub>62</sub> ]·14H <sub>2</sub> O	PC12	cell viability- 95.0%	[408]
K <sub>8</sub> [P <sub>2</sub> W <sub>17</sub> O <sub>61</sub> (Co <sup>II</sup> -OH <sub>2</sub> )]·16H <sub>2</sub> O		cell viability- 90.0%	
K <sub>8</sub> [P <sub>2</sub> W <sub>17</sub> O <sub>61</sub> (Ni <sup>II</sup> -OH <sub>2</sub> )]·17H <sub>2</sub> O		cell viability- 95.0%	
Aβ- K <sub>6</sub> P <sub>2</sub> W <sub>18</sub> O <sub>62</sub>		cell viability- 80.8%	
Aβ- K <sub>6</sub> P <sub>2</sub> W <sub>18</sub> O <sub>62</sub> -Co		cell viability- 90.0%	
Aβ- K <sub>6</sub> P <sub>2</sub> W <sub>18</sub> O <sub>62</sub> -Ni		cell viability- 105.0%	
Aβ- K <sub>6</sub> P <sub>2</sub> W <sub>18</sub> O <sub>62</sub> @AuNPs	PC12	cell viability- 65.0%	[409]
Aβ- K <sub>6</sub> P <sub>2</sub> W <sub>18</sub> O <sub>62</sub> @AuNPs-pep		cell viability- 90.0%	[411]
MSNs-K <sub>5</sub> P <sub>2</sub> W <sup>V</sup> W <sup>VI</sup> <sub>17</sub> O <sub>62</sub> -copolymer	PC12	cell viability- 92.6%	
MSNs- K <sub>5</sub> P <sub>2</sub> W <sup>V</sup> W <sup>VI</sup> <sub>17</sub> O <sub>62</sub> -copolymer upon NIR irradiation		cell viability- 54.8%	[407]
K <sub>8</sub> [P <sub>2</sub> CoW <sub>17</sub> O <sub>61</sub> ]	PC12	cell viability- 90.0%	
CeONP-K <sub>6</sub> P <sub>2</sub> W <sub>18</sub> O <sub>62</sub>	PC12	cell viability- 75.0%	[410]

PMAA-ChCl: poly(methacrylic acid)-chitosan hydrochloride; PMAA-CMCh: poly(methacrylic acid)-carboxymethyl chitosan; TMC: trimethyl chitosan; DBB: 4,4'-di(4-benzoato)-2,2'-bipyridine; R848: resiquimod; GG: gellan gum hydrogel; pep: peptide CLPFFD; CeONP: cerium oxide nanoparticles.

antibacterial properties [404]. In particular, the WD type has shown synergy effects with conventional antibiotics such as β-lactam antibiotics against *Staphylococcus aureus* [405,406].

In addition to the anticancer and antibacterial effects, transition metal-substituted WD POMs (K<sub>7</sub>P<sub>2</sub>W<sub>17</sub>O<sub>61</sub>M; M = Co<sup>II</sup>, Ni<sup>II</sup>) have shown the greatest inhibition effect on amyloid β (Aβ) aggregation and Aβ-heme peroxidase-like activity (critical steps in the development of Alzheimer's disease) [407,408]. WD POM-type structures built on nanoplatform-like gold nanoparticles (AuNPs), mesoporous silica nanoparticles (MSNs) or cerium oxide nanoparticles (CeONPs) were used as novel Aβ inhibitors [409–411]. WD POMs built in MSNs were successfully used in the photothermal treatment of AD. Under NIR laser illumination, a POM nanohybrid inhibited and disaggregated Aβ fibers, as well as crossed the blood–brain-barrier [411]. Co- and Ni-substituted



POMs showed greater inhibitory effects on amyloid A $\beta$  aggregation than a WD POM substituted with Mn<sup>III</sup>, Cu<sup>II</sup>, Fe<sup>II</sup> or a non-substituted WD, or other types of POMs such as Kegging or Anderson.

In addition to the anticancer properties of this type of POMs, it has been recently found that the hierarchical assembly of nMOFs incorporating WD POMs acts as a multifarious radio-enhancer for anticancer therapy [412]. The hierarchical assembly of nMOFs consists of Hf-based metalloxo clusters, an Ir-based bridging ligand, and a WD POM. It has been shown that this system acts as a radioelectric enhancer for the efficient generation of reactive oxygen species (ROSS), showing an excellent antitumor effect on colon cancer tumor models (MC38 and CT26 cell lines). The assembly facilitated synergy interactions among high-Z components, generating three types of ROSS: hydroxyl radicals ( $\cdot\text{OH}$ ) through the radiolysis of water, singlet oxygen ( $^1\text{O}_2$ ) through the photosensitization of DBB-Ir, and superoxide formation through  $\text{W}_{18}$  (Fig. 43).

The biological application of WD POMs is often related to their inhibition activity toward PMCA  $\text{Ca}^{II}$  and SERCAATPase [414]. The inhibitory effect against AbPPO4 has been tested on intact, mono-, tri- and hexa-lacunary forms of WD POMs. The monolacunary form,  $[\alpha_2\text{-P}_2\text{W}_{17}\text{O}_{61}]^{10-}$ , retains its structural integrity and exhibits the strongest inhibition of AbPPO4 ( $K_i = 6.5 \text{ mM}$ ), while the trilacunary type rearranges to a more stable monolacunary form and shows the weakest inhibition [415].

A number of studies with WD POM types have proved their antiviral effect. A screening study of POMs for anti-HIV-1 and HIV-2 activity demonstrated that organic moieties enhanced the inhibitory potential [416–418].

Interestingly, WD structures were also used as additive agents in protein crystallization [404].  $\text{K}_6[\text{P}_2\text{W}_{18}\text{O}_{62}]$  bound RNA polymerase II during speciation chain elongation and was successfully used for phasing a large protein [419]. In the recent study Leyssens et al. also presented the use of the  $\text{K}_{10}[\alpha_2\text{-P}_2\text{W}_{17}\text{O}_{61}] \cdot 20\text{H}_2\text{O}$  WD POM and the hafnium(IV)-substituted WD POM,  $\text{K}_{16}[\text{Hf}(\alpha_2\text{-P}_2\text{W}_{17}\text{O}_{61})_2] \cdot 19\text{H}_2\text{O}$ , as contrast-enhancing staining agents in X-ray microfocus computed tomography [420]. Imaging of rat, porcine and human blood vessels revealed microstructural differences between the type of blood vessels, which may be useful in computer modeling for future graft material design and for understanding the function of blood vessels and improving current disease treatments.

## 7. Conclusions and perspectives

Over the past two decades, we have seen dynamic development in the field of WD POMs which, when functionalized, lend themselves to easy post-functionalization with other organic or inorganic molecules, leading to advanced material design and an extensive range of applications. In this review, we have discussed the possibilities for the functionalization of the WD POM basic subunit and classified them according to modifications made in respective structural parts: templates/heteroatoms, addenda atoms (CAP modification: trilacunary and monolacunary, and belt modification) and non-conventional WD POM motifs (open and sandwich-type WD POMs). The review also presents an analysis of speciation in solution and includes ion distribution plots over a wide pH range for WD POMs, knowledge of which is essential for further modifications, as suboptimal selection of reaction conditions such as pH in the first place can prove detrimental to the WD POM subunit. In addition, the ionic interactions of negatively charged WD POM subunits with counter cations are also shown. As part of this review, we also discussed the path of further post-functionalization of the currently available hybrid WD POM platforms and classified them based on the available post-functionalization approaches into single and double linker modularities and the other different linker modularities, such as polymers with POMs. This review reveals how WD POM post-functionalization can generate materials with new and/or improved physicochemical properties with a significant impact on the development of their applications in the following scientific fields: energy-related applications, catalysis (photocatalysis, electrocatalysis), functional materials (sensors, optical materials, electrochromic materials, magnetic materials), biology/medicine (anticancer and antibacterial activity).

Additionally, to better illustrate the current trends and present less researched aspects of this field, we include below data from a meta-analysis of studies on WD POMs. Owing to the bibliometric data available in the Scopus database a network constructed on the basis of keywords can be generated, searching the latest scientific and technological developments regarding WD POMs. In the field of science and technology, the Scopus database was used, searching “Wells-Dawson” and “structure” (Fig. 44), “Wells-Dawson” and “properties” (Fig. 45) as combined keywords, in articles published until May 2024.

Duplicate papers found in more than one of the databases that did not focus on the selected keywords were excluded. VOSviewer software version 1.6.20 (<https://www.vosviewer.com>) was used to analyze the

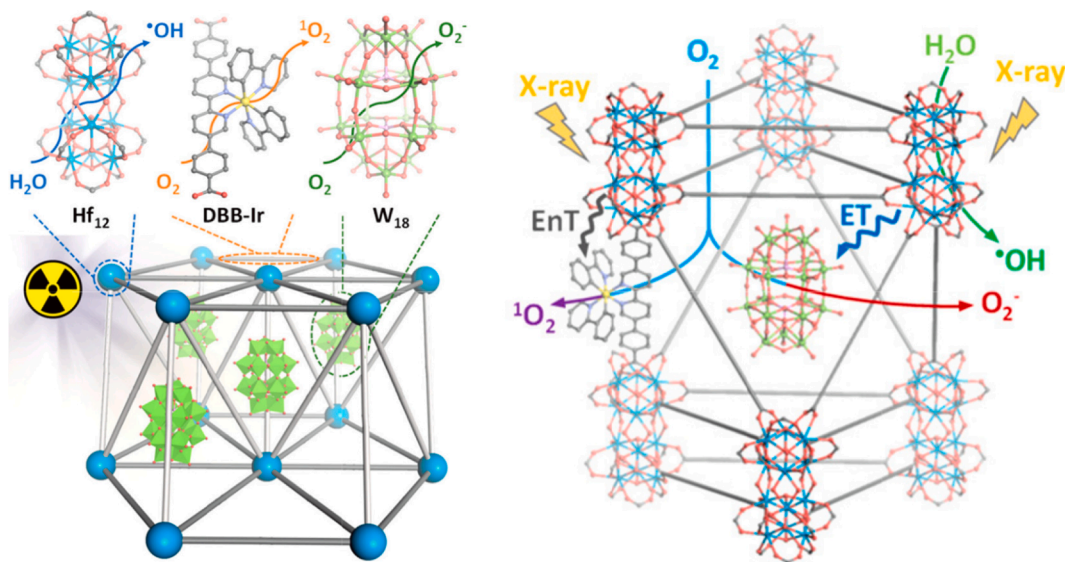


**Fig. 43.** The assembly of nMOF consisting of Hf-based metalloxo clusters ( $\text{Hf}_{12}$ ), an Ir-based bridging ligand (DBB-Ir), and a WD POM ( $\text{W}_{18}$ ) and mechanisms of ROS generation. EnT: energy; ET: electron transfer. Reproduced from [412] with permission of the copyright holders.

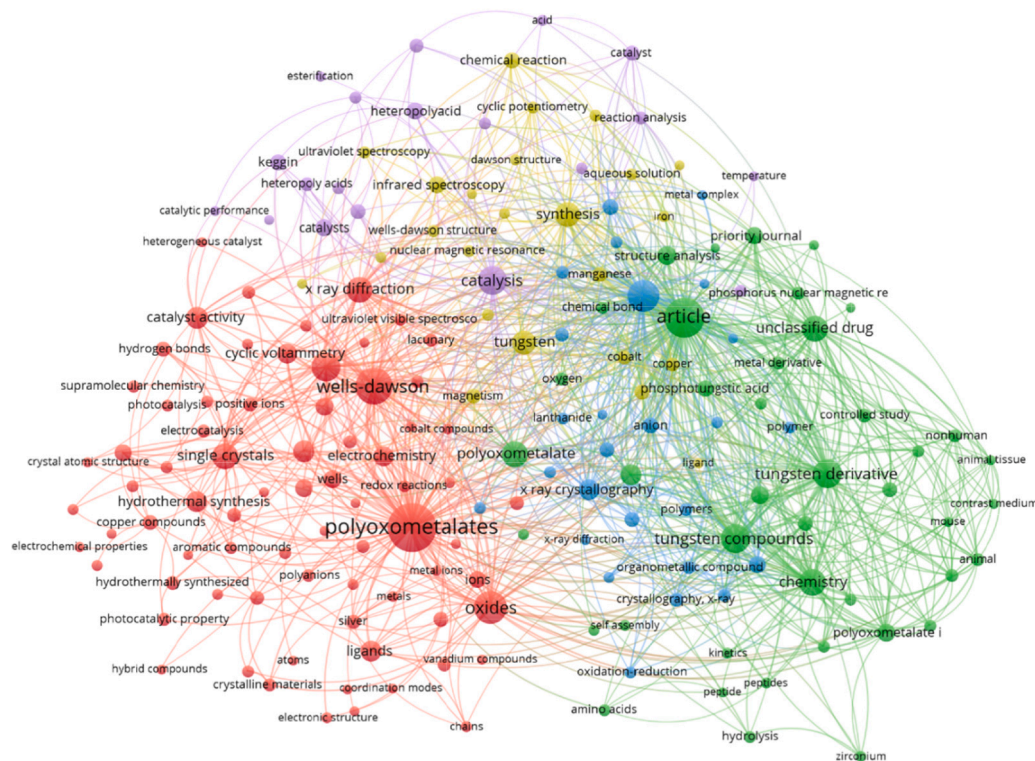


**Fig. 44.** A bibliometric map obtained with VOSviewer version 1.6.20 (<https://www.vosviewer.com>) [421] using “Wells-Dawson” and “structure” as keywords, recorded from the Scopus database.

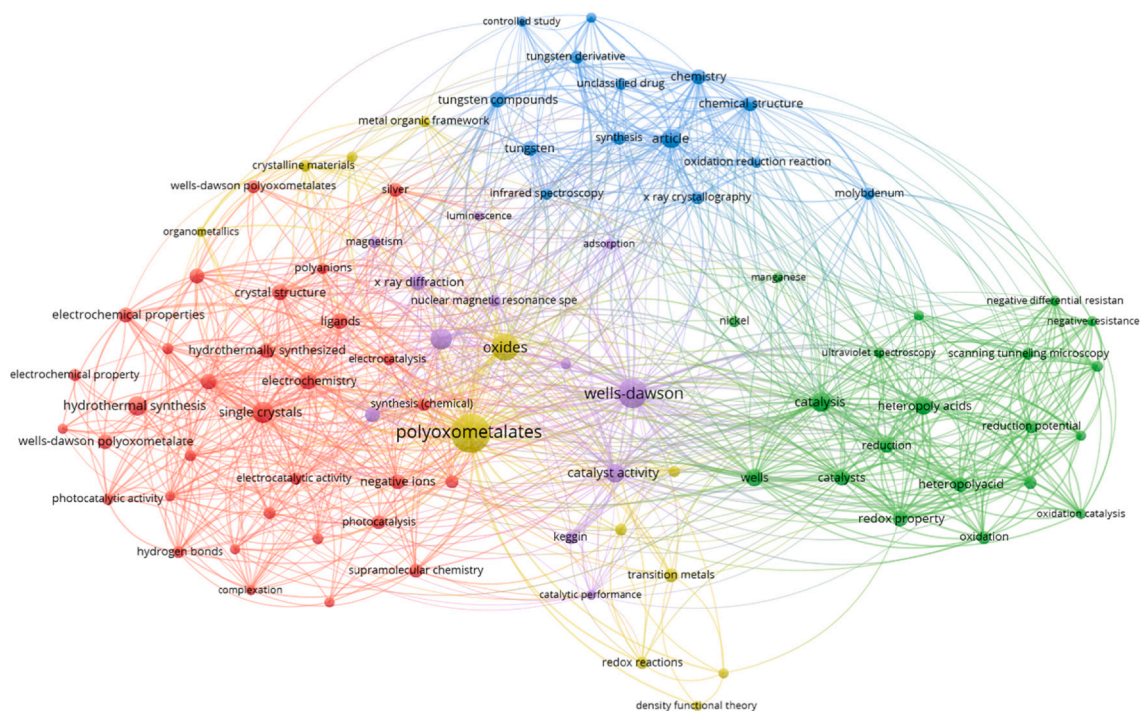


**Fig. 45.** A bibliometric map obtained with VOSviewer version 1.6.20 (<https://www.vosviewer.com>) [421] using “Wells-Dawson” and “properties” as keywords, recorded from the Scopus database.

data and generate the bibliometric maps [421]. Each keyword is represented by a circle and the lines show the frequency and relationships between them; the larger the circle, the more often the keyword appeared in publications. The keywords are assigned to a cluster, each cluster corresponding to a different research area and shown in a

different color. The combined “Wells-Dawson” and “structure” search gave five main clusters (Fig. 44), focusing mainly on (i) single crystals, X ray diffraction (red, 75 items), (ii) tungsten derivatives, unclassified drug (green, 42 items), (iii) chemical structure, metal complexes (blue, 26 items), (iv) synthesis (yellow, 24 items) and (v) catalysis (purple, 19



items). For the second network, the combination of “Wells-Dawson” and “properties” search recorded five main clusters (Fig. 45), focusing mainly on (i) single crystals, electrochemical properties (red, 32 items), (ii) catalysis, heteropoly acids (green, 20 items), (iii) synthesis, tungsten compounds (blue, 14 items), (iv) oxides, transition metals (yellow, 12 items) and (v) catalyst activity (purple, 12 items). The above meta-analysis clearly shows that mainly the archetypical tungsten WD POMs were employed for majority of the studies, but the hybrid systems are gaining more attention. Efficient protocols for integration with *d-/f*-block metal ions, small molecules or even polymers was demonstrated, therefore means necessary for improvement of the desired properties are already known. The concepts of supramolecular chemistry seem to be the another promising option to explore in this manner. Integration of WD POMs with MOFs was demonstrated and should be expanded into other well-defined porous materials such as Covalent Organic Frameworks (COFs). Tunable redox properties and acid/base character confer to the most often explored catalytic applications, including photo- and electrocatalysis. Whereas WD POMs can improve the properties of lithium-ion batteries, their application in sodium/zinc/aluminum-based energy storage systems is yet to be demonstrated. Finally, significant amount of WD POM studies targeted their biological properties, as anticancer and antibacterial agents or for their interactions with proteins. The latter can be potentially used in tackling the neurodegenerative diseases, but it remains to be seen *in vivo*.

Based on the research conducted so far, we expect that in the coming years, advances in the functionalization and post-functionalization approaches to WD POM subunits will further improve their physico-chemical properties and increase their importance in their downstream applications. However, for this to happen there are several challenges to overcome. One of the limitations associated with the synthesis is the presence of oxo groups on the WD POM surface, which can only bind to a

limited number of organic groups to form hybrid materials for further post-functionalization. In addition, the WD POM subunit itself has poor chemical stability, and conducting a chemical reaction in which the reactant is based on the POM subunit is limited by the pH value. Therefore, the rational design and synthesis of new WD POM hybrids that can combine WD POM subunits containing oxide groups with organic or inorganic linkers that enable further functionalization is the key task in advanced engineering, carrying the prospect of obtaining materials with excellent and improved properties that could be used in many scientific fields. A great advantage of WD POM-based materials is their ability to modify their acid-base and redox properties by changing their chemical composition, and their ability to accept and release electrons. In addition, WD POM hybrids have unique properties such as well-defined structure or Brønsted acidity. These features as well as the ability to modify and introduce suitable linkers will be crucial to improve electrochemical properties manifested in improved energy storage and delivery capabilities, and will also make WD POM hybrids even better catalysts for many chemical reactions. In addition, the applications of WD POM hybrids in biology and medicine are largely due to their shape and negative surface charge, resulting in specific interactions with various biomolecules, and further optimization of the charge and shape of the subunits could minimize potential toxicity and improve *in vivo* stability.

The most important features of WD-POMs and how they transform into the desired properties that have been discussed in this review are summarized in Fig. 46.

The future may bring even more POM-based applications, given the available strategies and the rapid development and progress in designing novel functionalizations of the WD POM subunit, so that the potential of WD POMs in various domains of technology could be fully leveraged.

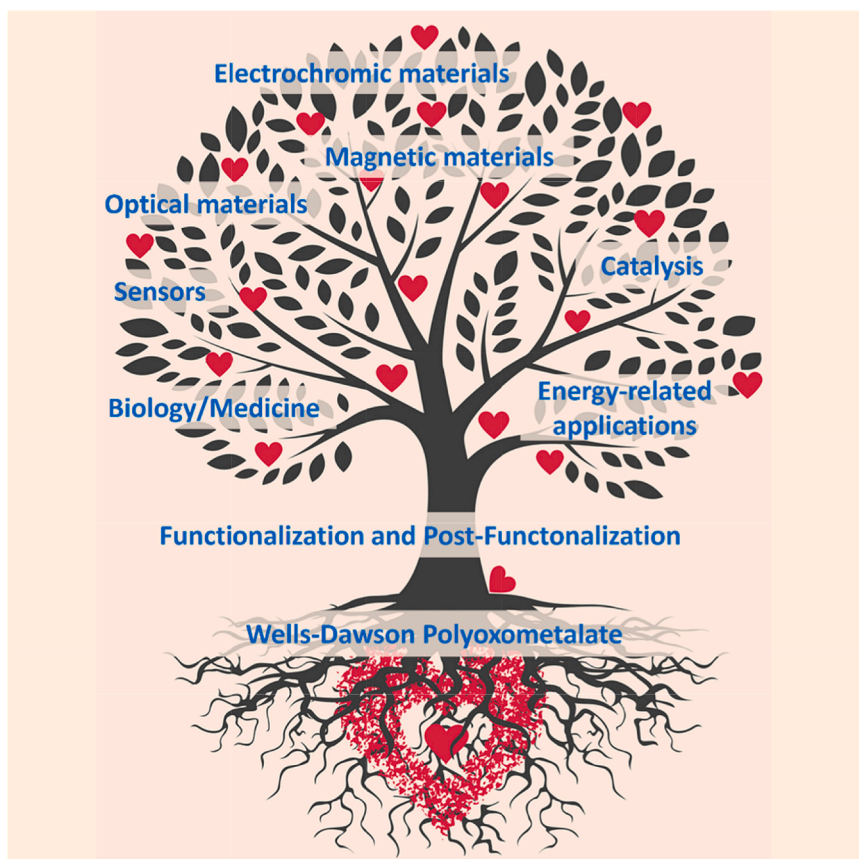


**Fig. 46.** Schematic visualization of a tree in which the roots of the WD POM expand into the tree trunk, and from there the respective closely related branches represent various applications.

## Declaration of competing interest

The authors declare that they have no known competing financial interests or personal relationships that could have appeared to influence the work reported in this paper.

## Data availability

Data will be made available on request.

## Acknowledgements

This work was supported by the National Science Centre, Poland (grant numbers UMO-2022/45/N/ST4/00632 (D.N.), UMO-2020/39/D/ST4/01182 (A.G.), UMO-2022/44/C/ST4/00017 (E.W.-S.), 2022/47/B/ST4/02310 (V.P.)). Daria Nowicka is a scholarship holder of the Adam Mickiewicz University in Poznan Foundation for the 2023/2024 academic year. Adam Gorczyński is a scholarship holder of the Polish Ministry of Education and Science for outstanding young scientists.

## References

- [1] N.I. Gumerova, A. Rompel, *Nat. Rev. Chem.* 2 (2018) 0112.
- [2] A.V. Anyushin, A. Kondinski, T.N. Parac-Vogt, *Chem. Soc. Rev.* 49 (2020) 382–432.
- [3] J.-X. Liu, X.-B. Zhang, Y.-L. Li, S.-L. Huang, G.-Y. Yang, *Coord. Chem. Rev.* 414 (2020) 213260.
- [4] M. Hutin, M. Rosnes, D.-L. Long, L. Cronin, *Comprehensive Inorganic Chemistry II* (second edition): From Elements to Applications, 2 (2013) 241–269.
- [5] M. Aureliano, N.I. Gumerova, G. Sciortino, E. Garribba, C.C. McLauchlan, A. Rompel, D.C. Crans, *Coord. Chem. Rev.* 454 (2022) 214344.
- [6] R. Sheng, R. Sun, L. Chen, R. Lv, Y. Li, T. Du, Y. Zhang, Y. Qi, *Crit. Rev. Anal. Chem.* 54 (2024) 315–332.
- [7] B. Yu, X. Zhao, J. Ni, F. Yang, *Chem. Phys. Mater.* 2 (2023) 20–29.
- [8] N. Ogiwara, T. Iwano, T. Ito, S. Uchida, *Coord. Chem. Rev.* 462 (2022) 214524.
- [9] J.M. Cameron, G. Guillemot, T. Galambos, S.S. Amin, E. Hampson, K. Mall Haidaraly, G.N. Newton, G. Izzet, *Chem. Soc. Rev.* 51 (2022) 293–328.
- [10] C. Dey, *J. Clust. Sci.* 33 (2022) 1–18.
- [11] M.J.W. Budyk, K. Staszak, A. Bajek, F. Pniewski, R. Jastrzab, M. Staszak, B. Tylkowski, K. Wieszczycka, *Coord. Chem. Rev.* 493 (2023) 215306.
- [12] Y. Zhang, Y. Li, H. Guo, Y. Guo, H.N. Miras, D.L. Long, L. Xu, L. Cronin, *Chemistry (Weinheim an der Bergstrasse, Germany)* 17 (2011) 7472–7479.
- [13] G. Izzet, B. Abécassis, D. Brouiri, M. Piot, B. Matt, S.A. Serapian, C. Bo, A. Proust, *J. Am. Chem. Soc.* 138 (2016) 5093–5099.
- [14] L. Vandebroek, Y. Mampaey, S. Antonyuk, L. Van Meervelt, T.N. Parac-Vogt, *Eur. J. Inorg. Chem.* 2019 (2019) 506–511.
- [15] Y. Gao, M. Choudhary, G.K. Such, C. Ritchie, *Chem. Sci.* 13 (2022) 2510–2527.
- [16] M.-T.-K. Ng, N.L. Bell, D.-L. Long, L. Cronin, *J. Am. Chem. Soc.* 143 (2021) 20059–20063.
- [17] I. Lindqvist, *Acta Crystallogr.* 5 (1952) 667–670.
- [18] J.F. Keggin, *Nature* 132 (1933) 351.
- [19] B. Dawson, *Acta Crystallogr.* 6 (1953) 113–126.
- [20] D.D. Dexter, J.V. Silverton, *J. Am. Chem. Soc.* 90 (1968) 3589–3590.
- [21] J.A. Fernández, X. López, C. Bo, C. de Graaf, E.J. Baerends, J.M. Poblet, *J. Am. Chem. Soc.* 129 (2007) 12244–12253.
- [22] H.T. Evans, *J. Am. Chem. Soc.* 70 (1948) 1291–1292.
- [23] J.S. Anderson, *Nature* 140 (1937) 850.
- [24] Y. Zhang, J. Liu, S.-L. Li, Z.-M. Su, Y.-Q. Lan, *Energy Chem.* 1 (2019) 100021.
- [25] L.E. Briand, G.T. Baronetti, H.J. Thomas, *Appl. Catal. A: Gen.* 256 (2003) 37–50.
- [26] S.-S. Wang, G.-Y. Yang, *Chem. Rev.* 115 (2015) 4893–4962.
- [27] Q. Hu, K. Li, X. Chen, Y. Liu, G. Yang, *Polyoxometalates 3* (2024) 9140048.
- [28] Z. Wei, S. Ru, Q. Zhao, H. Yu, G. Zhang, Y. Wei, *Green Chem.* 21 (2019) 4069–4075.
- [29] G. Dai, Q. Li, D. Zang, Y. Wei, *Green Chem.* 25 (2023) 6263–6269.
- [30] H. Yu, Q. Zhao, Z. Wei, Z. Wu, Q. Li, S. Han, Y. Wei, *Chem. Commun.* 55 (2019) 7840–7843.
- [31] Y.-F. Liu, C.-W. Hu, G.-P. Yang, *Chin. Chem. Lett.* 34 (2023) 108097.
- [32] Y. Liu, G. Zeng, Y. Cheng, L. Chen, Y. Liu, Y. Wei, G. Yang, *Chin. Chem. Lett.* 35 (2024) 108480.
- [33] X. Gao, R. Ma, Z. Liu, S. Wang, Y. Wu, G. Song, *Appl. Catal. B: Environ. Energy* 352 (2024) 124059.
- [34] Q. Hu, H. Zhou, Y. Ding, T. Wågberg, X. Han, *ACS Catal.* 14 (2024) 5898–5910.
- [35] A. Ebrahimi, L. Krivosudský, A. Cherevan, D. Eder, *Coord. Chem. Rev.* 508 (2024) 215764.
- [36] Y.-F. Liu, X.-L. Lin, B.-M. Ming, Q.-L. Hu, H.-Q. Liu, X.-J. Chen, Y.-H. Liu, G.-P. Yang, *Inorg. Chem.* 63 (2024) 5681–5688.
- [37] X. Wei, Y. Jiang, Y. Ma, H. Liao, S. Dai, P. An, Z.-Q. Wang, X.-Q. Gong, Z. Hou, *ACS Catal.* 14 (2024) 5344–5355.
- [38] J.M. Cameron, S. Fujimoto, K. Kastner, R.-J. Wei, D. Robinson, V. Sans, G. N. Newton, H.H. Oshio, *Chem. – Eur. J.* 23 (2017) 47–50.
- [39] N. Shi, Y. Ding, N. Li, F. Wen, D. Liu, *J. Environ. Chem. Eng.* 11 (2023) 110558.
- [40] S. Li, N. Li, G. Li, Y. Ma, M. Huang, Q. Xia, Q. Zhao, X. Chen, *Polyoxometalates 2* (2023) 9140024.
- [41] C. Gu, C. Li, N. Minezawa, S. Okazaki, K. Yamaguchi, K. Suzuki, *Nanoscale* 16 (2024) 8013–8019.
- [42] J.-Y. Zhang, Y. Song, J. Yang, W.-Y. Pei, J.-F. Ma, *Inorg. Chem. Front.* 11 (2024) 3011–3020.
- [43] S. Fu, S. Ullah Khan, R. Yang, H. Pang, C.-M. Au, H. Ma, X. Wang, G. Yang, W. Sun, W.-Y. Yu, *J. Colloid Interface Sci.* 666 (2024) 496–504.
- [44] K. Talbi, F. Penas-Hidalgo, A.L. Robinson, P. Gotico, W. Leibl, P. Mialane, M. Gomez-Mingot, M. Fontecave, A. Solé-Daura, C. Mellot-Draznieks, A. Dolbecq, *Appl. Catal. B: Environ. Energy* 345 (2024) 123681.
- [45] Y. Yang, K. Guo, M. Zhu, A. Zhang, M. Xing, Y. Lu, X. Bai, X. Ji, Y. Hu, S. Liu, *Inorg. Chem.* 63 (2024) 7876–7885.
- [46] M. Yamaguchi, K. Shioya, C. Li, K. Yonesato, K. Murata, K. Ishii, K. Yamaguchi, K. Suzuki, *J. Am. Chem. Soc.* 146 (2024) 4549–4556.
- [47] J.M. Clemente-Juan, E. Coronado, A. Gaita-Ariño, *Chem. Soc. Rev.* 41 (2012) 7464–7478.
- [48] Z.-X. Yang, F. Gong, D. Lin, Y. Huo, *Coord. Chem. Rev.* 492 (2023) 215205.
- [49] L. Martínez, P. Alborés, *Eur. J. Inorg. Chem.* 27 (2024) e202300687.
- [50] D.R.M. Clyde, D.L. Cortie, S. Granville, D.C. Ware, P.J. Brothers, J. Malmström, *Nano Lett.* 24 (2024) 2165–2174.
- [51] M. Palacios-Corella, V. García-López, J.C. Waerenborgh, B.J.C. Vieira, G. Mínguez Espallargas, M. Clemente-León, E. Coronado, *Chem. Sci.* 14 (2023) 3048–3055.
- [52] M.R. Horn, A. Singh, S. Alomari, S. Goberna-Ferrón, R. Benages-Vilau, N. Chodankar, N. Motta, K. Ostrikov, J. MacLeod, P. Sonar, P. Gomez-Romero, D. Dubal, *Energy Environ. Sci.* 14 (2021) 1652–1700.
- [53] C. Mu, Z. Du, W. Li, *Polyoxometalates 3* (2024) 9140062.
- [54] Q. Liu, Y. Cui, L. Zhu, D. Cheng, C. Wang, S. Lu, B. Li, X. Chen, H.-Y. Zang, *Polyoxometalates 2* (2023) 9140036.
- [55] L. Ni, J. Gu, X. Jiang, H. Xu, Z. Wu, Y. Wu, Y. Liu, J. Xie, Y. Wei, G. Diao, *Angew. Chem. Int. Ed. Engl.* 62 (2023) e202306528.
- [56] D. Pakulski, A. Gorczyński, D. Brykczynska, V. Montes-García, W. Czepa, I. Janica, M. Bielejewski, M. Kubicki, V. Patroniak, P. Samorì, A. Ciesielski, *Angew. Chem. Int. Ed.* 62 (2023) e202305239.
- [57] Á. Barros, B. Artetxe, U. Eletxigerra, E. Aranzabe, J.M. Gutiérrez-Zorrilla, *Materials* 16 (2023) 5054.
- [58] D. Pakulski, A. Gorczyński, W. Czepa, Z. Liu, L. Ortolani, V. Morandi, V. Patroniak, A. Ciesielski, P. Samorì, *Energy Storage Mater.* 17 (2019) 186–193.
- [59] C. Wang, B. Wang, H. Yang, Y. Wan, H. Fang, W. Bao, W. Wang, N. Wang, Y. Lu, *Chem. Eng. J.* 483 (2024) 149143.
- [60] H. Hu, L. Lian, X. Ji, W.-L. Zhao, H. Li, W. Chen, H.N. Miras, Y.-F. Song, *Coord. Chem. Rev.* 503 (2024) 215640.
- [61] S. Zhang, R. Liu, C. Streb, G. Zhang, *Polyoxometalates 2* (2023) 9140037.
- [62] A. Das, M. Mohapatra, S. Basu, *Carbon* 223 (2024) 119007.
- [63] Á. Barros, E. Aranzabe, B. Artetxe, J.C. Duburg, L. Gubler, J.M. Gutiérrez-Zorrilla, U. Eletxigerra, *ACS Appl. Energy Mater.* 7 (2024) 3729–3739.
- [64] E. Svensson Grape, J. Huang, D. Roychowdhury, T.T. Debelá, H. Chang, A. Jenkins, A.M. Schimpf, C.H. Hendon, C.K. Brozek, *ACS Appl. Energy Mater.* (2024).
- [65] A. Bijelic, M. Aureliano, A. Rompel, *Angew. Chem. Int. Ed.* 58 (2019) 2980–2999.
- [66] S. Lentink, D.E. Salazar Marcano, M.A. Moussawi, T.N. Parac-Vogt, *Angew. Chem. Int. Ed.* 62 (2023) e202303817.
- [67] A. Kondinski, *Polyoxometalates 3* (2024) 9140058.
- [68] L. Wang, P. Dai, H. Ma, T. Sun, J. Peng, *Inorg. Chem. Front.* 11 (2024) 1339–1365.
- [69] M. Tahmasebi, M. Mirzaei, M. Darroudi, J.T. Mague, *J. Mol. Struct.* 1309 (2024) 138102.
- [70] B. Li, X. Xu, Y. Lv, Z. Wu, L. He, Y.-F. Song, *Small* 20 (2024) 2305539.
- [71] H. Soria-Carrera, E. Atrián-Blasco, R. Martín-Rapún, S.G. Mitchell, *Chem. Sci.* 14 (2023) 10–28.
- [72] R. Khan, M. Tariq, K.H. Shah, S. Rani, N.A. Osman, H.M. Asif, S. Mehar, A. K. Alanazi, H.M. Abo-Dief, *J. Photoch. Photobiol. A* 442 (2023) 114774.
- [73] C. Zhang, R. Liu, X. Kong, H. Li, D. Yu, X. Fang, L. Wu, Y. Wu, *Int. J. Mol. Sci.* 24 (2023) 8858.
- [74] D. Nowicka, D. Marcinkowski, N. Vavra, M. Szymańska, M. Kubicki, G. Consiglio, W. Drożdż, A.R. Stefankiewicz, V. Patroniak, M. Fik-Jaskółka, A. Gorczyński, *Dalton Trans.* 53 (2024) 11678–11688.
- [75] M. Xu, C. Liu, Y. Wang, J. Wang, J. Feng, J. Sha, *J. Clust. Sci.* 32 (2021) 1–10.
- [76] C.-G. Liu, W. Guan, L.-K. Yan, Z.-M. Su, P. Song, E.-B. Wang, *J. Phys. Chem. C* 113 (2009) 19672–19676.
- [77] S. Liu, L. Xu, G.-G. Gao, B. Xu, *Thin Solid Films* 517 (2009) 4668–4672.
- [78] F. Xiao, X. Meng, L. Wang, J. Hao, C. Lv, Y. Wei, *Polyoxometalates 3* (2024) 9140055.



- [85] H.-X. Sheng, B.-Y. Lin, C.-Q. Chen, J. Du, P. Yang, *Polyoxometalates* 3 (2024) 9140060.
- [86] A. Bocian, W. Drożdż, M. Szymańska, J. Lewandowski, M. Fik-Jaskółka, A. Gorczyński, V. Patroniak, A.R. Stefankiewicz, *Nanoscale* 12 (2020) 4743–4750.
- [87] G. Markiewicz, D. Pakulski, A. Galanti, V. Patroniak, A. Ciesielski, A. R. Stefankiewicz, P. Samorì, *Chem. Commun.* 53 (2017) 7278–7281.
- [88] A. Blazević, A. Rempel, *Coord. Chem. Rev.* 307 (2016) 42–64.
- [89] D. Li, P. Ma, J. Niu, J. Wang, *Coord. Chem. Rev.* 392 (2019) 49–80.
- [90] D.E. Salazar Marcano, M.A. Moussawi, A.V. Anyushin, S. Lentink, L. Van Meerelt, I. Ivanović-Burmazović, T.N. Parac-Vogt, *Chem. Sci.* 13 (2022) 2891–2899.
- [91] P. Wang, Z. Wang, P. Wang, A.N. Chishti, H. Zhang, J. Shi, L. Ni, S. Jamil, Y. Wei, *Polyoxometalates* 3 (2024) 9140047.
- [92] S.-R. Li, W.-D. Liu, L.-S. Long, L.-S. Zheng, X.-J. Kong, *Polyoxometalates* 2 (2023) 9140022.
- [93] Q. Zhang, F. Li, L. Xu, *Polyoxometalates* 2 (2023) 9140018.
- [94] H. Zhang, W.-L. Zhao, H. Li, Q. Zhuang, Z. Sun, D. Cui, X. Chen, A. Guo, X. Ji, S. An, W. Chen, Y.-F. Song, *Polyoxometalates* 1 (2022) 9140011.
- [95] Z. Zeb, Y. Huang, L. Chen, W. Zhou, M. Liao, Y. Jiang, H. Li, L. Wang, L. Wang, H. Wang, T. Wei, D. Zang, Z. Fan, Y. Wei, *Coord. Chem. Rev.* 482 (2023) 215058.
- [96] B. Li, L. Wu, *Polyoxometalates* 2 (2023) 9140016.
- [97] C. Dey, *Coord. Chem. Rev.* 510 (2024) 215847.
- [98] H.M. Asif, R.B. Bi, M. Tariq, N. Shaheen, M. Khalid, M. Nadeem, M. Ali Khan, T. M. Ansari, *Russ. J. Inorg. Chem.* 66 (2021) 340–347.
- [99] L. Wang, W. Li, L. Wu, X. Dong, H. Hu, G. Xue, *Inorg. Chem. Commun.* 35 (2013) 122–125.
- [100] S.-M. Wang, J. Hwang, E. Kim, J. Mater. Chem. C. 7 (2019) 7828–7850.
- [101] S. Vanhaecht, G. Absillis, T.N. Parac-Vogt, *Dalton Trans.* 41 (2012) 10028–10034.
- [102] S. Vanhaecht, T. Quanten, T.N. Parac-Vogt, *Dalton Trans.* 46 (2017) 10215–10219.
- [103] S. Yoshitaka, Y. Shoko, H. Takeshi, M. Hideyuki, N. Kenji, B. Chem. Soc. Jpn. 80 (2007) 1965–1974.
- [104] B. Yan, R. Liang, K. Zheng, R. Li, P. Ma, J. Wang, J. Niu, *Inorg. Chem.* 60 (2021) 8164–8172.
- [105] M.-X. Li, Y. Zhang, Z.-M. Zhu, F. Su, L.-C. Zhang, X.-J. Sang, J. Coord. Chem. 73 (2020) 2437–2449.
- [106] J. Guo, D. Zhang, L. Chen, Y. Song, D. Zhu, Y. Xu, *Dalton Trans.* 42 (2013) 8454–8459.
- [107] G. Zhu, E.N. Glass, C. Zhao, H. Lv, J.W. Vickers, Y.V. Geletii, D.G. Musaev, J. Song, C.L. Hill, *Dalton Trans.* 41 (2012) 13043–13049.
- [108] S. Nellutla, J. van Tol, N.S. Dalal, L.-H. Bi, U. Kortz, B. Keita, L. Nadjo, G. A. Khitrov, A.G. Marshall, *Inorg. Chem.* 44 (2005) 9795–9806.
- [109] F.-Q. Zhang, J.-P. Gao, L.-K. Yan, W. Guan, R.-X. Yao, X.-M. Zhang, *Dalton Trans.* 46 (2017) 16145–16158.
- [110] X. Xu, H.-L. Dong, R.-L. Sang, L. Xu, *Chem. Commun.* 48 (2012) 12177–12179.
- [111] Q. Zheng, L. Vilà-Nadal, Z. Lang, J.-J. Chen, D.-L. Long, J.S. Mathieson, J. M. Poblét, L. Cronin, *J. Am. Chem. Soc.* 140 (2018) 2595–2601.
- [112] H.N. Miras, D.L. Long, L. Cronin, Chapter one - exploring self-assembly and the self-organization of nanoscale inorganic polyoxometalate clusters, in: R. van Eldik, L. Cronin (Eds.), *Adv. Inorg. Chem., Academic Press*, 2017, pp. 1–28.
- [113] I.M. Mbomekalle, B. Keita, L. Nadjo, P. Berthet, W.A. Neiwiert, C.L. Hill, M. D. Ritorto, T.M. Anderson, *Dalton Trans.* (2003) 2646–2650.
- [114] T. Ueda, M. Suzuki, T. Toya, J. Clust. Sci. 27 (2016) 501–511.
- [115] T. Minato, K. Suzuki, K. Kamata, N. Mizuno, *Chem. – Eur. J.* 20 (2014) 5946–5952.
- [116] C.J. Gomez-Garcia, J.J. Borrás-Almenar, E. Coronado, L. Ouahab, *Inorg. Chem.* 33 (1994) 4016–4022.
- [117] L.-H. Bi, E.-B. Wang, J. Peng, R.-D. Huang, L. Xu, C.-W. Hu, *Inorg. Chem.* 39 (2000) 671–679.
- [118] J. Luo, G. Jin, F. Zhang, Y. Liu, L. Chen, S. Xie, J. Zhao, *Eur. J. Inorg. Chem.* 2018 (2018) 143–152.
- [119] J. Xie, B.F. Abrahams, A.G. Wedd, *Chem. Commun.* (2008) 576–578.
- [120] G. Cao, J. Xiong, Q. Xue, S. Min, H. Hu, G. Xue, *Electrochim. Acta* 106 (2013) 465–471.
- [121] T. Rüther, V.M. Hultgren, B.P. Timko, A.M. Bond, W.R. Jackson, A.G. Wedd, *J. Am. Chem. Soc.* 125 (2003) 10133–10143.
- [122] M.K. Seery, L. Guerin, R.J. Forster, E. Gicquel, V. Hultgren, A.M. Bond, A. G. Wedd, T.E. Keyes, *J. Phys. Chem. A* 108 (2004) 7399–7405.
- [123] S.-S. Zhu, B. Yue, X.-Q. Shi, Y.-D. Gu, J. Liu, M.-Q. Chen, Y.-F. Huang, *J. Chem. Soc., Dalton Trans.* (1993) 3633–3634.
- [124] D.-L. Long, H. Abbas, P. Kögerler, L. Cronin, *Angew. Chem. Int. Ed.* 44 (2005) 3415–3419.
- [125] J. Yan, D.-L. Long, H.N. Miras, L. Cronin, *Inorg. Chem.* 49 (2010) 1819–1825.
- [126] P. Lapham, L. Vilà-Nadal, L. Cronin, V.P. Georgiev, *J. Phys. Chem. C* 125 (2021) 3599–3610.
- [127] Q. Zheng, M. Kupper, W. Xuan, H. Oki, R. Tsunashima, D.-L. Long, L. Cronin, *J. Am. Chem. Soc.* 141 (2019) 13479–13486.
- [128] Q. Han, X. Sun, J. Li, P. Ma, J. Niu, *Inorg. Chem.* 53 (2014) 2006–2011.
- [129] Z. Han, Q. Hao, Z. Wang, X. Zhai, *J. Chem. Crystallogr.* 43 (2013) 1–5.
- [130] L. Shi, X.-M. Gao, T.-Y. Liu, X.-H. Huang, Z.-H. Gong, Y.-P. Chen, Y.-Q. Sun, *Dalton Trans.* 47 (2018) 1347–1354.
- [131] S. He, Y. Xin, J. Li, Z. Zhu, P. Zhao, W. You, *Acta Crystallogr. Sect. C* 74 (2018) 1267–1273.
- [132] J. Gao, J. Yan, S. Beeg, D.-L. Long, L. Cronin, *Angew. Chem. Int. Ed.* 51 (2012) 3373–3376.
- [133] L. Liu, J. Jiang, L. Cui, J. Zhao, X. Cao, L. Chen, *Inorg. Chem.* 61 (2022) 1949–1960.
- [134] C. Busche, L. Vilà-Nadal, J. Yan, H.N. Miras, D.L. Long, V.P. Georgiev, A. Asenov, R.H. Pedersen, N. Gadegaard, M.M. Mirza, D.J. Paul, J.M. Poblét, L. Cronin, *Nature* 515 (2014) 545–549.
- [135] U. Kortz, M.T. Pope, *Inorg. Chem.* 33 (1994) 5643–5646.
- [136] M. Bugnola, R.E. Schreiber, Y. Kaufman, G. Leituss, L.J.W. Shimon, R. Neumann, *Eur. J. Inorg. Chem.* 2019 (2019) 482–485.
- [137] R.E. Schreiber, H. Cohen, G. Leituss, S.G. Wolf, A. Zhou, L. Que Jr., R. Neumann, *J. Am. Chem. Soc.* 137 (2015) 8738–8748.
- [138] F. Chauveau, P. Doppelt, J. Lefebvre, *Inorg. Chem.* 19 (1980) 2803–2806.
- [139] R. Ben-Daniel, A.M. Khenkin, R. Neumann, *Chem. – Eur. J.* 6 (2000) 3722–3728.
- [140] D.-L. Long, P. Kögerler, A.D.C. Parenty, J. Fielden, L. Cronin, *Angew. Chem. Int. Ed.* 45 (2006) 4798–4803.
- [141] J. Yan, D.L. Long, E.F. Wilson, L. Cronin, *Angew. Chem. Int. Ed.* 48 (2009) 4376–4380.
- [142] L. Vilà-Nadal, S.G. Mitchell, D.-L. Long, A. Rodríguez-Fortea, X. López, J. M. Poblét, L. Cronin, *Dalton Trans.* 41 (2012) 2264–2271.
- [143] D.-L. Long, Y.-F. Song, E.F. Wilson, P. Kögerler, S.-X. Guo, A.M. Bond, J.S. Hargreaves, L. Cronin, *Angew. Chem. Int. Ed.* 47 (2008) 4384–4387.
- [144] Y.-Y. Zhang, S.-X. Liu, C.-J. Yu, Q. Tang, D.-D. Liang, C.-D. Zhang, F.-J. Ma, S.-J. Li, W. Zhang, R.-K. Tan, *Inorg. Chem. Commun.* 13 (2010) 1418–1420.
- [145] L. Ni, F. Hussain, B. Spingler, S. Weyeneth, G.R. Patzke, *Inorg. Chem.* 50 (2011) 4944–4955.
- [146] J. Wang, S. Li, Y. Shen, J. Niu, *Cryst. Growth Des.* 8 (2008) 372–374.
- [147] M. Haouas, I.-M. Mbomekallé, N. Vila, P. de Oliveira, F. Taulelle, *Inorg. Chem.* 53 (2014) 5568–5574.
- [148] H. Li, C. Lian, L. Chen, J. Zhao, G.-Y. Yang, *Nanoscale* 12 (2020) 16091–16101.
- [149] Y. Zhang, B. Zeng, Y. Liu, P. Li, L. Chen, J. Zhao, *Eur. J. Inorg. Chem.* 2020 (2020) 3416–3425.
- [150] N. Shen, F. Tian, J. Chang, K.-L. Huang, Z.-H. Zhang, X. Feng, J. Gu, S.-C. Chen, M.-Y. He, Q. Chen, *Cryst. Eng. Comm.* 22 (2020) 3656–3663.
- [151] T.L. Joriss, M. Kozik, L.C.W. Baker, *Inorg. Chem.* 29 (1990) 4584–4586.
- [152] T. Minato, D. Salley, N. Mizuno, K. Yamaguchi, L. Cronin, K. Suzuki, *J. Am. Chem. Soc.* 143 (2021) 12809–12816.
- [153] S. Li, G. Li, P. Ji, J. Zhang, S. Liu, J. Zhang, X. Chen, *ACS Appl. Mater. Interfaces.* 11 (2019) 43287–43293.
- [154] A. Müller, E. Krickemeyer, H. Bögge, M. Schmidtman, F. Peters, *Angew. Chem. Int. Ed.* 37 (1998) 3359–3363.
- [155] O. Oms, A. Dolbecq, P. Mialane, *Chem. Soc. Rev.* 41 (2012) 7497–7536.
- [156] Y. Hayashi, *Coord. Chem. Rev.* 255 (2011) 2270–2280.
- [157] M. Nyman, *Dalton Trans.* 40 (2011) 8049–8058.
- [158] S.S. Amin, J.M. Cameron, M. Winslow, E.S. Davies, S.P. Argent, D. Robinson, G. N. Newton, *Eur. J. Inorg. Chem.* 2022 (2022) e202200019.
- [159] R. Contant, R. Thouvenot, *Inorg. Chim. Acta* 212 (1993) 41–50.
- [160] L. Vilà-Nadal, S. Romo, X. López, J. Poblét, *Structural and Electronic Features of Wells-Dawson, Polyoxometalates* (2012).
- [161] E. Janusson, N. de Kler, L. Vilà-Nadal, D.-L. Long, L. Cronin, *Chem. Commun.* 55 (2019) 5797–5800.
- [162] F.-Q. Zhang, W. Guan, L.-K. Yan, Y.-T. Zhang, M.-T. Xu, E. Hayfron-Benjamin, Z.-M. Su, *Inorg. Chem.* 50 (2011) 4967–4977.
- [163] L. Yan, X. López, J.J. Carbó, R. Sniatynsky, D.C. Duncan, J.M. Poblét, *J. Am. Chem. Soc.* 130 (2008) 8223–8233.
- [164] J. Zhang, A.M. Bond, P.J.S. Richardt, A.G. Wedd, *Inorg. Chem.* 43 (2004) 8263–8271.
- [165] C.R. Graham, R.G. Finke, *Inorg. Chem.* 47 (2008) 3679–3686.
- [166] I.-M. Mbomekalle, Y.W. Lu, B. Keita, L. Nadjo, *Inorg. Chem. Commun.* 7 (2004) 86–90.
- [167] X. Ma, P. Wang, Z. Liu, C. Xin, S. Wang, J. Jia, P. Ma, J. Niu, J. Wang, *Inorg. Chem.* 59 (2020) 8690–8698.
- [168] P. Huang, X.-J. Wang, J.-J. Qi, X.-L. Wang, M. Huang, H.-Y. Wu, C. Qin, Z.-M. Su, *J. Mater. Chem. A* 5 (2017) 22970–22974.
- [169] T. Zhang, L.-K. Yan, S. Cong, W. Guan, Z.-M. Su, *Inorg. Chem. Front.* 1 (2014) 65–70.
- [170] W. Guo, H. Lv, J. Bacs, Y. Gao, J.S. Lee, C.L. Hill, *Inorg. Chem.* 55 (2016) 461–466.
- [171] C.P. Pradeep, M.F. Misrahi, F.Y. Li, J. Zhang, L. Xu, D.L. Long, T. Liu, L. Cronin, *Angew. Chem. Int. Ed.* 48 (2009) 8309–8313.
- [172] C.P. Pradeep, D.-L. Long, G.N. Newton, Y.-F. Song, L. Cronin, *Angew. Chem. Int. Ed.* 47 (2008) 4388–4391.
- [173] P. Yin, C.P. Pradeep, B. Zhang, F.-Y. Li, C. Lydon, M.H. Rosnes, D. Li, E. Bitterlich, L. Xu, L. Cronin, T. Liu, *Chem. – Eur. J.* 18 (2012) 8157–8162.
- [174] J. Oble, B. Riffade, A. Noël, M. Malacria, S. Thorimbert, B. Hasenknopf, E. Lacôte, *Org. Lett.* 13 (2011) 5990–5993.
- [175] J. Li, I. Huth, L.-M. Chamoreau, B. Hasenknopf, E. Lacôte, S. Thorimbert, M. Malacria, *Angew. Chem. Int. Ed.* 48 (2009) 2035–2038.
- [176] H. Iridi, A. Boulmier, P. Bolle, A. Dolbecq, J.-N. Rebilly, F. Banse, L. Ruhlmann, H. Serier-Brault, R. Dessapt, P. Mialane, O. Oms, *J. Mater. Chem. C* 8 (2020) 637–649.
- [177] W. Chen, U. Tong, T. Zeng, C. Streb, Y.-F. Song, *J. Mater. Chem. C* 3 (2015) 4388–4393.
- [178] B. Riffade, D. Lachkar, J. Oble, J. Li, S. Thorimbert, B. Hasenknopf, E. Lacôte, *Org. Lett.* 16 (2014) 3860–3863.
- [179] I. Azcarate, I. Ahmed, R. Farha, M. Goldmann, X. Wang, H. Xu, B. Hasenknopf, E. Lacôte, L. Ruhlmann, *Dalton Trans.* 42 (2013) 12688–12698.

- [180] M.-P. Santoni, A.K. Pal, G.S. Hanan, M.-C. Tang, A. Furtos, B. Hasenknopf, *Dalton Trans.* 43 (2014) 6990–6993.
- [181] V. Kalyani, V.S.V. Satyanarayana, V. Singh, C.P. Pradeep, S. Ghosh, S.K. Sharma, K.E. Gonsalves, *Chem. – Eur. J.* 21 (2015) 2250–2258.
- [182] S. Martín, Y. Takashima, C.-G. Lin, Y.-F. Song, H.N. Miras, L. Cronin, *Inorg. Chem.* 58 (2019) 4110–4116.
- [183] R. Gupta, W. Huang, L.C. Francesconi, T. Polenova, *Solid State Nucl. Magn. Reson.* 84 (2017) 28–33.
- [184] M. Abbessi, R. Contant, R. Thouvenot, G. Herve, *Inorg. Chem.* 30 (1991) 1695–1702.
- [185] W.W. Laxson, S. Özkur, R.G. Finke, *Inorg. Chem.* 53 (2014) 2666–2676.
- [186] W. Xiao, S. Li, Y. Zhao, Y. Ma, N. Li, J. Zhang, X. Chen, *Dalton Trans.* 50 (2021) 8690–8695.
- [187] G. Zhang, E. Gadot, G. Gan-Or, M. Baranov, T. Tubul, A. Neyman, M. Li, A. Clotet, J.M. Poblet, P. Yin, I.A. Weinstock, *J. Am. Chem. Soc.* 142 (2020) 7295–7300.
- [188] X. Fang, M. Speldrich, H. Schilder, R. Cao, K.P. O'Halloran, C.L. Hill, P. Kögerler, *Chem. Commun.* 46 (2010) 2760–2762.
- [189] A.M. Khenkin, G. Leitus, L. Weiner, R. Neumann, *J. Clust. Sci.* 25 (2014) 687–693.
- [190] X.-X. Li, W.-H. Fang, J.-W. Zhao, G.-Y. Yang, *Chem. – Eur. J.* 20 (2014) 17324–17332.
- [191] Y.-C. Liu, C.-H. Fu, S.-T. Zheng, J.-W. Zhao, G.-Y. Yang, *Dalton Trans.* 42 (2013) 16676–16679.
- [192] Y. Sakai, Y. Kitakoga, K. Hayashi, K. Yoza, K. Nomiya, *Eur. J. Inorg. Chem.* 2004 (2004) 4646–4652.
- [193] C.P. Pradeep, D.-L. Long, P. Kögerler, L. Cronin, *Chem. Commun.* (2007) 4254–4256.
- [194] S. Li, Y. Zhou, N. Ma, J. Zhang, Z. Zheng, C. Streb, X. Chen, *Angew. Chem. Int. Ed.* 59 (2020) 8537–8540.
- [195] S. Li, Y. Zhao, S. Knoll, R. Liu, G. Li, Q. Peng, P. Qiu, D. He, C. Streb, X. Chen, *Angew. Chem. Int. Ed.* 60 (2021) 16953–16957.
- [196] S. Li, Y. Zhao, H. Qi, Y. Zhou, S. Liu, X. Ma, J. Zhang, X. Chen, *Chem. Commun.* 55 (2019) 2525–2528.
- [197] A.M. Khenkin, D. Kumar, S. Shaik, R. Neumann, *J. Am. Chem. Soc.* 128 (2006) 15451–15460.
- [198] K. Stroobants, G. Absillis, P.S. Shestakova, R. Willem, T.N. Parac-Vogt, *J. Clust. Sci.* 25 (2014) 855–866.
- [199] S. Vanhaecht, G. Absillis, T.N. Parac-Vogt, *Dalton Trans.* 42 (2013) 15437–15446.
- [200] W. Wang, N.V. Izarova, J. van Leusen, P. Kögerler, *Chem. Commun.* 56 (2020) 14857–14860.
- [201] A. Sap, L. Vandebroek, V. Goovaerts, E. Martens, P. Proost, T.N. Parac-Vogt, *ACS Omega* 2 (2017) 2026–2033.
- [202] L. Vandebroek, E. De Zitter, H.G.T. Ly, D. Conić, T. Mihaylov, A. Sap, P. Proost, K. Pierloot, L. Van Meervelt, T.N. Parac-Vogt, *Chem. – Eur. J.* 24 (2018) 10099–10108.
- [203] Q.-H. Luo, R.C. Howell, M. Dankova, J. Bartis, C.W. Williams, W.D. Horrocks, V. G. Young, A.L. Rheingold, L.C. Francesconi, M.R. Antonio, *Inorg. Chem.* 40 (2001) 1894–1901.
- [204] A. Ostuni, R.E. Bachman, M.T. Pope, *J. Clust. Sci.* 14 (2003) 431–446.
- [205] J. Iijima, H. Naruke, *J. Mol. Struct.* 1040 (2013) 33–38.
- [206] W. Huang, M. Schopfer, C. Zhang, R.C. Howell, L. Todaro, B.A. Gee, L. C. Francesconi, T. Polenova, *J. Am. Chem. Soc.* 130 (2008) 481–490.
- [207] G. Gao, L. Xu, W. Wang, W. An, Y. Qiu, *J. Mater. Chem.* 14 (2004) 2024–2029.
- [208] R. Wan, P. Ma, M. Han, D. Zhang, C. Zhang, J. Niu, J. Wang, *Dalton Trans.* 46 (2017) 5398–5405.
- [209] M. Sadakane, A. Ostuni, M.T. Pope, *J. Chem. Soc., Dalton Trans.* (2002) 63–67.
- [210] Q. Luo, R.C. Howell, J. Bartis, M. Dankova, W.D. Horrocks, A.L. Rheingold, L. C. Francesconi, *Inorg. Chem.* 41 (2002) 6112–6117.
- [211] C. Zhang, L. Bensaid, D. McGregor, X. Fang, R.C. Howell, B. Burton-Pye, Q. Luo, L. Todaro, L.C. Francesconi, *J. Clust. Sci.* 17 (2006) 389–425.
- [212] C. Boglio, G. Lenoble, C. Duhayon, B. Hasenknopf, R. Thouvenot, C. Zhang, R. C. Howell, B.P. Burton-Pye, L.C. Francesconi, E. Lacôte, S. Thorimbert, M. Malacria, C. Afonso, J.-C. Tabet, *Inorg. Chem.* 45 (2006) 1389–1398.
- [213] Y. Lu, Y. Xu, Y. Li, E. Wang, X. Xu, Y. Ma, *Inorg. Chem.* 45 (2006) 2055–2060.
- [214] M. Sadakane, M.H. Dickman, M.T. Pope, *Inorg. Chem.* 40 (2001) 2715–2719.
- [215] F. Hu, P. Ma, M. Han, R. Wan, J. Wang, J. Niu, *Inorg. Chem. Commun.* 67 (2016) 103–106.
- [216] X. Wang, Y. Liu, M. Jin, Y. Wu, L. Chen, J.-W. Zhao, *Cryst. Growth Des.* 17 (2017) 5295–5308.
- [217] M.A. AlDamen, M.O. Sinnokrot, S.B. Atta, R.A. Al Qawasmeh, C.J. Gómez-García, *J. Struct. Chem.* 61 (2020) 559–565.
- [218] Y.-Q. Jiao, C. Qin, X.-L. Wang, F.-H. Liu, P. Huang, C.-G. Wang, K.-Z. Shao, Z.-M. Su, *Chem. Commun.* 50 (2014) 5961–5963.
- [219] N.V. Izarova, L. Klač, P. de Oliveira, I.M. Mbomekalle, V. Peters, F. Haarmann, P. Kögerler, *Dalton Trans.* 44 (2015) 19200–19206.
- [220] S.S. Mal, M.H. Dickman, U. Kortz, A.M. Todea, A. Merca, H. Bögge, T. Glaser, A. Müller, S. Nellutla, N. Kaur, J. van Tol, N.S. Dalal, B. Keita, L. Nadjio, *Chem. – Eur. J.* 14 (2008) 1186–1195.
- [221] S. Yao, Z. Zhang, Y. Li, E. Wang, *Dalton Trans.* 39 (2010) 3884–3889.
- [222] X. Yi, N.V. Izarova, T. Ifikhar, J. van Leusen, P. Kögerler, *Inorg. Chem.* 58 (2019) 9378–9386.
- [223] S. Yao, Z. Zhang, Y. Li, Y. Lu, E. Wang, Z. Su, *Cryst. Growth Des.* 10 (2010) 135–139.
- [224] F. Hussain, U. Kortz, B. Keita, L. Nadjio, M.T. Pope, *Inorg. Chem.* 45 (2006) 761–766.
- [225] C.-H. Zhan, Q. Zheng, D.-L. Long, L. Vilà-Nadal, L. Cronin, *Angew. Chem. Int. Ed.* 58 (2019) 17282–17286.
- [226] S.S. Mal, M.H. Dickman, U. Kortz, *Chem. – Eur. J.* 14 (2008) 9851–9855.
- [227] L.-H. Bi, U. Kortz, *Inorg. Chem.* 43 (2004) 7961–7962.
- [228] N. Laronze, J. Marrot, G. Hervé, *Chem. Commun.* (2003) 2360–2361.
- [229] J. Feng, G. Sun, F. Pei, M. Liu, *J. Inorg. Biochem.* 92 (2002) 193–199.
- [230] S. Matsunaga, Y. Inoue, T. Otaki, H. Osada, K. Nomiya, *Z. Anorg. Allg. Chem.* 642 (2016) 539–545.
- [231] K. Dong, P. Ma, H. Wu, Y. Wu, J. Niu, J. Wang, *Inorg. Chem.* 58 (2019) 6000–6007.
- [232] I.M. Mbomekalle, B. Keita, L. Nadjio, W.A. Neiwert, L. Zhang, K.I. Hardcastle, C. L. Hill, T.M. Anderson, *Eur. J. Inorg. Chem.* 2003 (2003) 3924–3928.
- [233] Z. Wang, X. Xin, M. Zhang, Z. Li, H. Lv, G.-Y. Yang, *Sci. China Chem.* 65 (2022) 1515–1525.
- [234] I.F. Bamba, C. Falaise, J. Marrot, G.K. Gbassi, P. Atheba, R. Guillot, M. Haouas, E. Cadot, *Inorg. Chem.* 61 (2022) 8309–8319.
- [235] L. Ruhlmann, D. Schaming, I. Ahmed, A. Courville, J. Canny, R. Thouvenot, *Inorg. Chem.* 51 (2012) 8202–8211.
- [236] F. Doungmene, P.A. Aparicio, J. Ntuenou, C.S.A. Mezui, P. de Oliveira, X. López, I.M. Mbomekallé, *Electrochim. Acta* 125 (2014) 674–682.
- [237] M.R. Farsani, F. Jalilian, B. Yadollahi, H.A. Rudbari, *Polyhedron* 76 (2014) 102–107.
- [238] X. Fang, T.M. Anderson, C.L. Hill, *Angew. Chem. Int. Ed.* 44 (2005) 3540–3544.
- [239] R.G. Finke, M.W. Drooge, *Inorg. Chem.* 22 (1983) 1006–1008.
- [240] M. Lebrini, I.M. Mbomekallé, A. Dolbecq, J. Marrot, P. Berthet, J. Ntuenou, F. Sécheresse, J. Vigneron, A. Etcheberry, *Inorg. Chem.* 50 (2011) 6437–6448.
- [241] C. Costa-Coquelard, S. Sorgues, L. Ruhlmann, J. Phys. Chem. A 114 (2010) 6394–6400.
- [242] D. Schaming, R. Farha, H. Xu, M. Goldmann, L. Ruhlmann, *Langmuir* 27 (2011) 132–143.
- [243] D. Schaming, C. Costa-Coquelard, S. Sorgues, L. Ruhlmann, I. Lampre, *Appl. Catal. A: Gen.* 373 (2010) 160–167.
- [244] N.I. Gumerova, A. Rompel, *Chem. Soc. Rev.* 49 (2020) 7568–7601.
- [245] N.I. Gumerova, A. Rompel, *Sci. Adv.* 9 (2023) eadi0814.
- [246] R. Contant, A. Teze, *Inorg. Chem.* 24 (1985) 4610–4614.
- [247] L.-Y. Guo, M. Jagodić, S.-Y. Zeng, Z. Wang, Z.-Q. Shi, X.-P. Wang, C.-H. Tung, D. Sun, *Dalton Trans.* 45 (2016) 8404–8411.
- [248] X. Fang, P. Kögerler, *Chem. Commun.* (2008) 3396–3398.
- [249] L. Pettersson, I. Andersson, L.O. Oehman, *Inorg. Chem.* 25 (1986) 4726–4733.
- [250] L. Pettersson, I. Andersson, L.-O. Öhman, I. Persson, F. Salvatore, *Acta Chem.* 39a (1985) 53–58.
- [251] A. Misra, K. Kozma, C. Streb, M. Nyman, *Angew. Chem. Int. Ed.* 59 (2020) 596–612.
- [252] D.E. Salazar Marcano, S. Lentink, M.A. Moussawi, T.N. Parac-Vogt, *Inorg. Chem.* 60 (2021) 10215–10226.
- [253] A. Proust, B. Matt, R. Villanneau, G. Guillemot, P. Gouzerh, G. Izzet, *Chem. Soc. Rev.* 41 (2012) 7605–7622.
- [254] S. Thorimbert, B. Hasenknopf, E. Lacôte, *Isr. J. Chem.* 51 (2011) 275–280.
- [255] A.J. Kibler, G.N. Newton, *Polyhedron* 154 (2018) 1–20.
- [256] J. Zhang, Y. Huang, G. Li, Y. Wei, *Coord. Chem. Rev.* 378 (2019) 395–414.
- [257] H.M. Asif, Y. Zhou, L. Zhang, N. Shaheen, D. Yang, J. Li, Y. Long, A. Iqbal, Y. Li, *Inorg. Chem.* 56 (2017) 9436–9447.
- [258] M.-P. Santoni, A.K. Pal, G.S. Hanan, A. Proust, B. Hasenknopf, *Inorg. Chem.* 50 (2011) 6737–6745.
- [259] T. Auvray, M.-P. Santoni, B. Hasenknopf, G.S. Hanan, *Dalton Trans.* 46 (2017) 10029–10036.
- [260] M. Glöb, R. Pütt, M. Moors, E. Kentzinger, W. Pyckhout-Hintzen, K.Y. Monakhov, *Nanoscale* 11 (2019) 4267–4277.
- [261] I. Azcarate, Z. Huo, R. Farha, M. Goldmann, H. Xu, B. Hasenknopf, E. Lacôte, L. Ruhlmann, *Chem. – Eur. J.* 21 (2015) 8271–8280.
- [262] D. Lachkar, D. Vilona, E. Dumont, M. Lelli, E. Lacôte, *Angew. Chem. Int. Ed.* 55 (2016) 5961–5965.
- [263] J. Lesage, A. Pontes da Costa, G. Pemboung, L. Ruhlmann, B. Hasenknopf, E. Lacôte, J. Rieger, *Polymer* 57 (2015) 173–182.
- [264] J. Lesage de la Haye, P. Beaunier, L. Ruhlmann, B. Hasenknopf, E. Lacôte, J. Rieger, *Chem. Plus. Chem.* 79 (2014) 250–256.
- [265] S. Barety, S. Piligkos, B. Hasenknopf, P. Gouzerh, E. Lacôte, S. Thorimbert, M. Malacria, *J. Am. Chem. Soc.* 127 (2005) 6788–6794.
- [266] C. Boglio, K. Micoine, É. Derat, R. Thouvenot, B. Hasenknopf, S. Thorimbert, E. Lacôte, M. Malacria, *J. Am. Chem. Soc.* 130 (2008) 4553–4561.
- [267] H.G.T. Ly, T. Mihaylov, G. Absillis, K. Pierloot, T.N. Parac-Vogt, *Inorg. Chem.* 54 (2015) 11477–11492.
- [268] C.R. Mayer, C. Roch-Marchal, H. Lavanant, R. Thouvenot, N. Sellier, J.-C. Blais, F. Sécheresse, *Chem. – Eur. J.* 10 (2004) 5517–5523.
- [269] F. Odobel, M. Séverac, Y. Pellegrin, E. Blart, C. Fosse, C. Cannizzo, C.R. Mayer, K. J. Elliott, A. Harriman, *Chem. – Eur. J.* 15 (2009) 3130–3138.
- [270] B. Matt, S. Renaudineau, L.M. Chamoreau, C. Afonso, G. Izzet, A. Proust, *J. Org. Chem.* 76 (2011) 3107–3112.
- [271] A.V. Anyushin, S. Vanhaecht, T.N. Parac-Vogt, *Inorg. Chem.* 59 (2020) 10146–10152.
- [272] E. Hampson, J.M. Cameron, S. Amin, J. Kyo, J.A. Watts, H. Oshio, G.N. Newton, *Angew. Chem. Int. Ed.* 58 (2019) 18281–18285.
- [273] E. Hampson, J.M. Cameron, J.A. Watts, G.N. Newton, *Chem. Commun.* 56 (2020) 8237–8240.
- [274] K. Kastner, A.J. Kibler, E. Karjalainen, J.A. Fernandes, V. Sans, G.N. Newton, *J. Mater. Chem. A* 5 (2017) 11577–11581.
- [275] M. Glöb, R. Pütt, M. Moors, E. Kentzinger, S. Karthäuser, K.Y. Monakhov, *Adv. Mater. Interfaces* 9 (2022) 2200461.

- [276] Y. Hou, C.L. Hill, *J. Am. Chem. Soc.* 115 (1993) (1830) 11823.
- [277] D. Vilona, M. Lelli, E. Dumont, E. Lacôte, *Chem. – Eur. J.* 27 (2021) 17761–17764.
- [278] H. Zeng, G.R. Newkome, C.L. Hill, *Angew. Chem. Int. Ed.* 39 (2000) 1771–1774.
- [279] P. Yin, T. Li, R.S. Forgan, C. Lydon, X. Zuo, Z.N. Zheng, B. Lee, D. Long, L. Cronin, T. Liu, *J. Am. Chem. Soc.* 135 (2013) 13425–13432.
- [280] M. Piot, S. Hupin, H. Lavanant, C. Afonso, L. Bouteiller, A. Proust, G. Izzet, *Inorg. Chem.* 56 (2017) 8490–8496.
- [281] B. Matt, X. Xiang, A.L. Kaledin, N. Han, J. Moussa, H. Amouri, S. Alves, C.L. Hill, T. Lian, D.G. Musaev, G. Izzet, A. Proust, *Chem. Sci.* 4 (2013) 1737–1745.
- [282] F. Zonneville, M.T. Pope, *J. Am. Chem. Soc.* 101 (1979) 2731–2732.
- [283] M. Boujita, J. Boixel, E. Blart, C.R. Mayer, F. Odobel, *Polyhedron* 27 (2008) 688–692.
- [284] B. Matt, C. Coudret, C. Viala, D. Jouvenot, F. Loiseau, G. Izzet, A. Proust, *Inorg. Chem.* 50 (2011) 7761–7768.
- [285] W.-K. Miao, Y.-K. Yan, X.-L. Wang, Y. Xiao, L.-J. Ren, P. Zheng, C.-H. Wang, L.-X. Ren, W. Wang, *ACS Macro Lett.* 3 (2014) 211–215.
- [286] W.-K. Miao, A. Yi, Y.-K. Yan, L.-J. Ren, D. Chen, C.-H. Wang, W. Wang, *Polym. Chem.* 6 (2015) 7418–7426.
- [287] Z. Huo, I. Azcarate, R. Farha, M. Goldmann, H. Xu, B. Hasenknopf, E. Lacôte, L. Ruhlmann, *J. Solid State Electrochem.* 19 (2015) 2611–2621.
- [288] G. Wang, T. Chen, S. Li, H. Pang, H. Ma, *Dalton Trans.* 46 (2017) 13897–13902.
- [289] F. Gomollón-Bel, *Chem. Int.* 41 (2019) 12–17.
- [290] M. Kato, M. Kamigaito, M. Sawamoto, T. Higashimura, *Macromol.* 28 (1995) 1721–1723.
- [291] J.-S. Wang, K. Matyjaszewski, *J. Am. Chem. Soc.* 117 (1995) 5614–5615.
- [292] K. Matyjaszewski, N.V. Tsarevsky, *J. Am. Chem. Soc.* 136 (2014) 6513–6533.
- [293] Y. Han, Y. Xiao, Z. Zhang, B. Liu, P. Zheng, S. He, W. Wang, *Macromol.* 42 (2009) 6543–6548.
- [294] S.-J. Yu, Y.-K. Han, W. Wang, *Polymer* 162 (2019) 73–79.
- [295] Y.-K. Han, Z.-J. Zhang, Y.-L. Wang, N. Xia, B. Liu, Y. Xiao, L.-X. Jin, P. Zheng, W. Wang, *Macromol. Chem. Phys.* 212 (2011) 81–87.
- [296] J. Lesage de La Haye, J.-M. Guigner, E. Marceau, L. Ruhlmann, B. Hasenknopf, E. Lacôte, J. Rieger, *Chem. – Eur. J.* 21 (2015) 2948–2953.
- [297] P. He, B. Xu, H. Liu, S. He, F. Saleem, X. Wang, *Sci. Rep.* 3 (2013) 1833.
- [298] P. He, B. Xu, X. Xu, L. Song, X. Wang, *Chem. Sci.* 7 (2016) 1011–1015.
- [299] M.A. Moussawi, N. Leclerc-Laronze, S. Floquet, P.A. Abramov, M.N. Sokolov, S. Cordier, A. Ponchel, E. Monflier, H. Bricout, D. Landy, M. Haouas, J. Marrot, E. Cadot, *J. Am. Chem. Soc.* 139 (2017) 12793–12803.
- [300] M.-B. Hu, Z.-Y. Hou, W.-Q. Hao, Y. Xiao, W. Yu, C. Ma, L.-J. Ren, P. Zheng, W. Wang, *Langmuir* 29 (2013) 5714–5722.
- [301] M. Piot, B. Abécassis, D. Broui, C. Troufflard, A. Proust, G. Izzet, *Proc. Natl. Acad. Sci.* 115 (2018) 8895–8900.
- [302] Q. Liu, P. He, H. Yu, L. Gu, B. Ni, D. Wang, X. Wang, *Sci. Adv.* 5 (2019) eaax1081.
- [303] L.-L. Zhang, W.-K. Miao, L.-J. Ren, Y.-K. Yan, W. Wang, *Chin. J. Polym. Sci.* 39 (2021) 716–724.
- [304] Q. Li, L. Zhang, J. Dai, H. Tang, Q. Li, H. Xue, H. Pang, *J. Chem. Eng.* 351 (2018) 441–461.
- [305] F.M.B. Gusmão, D. Mladenović, K. Radinović, D.M.F. Santos, B. Šljukić, *Energies* 15 (2022) 9021.
- [306] N.K. Sah, S.J. Phukan, D.N. Madhusudan, K. Sankaranarayanan, M. Roy, S. Garai, *Polyoxometalate-Induced Nano-Engineered Composite Materials: Supercapacitor Applications*, in: *Nanomater. Sustainable Energy Appl.*, CRC Press, 2024, pp. 50–76.
- [307] K. Li, T. Liu, J. Ying, A. Tian, X. Wang, *J. Mater. Chem. A* 12 (2024) 13576–13604.
- [308] M. JE, P.R. Chandewar, D. Shee, S.S. Mal, *RSC Adv.* 13 (2023) 26744–26754.
- [309] N.S. Mughal, D.A. Walsh, G.N. Newton, *ACS Appl. Energy Mater.* 3 (2020) 12308–12315.
- [310] S.S. Amin, J.M. Cameron, R.B. Cousins, J. Wrigley, L. Liirò-Peluso, V. Sans, D. A. Walsh, G.N. Newton, *Inorg. Chem. Front.* 9 (2022) 1777–1784.
- [311] C. Fleming, D.-L. Long, N. McMillan, J. Johnston, N. Bovet, V. Dhanak, N. Gadegaard, P. Kögerler, L. Cronin, M. Kadodwala, *Nat. Nanotechnol.* 3 (2008) 229–233.
- [312] M. Vasilopoulou, A.M. Douvas, L.C. Palilis, S. Kennou, P. Argitis, *J. Am. Chem. Soc.* 137 (2015) 6844–6856.
- [313] A.M. Douvas, D. Tsikritzis, C. Tselios, A. Haider, A.S. Mougharbel, U. Kortz, A. Hiskia, A.G. Coutsolelos, L.C. Palilis, M. Vasilopoulou, S. Kennou, P. Argitis, *Phys. Chem. Chem. Phys.* 21 (2019) 427–437.
- [314] S.N.S., N. Basu, M. Cahay, S.M.N., S.S. Mal, P.P. Das, *Physica Status Solidi (a)* 217 (2020) 2000306.
- [315] W. Sun, C. He, T. Liu, C. Duan, *Chem. Commun.* 55 (2019) 3805–3808.
- [316] J.J. Walsh, C.T. Mallon, A.M. Bond, T.E. Keyes, R.J. Forster, *Chem. Commun.* 48 (2012) 3593–3595.
- [317] I. Ahmed, R. Farha, M. Goldmann, L. Ruhlmann, *Chem. Commun.* 49 (2013) 496–498.
- [318] J. Walsh, J. Zhu, A. Bond, R. Forster, T. Keyes, *J. Electroanal. Chem.* 706 (2013) 93–101.
- [319] A. Harriman, K.J. Elliott, M.A.H. Alamir, L.L. Pleux, M. Séverac, Y. Pellegrin, E. Blart, C. Fosse, C. Cannizzo, C.R. Mayer, F. Odobel, *J. Phys. Chem. C* 113 (2009) 5834–5842.
- [320] H. Sun, L.-Y. Guo, J.-S. Li, J.-P. Bai, F. Su, L.-C. Zhang, X.-J. Sang, W.-S. You, Z.-M. Zhu, *Chem. Sus. Chem.* 9 (2016) 1125–1133.
- [321] I. Ahmed, R. Farha, Z. Huo, C. Allain, X. Wang, H. Xu, M. Goldmann, B. Hasenknopf, L. Ruhlmann, *Electrochim. Acta* 110 (2013) 726–734.
- [322] K.J. Elliott, A. Harriman, L. Le Pleux, Y. Pellegrin, E. Blart, C.R. Mayer, F. Odobel, *Phys. Chem. Chem. Phys.* 11 (2009) 8767–8773.
- [323] H.M. Asif, H.F. Ashfaq, Y. Zhou, L. Zhang, A. Iqbal, X. Hu, F.K. Shehzad, *Dalton Trans.* 52 (2023) (1858) 11850–11851.
- [324] B. Matt, J. Fize, J. Moussa, H. Amouri, A. Pereira, V. Artero, G. Izzet, A. Proust, *Energy Environ. Sci.* 6 (2013) 1504–1508.
- [325] A. Panagiotopoulos, A.M. Douvas, 9 (2016) 3213–3219.
- [326] Z.-M. Zhang, T. Zhang, C. Wang, Z. Lin, L.-S. Long, W. Lin, *J. Am. Chem. Soc.* 137 (2015) 3197–3200.
- [327] H. Li, S. Yao, H.-L. Wu, J.-Y. Qu, Z.-M. Zhang, T.-B. Lu, W. Lin, E.-B. Wang, *Appl. Catal. B: Environ.* 224 (2018) 46–52.
- [328] J. Tian, Z. Xu, D.-W. Zhang, H. Wang, S.-H. Xie, D.-W. Xu, Y.-H. Ren, H. Wang, Y. Liu, L. Zhanting, *Nat. Commun.* 7 (2016) 11580.
- [329] L. Jiao, Y. Dong, X. Xin, L. Qin, H. Lv, *Appl. Catal. B: Environ.* 291 (2021) 120091.
- [330] M. Alaaeddine, Q. Zhu, D. Fichou, G. Izzet, J.E. Rault, N. Barrett, A. Proust, L. Tortech, *Inorg. Chem. Front.* 1 (2014) 682–688.
- [331] X.-W. Guo, X.-H. Li, Z.-J. Liu, W.-L. Chen, X.-T. Zheng, E.-B. Wang, Z.-M. Su, *Inorg. Chem. Front.* 4 (2017) 1187–1191.
- [332] X.-Y. Yang, M.-T. Li, N. Sheng, J.-S. Li, G.-D. Liu, J.-Q. Sha, J. Jiang, *Cryst. Growth Des.* 18 (2018) 5564–5572.
- [333] M. Li, L. Cong, J. Zhao, T. Zheng, R. Tian, J. Sha, Z. Su, X. Wang, *J. Mater. Chem. A* 5 (2017) 3371–3376.
- [334] J. Hu, H. Diao, W. Luo, Y.-F. Song, *Chem. – Eur. J.* 23 (2017) 8729–8735.
- [335] B.-W. Cong, Z.-H. Su, Z.-F. Zhao, B. Wang, *CrystEngComm* 19 (2017) 7154–7161.
- [336] H. Zhang, Z. Ma, S. Duan, Y. Liu, X. Jiang, Q. Zhou, M. Chen, L. Ni, G. Diao, *Electrochim. Acta* 428 (2022) 140868.
- [337] M. Wang, D. Yin, Y. Cao, X. Dong, G. Gao, X. Hu, C. Jin, L. Fan, J. Yu, H. Liu, *Chin. Chem. Lett.* 33 (2022) 4350–4356.
- [338] H.D. Pratt III, T.M. Anderson, *Dalton Trans.* 42 (2013) 15650–15655.
- [339] S. Chinnathambi, M. Ammam, *J. Power Sources* 284 (2015) 524–535.
- [340] C. Mu, X. Wang, Z. Ma, X. Liu, W. Li, J. Mater. Chem. A. 10 (2022) 7207–7217.
- [341] F.M. Mulder, B.M.H. Weninger, J. Middelkoop, F.G.B. Ooms, H. Schreuders, *Energy Environ. Sci.* 10 (2017) 756–764.
- [342] J.-J. Chen, M.D. Symes, L. Cronin, *Nat. Chem.* 10 (2018) 1042–1047.
- [343] N. Dupré, P. Rémy, K. Micoine, C. Boglio, S. Thorimbert, E. Lacôte, B. Hasenknopf, M. Malacria, *Chem. – Eur. J.* 16 (2010) 7256–7264.
- [344] A. Rajan, A.S. Mougharbel, S. Bhattacharya, T. Nisar, V. Wagner, U. Kortz, *Inorg. Chem.* 59 (2020) 13042–13049.
- [345] F. de Azambuja, T.N. Parac-Vogt, *ACS Catal.* 9 (2019) 10245–10252.
- [346] G.-P. Yang, S.-X. Shang, B. Yu, C.-W. Hu, *Inorg. Chem. Front.* 5 (2018) 2472–2477.
- [347] A. Modvig, C. Kumpidat, A. Riisager, J. Albert, *Materials* 12 (2019) 2175.
- [348] S.E. Collins, S.R. Matkovic, A.L. Bonivardi, L.E. Briand, *J. Phys. Chem. C* 115 (2011) 700–709.
- [349] S.L. Giles, J.G. Lundin, R.B. Balow, P.E. Pehrsson, J.H. Wynne, *Appl. Catal. A: Gen.* 542 (2017) 306–310.
- [350] C. Streb, *Dalton Trans.* 41 (2012) 1651–1659.
- [351] S.M. Mousavi, S.A. Hashemi, S. Bahrani, S. Mosleh, W.-H. Chiang, K. Yousefi, S. Ramakrishna, L.C. Wei, N. Omidifar, *Environ. Sci. and Pollut. Res.* 29 (2022) 56055–56067.
- [352] G. Marci, E.I. García-López, L. Palmisano, *Eur. J. Inorg. Chem.* 2014 (2014) 21–35.
- [353] L. Li, Q.-Y. Wu, Y.-H. Guo, C.-W. Hu, *Microporous Mesoporous Mater.* 87 (2005) 1–9.
- [354] S. Jiang, Y. Guo, C. Wang, X. Qu, L. Li, *J. Colloid Interface Sci.* 308 (2007) 208–215.
- [355] J. Lü, J.-X. Lin, X.-L. Zhao, R. Cao, *Chem. Commun.* 48 (2012) 669–671.
- [356] B. Keita, L. Nadjio, *J. Mol. Catal. A: Chem.* 262 (2007) 190–215.
- [357] B. Keita, I.-M. Mbomekalle, L. Nadjio, P. de Oliveira, A. Ranjbari, R. Contant, *C. R. Chim.* 8 (2005) 1057–1066.
- [358] B. Keita, R. Contant, P. Mialane, F. Sécheresse, P. de Oliveira, L. Nadjio, *Electrochem. Commun.* 8 (2006) 767–772.
- [359] Y. Yang, S. Liu, C. Li, S. Li, G. Ren, F. Wei, T. Qun, *Inorg. Chem. Commun.* 17 (2012) 54–57.
- [360] X. Zhao, D. Liang, S. Liu, C. Sun, R. Cao, C. Gao, Y. Ren, Z. Su, *Inorg. Chem.* 47 (2008) 7133–7138.
- [361] L. Liu, B. Wang, J.H. Lv, K. Yu, L. Wang, H. Zhang, S. Wang, B.B. Zhou, *Cryst. Eng. Comm.* 19 (2017) 5653–5661.
- [362] S. Imar, M. Yaqub, C. Maccato, C. Dickinson, F. Laffir, M. Vagin, T. McCormac, *Electrochim. Acta* 184 (2015) 323–330.
- [363] N. Fay, E. Dempsey, T. McCormac, *J. Electroanal. Chem.* 574 (2005) 359–366.
- [364] B. Keita, I. Mbomekallé, L. Nadjio, R. Contant, *Electrochem. Commun.* 3 (2001) 267–273.
- [365] M. Zhou, L.P. Guo, F.Y. Lin, H.X. Liu, *Anal. Chim. Acta* 587 (2007) 124–131.
- [366] D. Martel, A. Kuhn, *Electrochim. Acta* 45 (2000) 1829–1836.
- [367] J.-J. Chen, L. Vilà-Nadal, A. Solé-Daura, G. Chisholm, T. Minato, C. Busche, T. Zhao, B. Kandasamy, A.Y. Ganin, R.M. Smith, I. Colliard, J.J. Carbó, J. M. Poblet, M. Nyman, L. Cronin, *J. Am. Chem. Soc.* 144 (2022) 8951–8960.
- [368] M. Ammam, *J. Mater. Chem. A* 1 (2013) 6291–6312.
- [369] N. Anwar, M. Vagin, F. Laffir, G. Armstrong, C. Dickinson, T. McCormac, *Analyst* 137 (2012) 624–630.
- [370] C. Zhou, S. Li, W. Zhu, H. Pang, H. Ma, *Electrochim. Acta* 113 (2013) 454–463.
- [371] F. Boussema, A.J. Gross, F. Hmidia, B. Ayed, H. Majdoub, S. Cosnier, A. Maaref, M. Holzinger, *Biosens. Bioelectron.* 109 (2018) 20–26.
- [372] P. He, B. Xu, P.P. Wang, H. Liu, X. Wang, *Adv. Mater.* 26 (2014) 4339–4344.



- [373] G.-G. Gao, L. Xu, W. Wang, Z. Wang, Y. Qiu, E. Wang, J. Electrochem. Soc. 152 (2005) H102–H106.
- [374] M. Rouhani, A. Soleymanpour, Mater. Sci. Eng. C Mater. Biol. Appl. 117 (2020) 111287.
- [375] Q. Li, M. Xu, X. Li, S. Li, L. Hou, Y. Chen, J. Sha, Analyst 145 (2020) 4021–4030.
- [376] X. Liu, Q. Zheng, D. Jia, W. Wang, H. Zhao, X. Tao, J. Sha, J. Clust. Sci. 34 (2023) 3095–3103.
- [377] S. Muqaddas, H. Aslam, S. Ul Hassan, A. Raza Ashraf, M. Adeel Asghar, M. Ahmad, A. Nazir, R. Shoukat, M. Kaleli, S. Mostafa Ibrahim, S. Kyürekli, A. Haider, A. Ali, Mater. Sci. Eng. B. 293 (2023) 116446.
- [378] I. Sakthinathan, N. Yamasaki, D. Barreca, C. Maccato, T. Ueda, T. McCormac, Electrochim. Acta 462 (2023) 142689.
- [379] S.U. Hassan, Y. Zhou, L. Zhang, Z. Shi, D. Yang, H.M. Asif, N. Qu, J. Phys. Chem. C 120 (2016) 7757–7766.
- [380] Y. Zhang, Y. Li, J. Pang, Y. Liu, P. Li, L. Chen, J. Zhao, Inorg. Chem. 58 (2019) 7078–7090.
- [381] G. Gao, L. Xu, W. Wang, Z. Wang, Y. Qiu, E. Wang, Electrochim. Acta 50 (2005) 1101–1106.
- [382] G. Gao, L. Xu, W. Wang, W. An, Y. Qiu, Z. Wang, E. Wang, J. Phys. Chem. B 109 (2005) 8948–8953.
- [383] J. Zhang, X. Wang, G. Wang, Y. Feng, C. Zhang, T. Pang, G. Gao, L. Fan, H. Liu, Chin. Chem. Lett. 34 (2022) 107231.
- [384] S.-M. Wang, L. Liu, W.-L. Chen, E.-B. Wang, Electrochim. Acta 113 (2013) 240–247.
- [385] C. Boskovic, Acc. Chem. Res. 50 (2017) 2205–2214.
- [386] X. Fang, P. Kögerler, M. Speldrich, H. Schilder, M. Luban, Chem. Commun. 48 (2012) 1218–1220.
- [387] M. Ibrahim, Y. Xiang, B.S. Bassil, Y. Lan, A.K. Powell, P. de Oliveira, B. Keita, U. Kortz, Inorg. Chem. 52 (2013) 8399–8408.
- [388] J. Goura, M. Choudhari, T. Nisar, T. Balster, J.K. Bindra, J. Kinyon, B. Ali, T. McCormac, N.S. Dalal, V. Wagner, U. Kortz, Inorg. Chem. 59 (2020) 13034–13041.
- [389] M. Ibrahim, A. Baksi, Y. Peng, F.K. Al-Zeidaneen, I.M. Mbomekallé, P. de Oliveira, C.E. Anson, Molecules 25 (2020) 4229.
- [390] J. Jia, P. Ma, P. Zhang, D. Zhang, C. Zhang, J. Niu, J. Wang, Dalton Trans. 47 (2018) 6288–6292.
- [391] R. Pütt, P. Kozłowski, I. Werner, J. Griebel, S. Schmitz, J. Warneke, K. Y. Monakhov, Inorg. Chem. 60 (2021) 80–86.
- [392] Y. Liu, S. Tian, S. Liu, E. Wang, Transit. Met. Chem. 30 (2005) 113–117.
- [393] J. Hu, S.K. Tan, M.G.L. Lim, S.H. Chang, G. Cui, S. Liu, K. Narasimhan, S.Y. New, X. Wang, C. Chen, H. Chakravarty, P.R. Kolatkar, K.Y. Tam, Q. Lu, X. Su, R. Jauch, E. Cheung, Biochem. J. 475 (2018) 1965–1977.
- [394] X.H. Wang, J.F. Liu, J. Coord. Chem. 51 (2000) 73–82.
- [395] W. Xiao-Hong, H. Jiang-Hua, Z. Rong-Chang, L. Jing-Fu, Chin. J. Chem. 21 (2003) 415–418.
- [396] L. Pérez-Álvarez, L. Ruiz-Rubio, B. Artetxe, M.d. Vivanco, J.M. Gutiérrez-Zorrilla, J.L. Vilas-Vilela, Carbohydr. Polym. 213 (2019) 159–167.
- [397] Azizullah, M. Al-Rashida, A. Haider, U. Kortz, S.A. Joshi, J. Iqbal, Chem. Select 3 (2018) 1472–1479.
- [398] R.N. Azizullah, A. Ur, U. Haider, S. Kortz, M. Afridi, S.A. Sohail, J.I. Joshi, Int. J. Pharm. 533 (2017) 125–137.
- [399] F. Pu, E. Wang, H. Jiang, J. Ren, Mol. Biosyst. 9 (2013) 113–120.
- [400] R. Prudent, V. Moucadet, B. Laudet, C. Barette, L. Lafanechère, B. Hasenknopf, J. Li, S. Bareyt, E. Lacôte, S. Thorimbert, M. Malacria, P. Gouzerh, C. Cochet, Chem. Biol. 15 (2008) 683–692.
- [401] K. Narasimhan, S. Pillay, N.R. Bin Ahmad, Z. Bikadi, E. Hazai, L. Yan, P. R. Kolatkar, K. Pervushin, R. Jauch, ACS Chem. Biol. 6 (2011) 573–581.
- [402] C. Pimpão, I.V. da Silva, A.F. Mósca, J.O. Pinho, M.M. Gaspar, N.I. Gumerova, A. Rompel, M. Aureliano, G. Soveral, Int. J. Mol. Sci. 21 (2020) 2467.
- [403] Y. Liu, Y.-Y. Han, S. Lu, Y. Wu, J. Li, X. Sun, J. Yan, Biomater. Sci. 10 (2022) 1257–1266.
- [404] A. Bijelic, M. Aureliano, A. Rompel, Chem. Commun. 54 (2018) 1153–1169.
- [405] N. Fukuda, T. Yamase, Y. Tajima, Biol. Pharm. Bull. 22 (1999) 463–470.
- [406] M. Inoue, T. Suzuki, Y. Fujita, M. Oda, N. Matsumoto, T. Yamase, J. Inorg. Biochem. 100 (2006) 1225–1233.
- [407] J. Geng, M. Li, J. Ren, E. Wang, X. Qu, Angew. Chem. Int. Ed. 50 (2011) 4184–4188.
- [408] N. Gao, H. Sun, K. Dong, J. Ren, T. Duan, C. Xu, X. Qu, Nat. Commun. 5 (2014) 3422.
- [409] N. Gao, H. Sun, K. Dong, J. Ren, X. Qu, Chem. – Eur. J. 21 (2015) 829–835.
- [410] Y. Guan, M. Li, K. Dong, N. Gao, J. Ren, Y. Zheng, X. Qu, Biomater. 98 (2016) 92–102.
- [411] M. Ma, N. Gao, Y. Sun, X. Du, J. Ren, X. Qu, Adv. Healthc. Mater. 7 (2018) 1800320.
- [412] G. Lan, K. Ni, S.S. Veroneau, T. Luo, E. You, W. Lin, J. Am. Chem. Soc. 141 (2019) 6859–6863.
- [413] G. Geisberger, E.B. Gyenge, C. Maake, G.R. Patzke, Carbohydr. Polym. 91 (2013) 58–67.
- [414] M. Aureliano, G. Fraqueza, M. Berrocal, J.J. Cordoba-Granados, N.I. Gumerova, A. Rompel, C. Gutierrez-Merino, A.M. Mata, J. Inorg. Biochem. 236 (2022) 111952.
- [415] R. Lampl, J. Breibeck, N.I. Gumerova, M.S. Galanski, A. Rompel, Sci. Rep. 11 (2021) 19354.
- [416] A. Flütsch, T. Schroeder, M.G. Grütter, G.R. Patzke, Bioorg. Med. Chem. Lett. 21 (2011) 1162–1166.
- [417] M. Witvrouw, H. Weigold, C. Pannecouque, D. Schols, E. De Clercq, G. Holan, J. Med. Chem. 43 (2000) 778–783.
- [418] R. Francese, A. Civra, M. Rittà, M. Donalisio, M. Argenziano, R. Cavalli, A. S. Mougharbel, U. Kortz, D. Lembo, Antiviral Res. 163 (2019) 29–33.
- [419] J. Fu, A.L. Gnat, D.A. Bushnell, G.J. Jensen, N.E. Thompson, R.R. Burgess, P. R. David, R.D. Kornberg, Cell 98 (1999) 799–810.
- [420] L. Leyssens, T. Balcaen, M. Pétré, N. Béjar Ayllón, W. El Aazmani, A. de Pierpont, G. Pyka, V. Lacroix, G. Kerckhofs, Acta Biomater. 164 (2023) 303–316.
- [421] N.J. van Eck, L. Waltman, Scientometrics 84 (2010) 523–538.